



VCU

Virginia Commonwealth University
VCU Scholars Compass

Theses and Dissertations


Graduate School

2018

Experimental Evaluation of Uranyl Transport into Mesoporous Silica Gel using Fluorescence

Brandon M. Dodd
Virginia Commonwealth University

Follow this and additional works at: <https://scholarscompass.vcu.edu/etd>

 Part of the [Environmental Indicators and Impact Assessment Commons](#), [Nuclear Engineering Commons](#), [Other Mechanical Engineering Commons](#), [Physical Chemistry Commons](#), and the [Water Resource Management Commons](#)

© The Author

Downloaded from

<https://scholarscompass.vcu.edu/etd/5336>

This Dissertation is brought to you for free and open access by the Graduate School at VCU Scholars Compass. It has been accepted for inclusion in Theses and Dissertations by an authorized administrator of VCU Scholars Compass. For more information, please contact libcompass@vcu.edu.

© Brandon Dodd 2018
All Rights Reserved

**Experimental Evaluation of Uranyl Transport into Mesoporous Silica Gel using
Fluorescence**

A dissertation submitted in partial fulfillment of the requirements for the degree of Doctor of
Philosophy at Virginia Commonwealth University.

by

BRANDON MICHAEL DODD

Bachelor of Science, Virginia Military Institute, USA, 2014

Master of Science, Virginia Commonwealth University, USA, 2015

Director: Dr. Gary C. Tepper

Professor and Chair, Department of Mechanical and Nuclear Engineering

Virginia Commonwealth University

Richmond, Virginia

April, 2018

Acknowledgements

I would not have made it to this day without the help and support of my friends, family, and professors.

I would first like to thank my advisor, Dr. Gary Tepper. He began supporting my research when I was still an undergrad visiting VCU for the summer, and he encouraged me to return to VCU for graduate school. Since becoming a graduate student, he has allowed me to control my own future through my course work and research and has supported me throughout my graduate studies. I have enjoyed discussing my research results and direction with him in our many planned and impromptu meetings over my years at VCU.

I would like to thank my committee members: Dr. Hooman Tafreshi, Dr. Jessika Rojas, Dr. Dmitry Pestov, and Dr. Garry Glaspell. They have all been so helpful by bringing their individual expertise to assist me throughout my dissertation project. They have always been available any time I have needed to discuss different components of my project, and they have assisted me with furthering my knowledge of porous media, particle interaction and radiation, and chemistry.

I would also like to thank Dr. Karla Mossi for all the help she has given me in determining the courses that I had to take and what options were available to me. She has also always let me know about any opportunity that she thought I might be interested in.

Dr. Goddard always thought of me when opportunities arose such as the Nuclear Facilities Experience and founding an Institute of Nuclear Materials Management chapter at VCU. He has

also allowed me access to gamma spectroscopy instruments and taught me so much about conventional radiation detection.

Dr. Ibrahim Guven has always shown me respect for my experimental abilities and always trusted me with his samples. I appreciate how he has always treated me as a respected research partner and more than as just a student.

I must thank my friends who have made my time at VCU a time I will never forget and will dearly miss when it is over: Brandon Campbell, Daniel Tincher, Dale Farkas, Ben Spence, and Taylor Britt. It has been a great experience being able to work with my friends and to build a relationship with each of you. I have appreciated working on course work together and the times when we just needed a break and took time to talk about anything else. They have expanded my mind to all different areas; from respiratory drug delivery and smart material to nuclear power plant simulations and radiation transport. I appreciate everything they have thought me along the way and all the good times we have had outside of school.

To my parents, who have supported me and let me live with them during my graduate studies, thank you. They have both been patient as I have taken this time to get my graduate degrees and assisted me with everything I have needed. I appreciate everything they have done for me and hope to one day be able to repay them in some way.

Last, I would like to thank my fiancée, Kari Norquist, a person without whom I would not be here today. Kari has believed in me more than anybody else from the summer we first met until today. She has never questioned my ability to get to this point in my career, even when I have. She has always been there to support me and has always told me I could accomplish anything to which I set my mind. She has been patient while I finish my doctorate degree even when she

was trying to start our future. I appreciate everything she has done for me, from letting me do homework on weekends when she was in town to assisting me with editing many of my papers.

Thank you all so much, I would not be here without all of you.

Table of Contents

Acknowledgements.....	ii
Table of Contents.....	v
List of Figures.....	viii
List of Tables.....	xi
Abstract.....	xiii
Chapter 1: Motivation and Objectives.....	1
Chapter 2: Background.....	7
2.1 Uranium in Nature.....	7
2.2 Environmental Contamination from Uranium Processing and Its Impact.....	8
2.3 Current Methods of Uranium Detection in Water.....	21
2.3 Uranium Fluorescence.....	24
2.4 Silica Gel Synthesis and Characterization.....	26
2.5 Silica Gel Fluorescent Enhancement of Uranyl.....	30
Chapter 3: Flow Enhanced Kinetics of Uranyl (UO ₂) transport nano-porous silica gel.....	32
3.1 Introduction.....	32
3.2 Spectra testing with Silica gel and Fluorescent Enhancement.....	32

3.3 Static Fluid Time Constant	36
3.4 Flow Enhanced Time Constant.....	39
3.5 Results and Discussion	43
3.6 Conclusions.....	47
Chapter 4: Table Top Instrument Development	49
4.1 Flow cell design	49
4.2 Hardware Holder Design	53
4.3 Circuit and Program Development	55
4.4 Current Status.....	63
4.5 Develop a final hand-held design for the instrument.....	64
Chapter 5: Uranyl Adsorption Kinetics within Silica Gel: Dependence on Flow Velocity and Concentration	66
5.1 Introduction.....	66
5.2 Experimental Methodology	68
5.3 Results and Discussion	71
5.4 Conclusions.....	74
Chapter 6: Uranyl Fluorescence Lifetime in Nanoporous Silica Gel: The Influence of Pore Size, pH and Water	76
6.1 Introduction.....	76
6.2 Experimental Methodology	78

6.3 Results and Discussion	80
6.4 Conclusions.....	85
Chapter 7: The Effect of Cations on Fluorescence and Kinetics of Uranyl in Nanoporous Silica Gel.....	86
7.1 Introduction.....	86
7.2 Experimental Methodology	88
7.3 Results and Discussion	92
7.4 Conclusions.....	96
Chapter 8: Gamma Spectroscopy of Uranium Adsorbed in Nanoporous Silica Gel	98
8.1 Introduction.....	98
8.2 Experimental Methodology	101
8.3 Results and Discussion	106
8.4 Conclusions.....	111
Chapter 9: Conclusions.....	113
List of References	118
VITA.....	128

List of Figures

Figure 2.1: The Quinta do Bispo uranium mine filled with effluent (17).	12
Figure 2.2: Map of uranium mining and milling sites in Portugal (3).	14
Figure 2.3: Jablonski Diagram for Uranyl in aqueous solutions(42).	25
Figure 3.1: a) Silica-filled nylon bag; b) 20x optical image of the nylon mesh; c) optical image of SG-3; d) SEM image of SG-1; e) SEM image of SG-3; and f) SEM image of SG-5.	34
Figure 3.2: Fluorescent spectrum of uranyl for silica gels and without silica gel present.	36
Figure 3.3: Normalized florescent intensity vs. time obtained for SG-4 in a quiescent solution.	37
Figure 3.4: Time constant in static fluid versus silica gel pore size.	38
Figure 3.5: a) Schematic of flow system; and b) internal geometry of the silica strainer.	40
Figure 3.6: a) Section view of the first strainer insert, b) Picture the assembled strainer with insert.	41
Figure 3.7: Section view of the second version of the strainer insert.	42
Figure 3.8: Section view of the final version of the strainer insert.	42
Figure 3.9: a) Normalized florescent intensity vs. time obtained for SG-4 in a quiescent solution as seen in Figure 3.3 above; b) Normalized florescent intensity vs. time obtained for SG-3 at 1 gph.	44
Figure 3.10: a) Schematic representation of uranyl transport into silica gel pack beds in quiescent solution and b) in presence of flow.	45
Figure 3.11: Time constant in presence of flow.	46

Figure 4.1: a) The top view of the flow cell lid, b) the bottom view of the flow cell lid, c) the section view of the flow cell base without barbed hose fitting installed, d) fully assembled flow cell.....	50
Figure 4.2: The second flow cell design section view.....	51
Figure 4.3: The third flow cell design section view.....	52
Figure 4.4: The section view of the final flow cell.....	52
Figure 4.5: Hardware holder section view and right side view.....	53
Figure 4.6: Second revised hardware holder section and right side view.....	54
Figure 4.7: Third revision hardware holder revision section view.....	55
Figure 4.8: Excitation scan of Uranyl Nitrate in silica gel.....	56
Figure 4.9: Uranyl emission with different excitation UVLEDs.....	57
Figure 4.10: UVLED output by wavelength: a) 365nm, b) 325nm, c)310nm, d) 280nm to include 114° (1,2) and 24° (3,4) viewing angle.....	58
Figure 4.11: Circuit schematic for the UVLED portion of the table top instrument.....	59
Figure 4.12: Time based emission scan of 280nm 24viewing angle UVLED.....	61
Figure 4.13: Time based emission scan of 280nm 24viewing angle UVLED using port control programing.....	62
Figure 5.1: a) Low velocity system bag, b) high velocity system bag.....	69
Figure 5.2: Schematic of the custom flow system.....	70
Figure 5.3: a) Normalized florescent intensity vs. time with silica gel saturation; b) Normalized florescent intensity vs. time in the linear region.....	72
Figure 5.4: Concentration as a function of response time.....	73
Figure 6.1: Figure 1: Lifetime measurement scan.....	79

Figure 6.2: Fluorescent spectra for uranyl adsorbed in silica	81
Figure 6.3: Lifetime as a function of pore size	82
Figure 6.4: Lifetimes after the samples remained dry for 204 days.	83
Figure 6.5: Spectra of a uranyl silica samples after drying for 204 day and when resubmerged in DI water	84
Figure 7.1: Full spectra of Uranyl.....	90
Figure 7.2: Fluorescent intensity as a function of time.....	91
Figure 7.3: EDS Spectrum for the Calcium cation sample.....	92
Figure 7.4: a) Stern-Volmer plot for Na ⁺ , b) Stern-Volmer plot for Mg ²⁺	93
Figure 7.5: Time constant results for each cation	94
Figure 7.6: Weight percent of uranium measure using EDS	95
Figure 8.1: ²³⁸ U decay chain (93)	100
Figure 8.2: Gamma spectra of the silica-5 natural diffusion sample	104
Figure 8.3: Activity as a function of half-life for ^{234m} Pa	107
Figure 8.4: Weighted average total uranium mass captured per silica surface area as a function of silica gel pore size.....	109
Figure 8.5: Mass of uranium captured as a function or silica gel pore size under flow conditions	110

List of Tables

Table 2.1: Concentrations of radionuclides dissolved in surface water and mine discharges	14
Table 2.2: Concentrations of radionuclides in the dissolved phase and particulates in irrigation wells (3).	15
Table 2.3: Concentrations of radionuclides in crops from the Quarta-Feira Valley ($\mu\text{g}/\text{kg}$)(19).	16
Table 3.1: Physical properties of silica gel	33
Table 3.2: Parameters for static fluid scans	35
Table 3.3: Spectrometer slit settings	35
Table 3.4: Parameters for static fluid scans.	37
Table 3.5: Spectrometer slit settings for flow enhanced scans.	40
Table 4.1: UVLED Specifications.	56
Table 5.1: Experimental Constants	74
Table 6.1 Physical properties of silica gels.....	78
Table 6.2: Spectrometer settings from spectral scans.....	79
Table 6.3: Spectrometer settings from lifetime scans.....	80
Table 7.1: Concentrations of cations found in fresh water(85–91)	88
Table 7.2: Ion Sources	89
Table 7.3: Spectrofluorometer settings for full spectra scans.....	89
Table 7.4: Spectrometer settings from time-based scans.....	90
Table 7.5: Concentrations of cations tested.	93

Table 7.6: Stern-Volmer Coefficients.....	93
Table 8.1: Manufacturer reported physical characteristics for the silica gel	102
Table 8.2: ^{234m}Pa and ^{238}U initial activities based on best fit curves for each silica gel sample.	107
Table 8.3: Measured uranium enrichment with uncertainty for each silica sample	108
Table 8.4: Filtration Efficiency.....	111

Abstract

EXPERIMENTAL EVALUATION OF URANYL TRANSPORT INTO MESOPOROUS SILICA GEL USING FLUORESCENCE

By Brandon Michael Dodd

A dissertation submitted in partial fulfillment of the requirements for the degree of Doctor of Philosophy at Virginia Commonwealth University.

Virginia Commonwealth University, 2018

Director: Dr. Gary C. Tepper

Professor and Chair, Department of Mechanical and Nuclear Engineering

This research investigated parameters that can affect the use of nanoporous silica gel as a media for accumulating a detectable amount of uranium. The unique fluorescence of the Uranyl (UO_2^{2+}) ion was used to evaluate the transport kinetics and accumulation within silica gel in a static fluid and under pressure driven flow. The addition of fluid flow decreased the time constant from on the order of an hour to approximately 2s with a very low fluid velocity of 0.36cm/s. The 0.36cm/s fluid velocity was found to be the critical velocity above which there was no gain in time constant. A table top instrument was developed that can detect trace amounts of uranium in solution. The table top instrument was used to investigate how the time constant depends on the uranyl concentration, which led to the development of a new time-based method

for quantifying the uranyl concentration. The time-based method of detection uses a preset threshold and, based on the time it takes to reach that threshold, the concentration in the water sample can be determined. The lifetime of uranyl in complex with silica increased to approximately 120us, allowing for gated detection and background discrimination. In addition to the fluorescent contaminants, competing cations were tested to determine how they affect the fluorescence and transport kinetics of the uranyl. The cations tested were Mn^{2+} , Ca^{2+} , Mg^{2+} , Na^+ , K^+ , and Li^+ . The result shows that within the natural concentrations, Mg^{2+} , Na^+ , and K^+ did quench the fluorescent of the uranyl ions by collision quenching. The time constant was also examined in the presence of each cation and showed that Ca^{2+} , Mg^{2+} , Na^+ , and K^+ decreased the adsorption time constant. Future studies in this area should be directed toward the development of a portable version of the instrument.

Chapter 1: Motivation and Objectives

Uranium is a ubiquitous, heavy, naturally occurring, radioactive element that is both chemically and radiologically toxic. Elevated concentrations of uranium in water and soil can be linked to activities such as uranium mining, nuclear fuel preparation, and disposal (1–3). Monitoring the concentration of uranium in the environment is of interest to organizations involved in activities such as national security, non-proliferation, water quality, and environmental impact studies (4,5). The impact studies have mainly focused on the area of human consumption because the EPA has established a maximum contamination level (MCL) of $30\mu\text{g/L}$ (4). Water with levels greater than the MCL have been linked to nephrotoxicity, osteotoxicity, liver damage, and increased risk of cancer (6–9). It has been discovered that two of the largest aquifers in the U.S., High Plains (HP) and Central Valley (CV), have contamination levels higher than the MCL. These two aquifers are the main source of water to wells for areas where almost 6 million people live, covering an area of 22375km^2 (7). These aquifers are also used to water 56700km^2 of farmland (7). These contaminated water sources need to be constantly monitored to check the status of the natural level of uranium. This monitoring is currently being done by gathering samples from the source and transporting them back to a lab to be tested.

Currently, the main methods for detecting uranium in water: alpha-spectrometry, gamma spectroscopy, inductively coupled plasma mass spectrometry, and fluorimetry. All three of these

methods have different sample preparations and laboratory equipment needed to properly perform the test. While these test are very accurate with detection limits of $0.1\mu\text{g/L}$, the need for laboratory equipment and extensive sample preparations make them impractical for field use (10). Currently, if an individual wants to know the uranium level in a water source, they will receive a testing kit from the local health department office to collect a water sample, and then it is sent to a laboratory for one or more of the aforementioned tests to be performed(8). The duration of this process, from acquiring a test kit until final results are received, will take considerably longer than if an instrument could be brought directly to the water source and provide rapid results.

One objective of this study is to develop a hand-held instrument to rapidly detect uranium in aqueous solutions by the observation of its fluorescent properties. Development of this technology will allow field testing of natural water sources and possible in-home testing of well water. In order to develop an instrument that can be hand-held, accurate, and fast, there would need to be significant technological advances. Requirements for a field testing device are that the sample preparation must be minimal; the equipment must be portable, battery powered, and small in overall size; and it should be simple to operate while maintaining the high level of accuracy that is currently accepted for the other methods. This instrument also needs to produce results in a rapid manner with minimal testing. Ideally, this device will be able to take a small water sample directly from the source and output the concentration of uranium in the water within minutes.

Objective 1: Examine the transport of uranyl into nanoporous silica gel and parameters that can affect it.

The current methods of detection of uranium in water are slow and must be performed in a laboratory environment. In order to minimize the time it takes to perform a measurement, the current timing needs to be characterized. Characterization of the transport kinetics will be based

on the uranyl concentration and fluid velocity needed for uranyl to full accumulate on the silica. Uranyl has a high affinity towards silica, so it can be used as a binding medium. The time for a measurement in the method used in this work is considered to be the time it takes for the uranyl to be fully accumulated on the surface on the silica, which is related to the time constant. In static fluid the time constant was on the order of an hour. The original idea was that changing the pore size of the silica gel would increase the gel permeability and decrease the time constant. This hypothesis was tested and shown to be successful, but it did not reduce the time constant to a point that would be considered sufficient for rapid detection. The next hypothesis was that using forced fluid flow to penetrate the silica gel pores would increase the rate at which the uranyl is deposited in the silica. This hypothesis eliminates the slow diffusion process that was the controlling mechanism in the previously mentioned method. The flow enhancement was very successful and reduced the time constant from the original hour to approximately a second. The tasks required for objective 1 are listed below.

Task 1.1: Evaluate the time constant for uranyl transport into nanoporous silica gel

- Status: Complete and published (Dodd et al. 2016)

Task 1.2: Investigate the effect of silica gel physical properties, uranyl concentration, and forced fluid flow on the transport kinetics.

- Status: Property of pore size and forced fluid flow are complete and published (Dodd et al. 2016)

Task 1.3: Evaluate the mass adsorbed into nanoporous silica gel.

- Status: Complete

Objective 2: Examine the parameters that affect the development of the table top instrument

The purpose of this objective is to identify the critical components needed to perform uranium detection. The hardware needs to have the ability to pump water through the silica gel bag, excite the entrapped uranyl, detect the fluorescent output of the uranyl, and relay and process the signal of the fluorescent detection. These specific abilities were intended to be performed by the smallest and lowest power-consuming devices because of the final goal of a hand-held battery operated device. The hardware components that were selected were a 12VDC peristaltic pump, a low voltage PMT with an analog signal output, a 280nm UVLED for excitation, and an Arduino UNO microcontroller. After the hardware was identified, the layout and flow cell needed to be addressed. The layout of the UVLED and the PMT was critical in order to have optimal excitation and fluorescent detection, while limiting light contamination. This was achieved with a custom 3d printed housing design that held the PMT, UVLED, optical filter, and the flow cell. In parallel to designing the hardware holder, a custom flow cell was designed that allows the water to flow through the silica gel bag from the top side of the bag and down to the exit. Once all of the hardware was laid out and the circuit was designed to power all of the components, a program was written that controls the pump speed and timing, gated excitation, and reads the analog signal from the PMT. The final step to the table top instrument set up was to test the detection limits of this configuration, which is currently at 3.9ppb. This limit of detection was the detection limit without increasing the PMT gain significantly and without using the time based detection method. The tasks required for objective 2 are listed below.

Task 2.1 Evaluate the performance of LEDs and PMT needed to detect uranyl fluorescence.

- Status: Complete

Task 2.2 Examine how uranyl concentration affects flow cell design, and optimize the hardware holder to limit light contamination.

- Status: Complete

Task 2.3 Evaluate sensitivity and find the detection limit of the table top instrument.

- Status: Complete

Task 2.4 Develop a method for gated detection to eliminate possible contaminants.

- Status: Complete

Objective 3: Perform calibration and contamination studies

The purpose of this section is to extensively test the uranium detection components and software. This will include testing all variables that must either be set or maintain their variability in the final calibration. The variables that need to be tested are the PMT gain through the Vcontrol, pumping time, and silica gel used. Once the final detection limit has been reached, these variables may be fixed in order to simplify the calibration. This calibration will need to take into account additional variables that can affect the detection such as water temperature and pH. The water temperature can affect the mobility of the uranyl into the silica gel matrix, and the pH is known to affect the fluorescent output of the uranyl. All of these possible variations must be taken into account when developing a robust calibration of the system. Once the calibration has been developed and tested, the contamination study can begin. The contaminants that will be tested will all produce light at wavelengths within the bandwidth of the optical filter used. Gated detection is another method that can be used to eliminate contaminants; therefore, fluorescent

lifetimes that differ from the lifetime of uranyl can be eliminated. Another avenues that will need to be addressed is initial filtration that could eliminate contaminants as long as the filter media used will not affect the uranyl. All of these test will be performed using the table top set up, and the results will be used in development of the final design.

Task 3.1 Analyze the uranyl concentration and pH effects on detection

- Status: Complete

Task 3.2 Investigate how possible contaminants affect detection.

- Status: Complete

Chapter 2: Background

2.1 Uranium in Nature

Natural uranium can be found in three isotopes: U^{234} , U^{235} , and U^{238} , with U^{238} being the most abundant. All of these isotopes can decay by either alpha or gamma emission (10). Uranium that is present in water can come from a number of sources both man-made and natural. The man-made sources range from mining to storage and disposal of spent nuclear fuel. The natural sources can be from erosion of large natural deposits or ubiquitous uranium. For example, the ubiquitous uranium concentration in soil is 3mg/kg of soil (11). Uranium in nature is commonly found in two forms: the tetravalent state or the hexavalent state. The tetravalent state of uranium is not water soluble, but the hexavalent state is water soluble (12). The hexavalent uranium in nature is most commonly found in an oxidized ionic form known as uranyl, with the chemical formula UO_2^{2+} (13,14). Uranyl readily complexes with nitrate, carbonate, phosphate, or sulfate ions, and all of these forms are water soluble (7,11,15). The stability of these uranium complexes can be affected by many geological processes such as precipitation, absorption, complexation with soil or other chemical species, and changes in pH (15). These processes often cause the accumulation of uranium in granite and sedimentary rocks, the most common which is uraninite (16). The uranium that is not deposited through normal geological processes or eroded from deposits will travel through ground water. The ground water contamination, which is usually in very small amounts, leads to the contamination of drinking water, plants, and animals, including humans. The normal level of contamination is usually 10^{-7} g of uranium/g of ocean water, plants, or animals (16). While

the normal levels are considerably lower than the MCL published by the EPA, there are regions where the levels exceed 180 times the MCL; these regions include a large portion of the U.S. (7). The elevated levels of uranium in these regions have sparked an interest in the development of a field instrument to detect uranium in water.

2.2 Environmental Contamination from Uranium Processing and Its Impact.

Introduction

Uranium is a naturally occurring element that, at naturally occurring concentrations, is not typically an environmental or health concern; however, elevated levels can be detrimental to the environment and living organisms. Elevated levels of uranium are associated with mining and milling of uranium ore, storage of nuclear waste, and other aspects of the nuclear fuel cycle, which can all cause uranium contamination. Though the nuclear fuel cycle is associated with uranium contamination today, it was not the initial reason. In the 1930s, Pierre and Marie Curie discovered that radium has important applications, specifically towards the treatment of cancer. Radium is a decay product of uranium, so the demand for radium drove the beginning of uranium mining. Initially, radium was considered the product of interest, so the uranium was deemed unimportant and was discarded as waste. Then, in 1938, Otto Hahn demonstrated the first nuclear fission reaction. The demonstration of fission showed that uranium had potentially useful applications. The first application that caused a large expansion in mining was the concept of a nuclear weapon during World War II. Next, in 1956, the United Kingdom began using nuclear energy to produce commercial electricity with Calder Hall (17). The development of nuclear weapons and commercial nuclear powers caused a steady increase in the demand for uranium until the end of the cold war. After the cold war ended in 1991, the uranium supply was stabilized, and there was no longer a large need for new uranium mines. Once the need to create

new uranium mines slowed, characterizing contamination at the mining, milling and processing sites began.

The contamination characterization of these site is challenging because measuring alpha and gamma spectrums in the field is very difficult due to the significant background signature, unknown source sizes and strengths, and a long list of potentially present attenuators that can affect the measurements results. That leaves two main avenues for characterization: 1) using a simple detector to determine the dose at specific locations on the site, and 2) collecting samples for more time consuming measurements in a laboratory setting. Both techniques are used to characterize the uranium content in the left over waste, soil on site, soil in the surrounding area, construction materials, surface and ground waters on the site, and any water sources into which the water runs off (5,17–21). In addition to looking in the immediate vicinity of the site, there is also contamination that travels a significant distance through the water ways and can contaminate farm land that is not adjacent to the nuclear sites. This contamination of the surrounding areas has raised concerns because it has been found to contaminate local food and water supplies of the general populous at levels that are not safe for humans (4,17,19). This has led to people having health issues caused by having high levels of uranium in their bodies (17). The next step for most of the nuclear facilities that have had contamination issues is to develop a plan for remediation of their sites in order to stop further contamination.

Causes of environmental contamination

Contamination caused by nuclear sites is classified as an elevated level of nuclear material that is present on the site and in the surrounding areas that can be linked back to a specific location or event. Most commonly, this is linked to mining and milling of uranium and

storage of nuclear waste. These links are because those processes have the highest potential for the uranium to interact with the environment.

The first and most concerning aspect of the fuel cycle in terms of contamination is uranium milling. Uranium milling is a large concern because the tailings are still radioactive and contain long lived radionuclides such as left over uranium and thorium (19,22). The forms of the tailings are typically in large heaps or sludge/slime that remain from in-situ leaching. The large heaps are piles of uranium milling by-product that still contain residual uranium and other decay products. The heaps are left unprotected from the elements which allows rain water to contaminate the runoff, surface water, and the soil (17–19,21–23). In addition to water contamination, there is air bourn dust and radiation that can be released from these large piles of waste (22,24). The waste piles at some locations also went through the process of leaching. This leaching was performed with sulphuric acid, which leaches the uranium out of the remaining ore, but it also leaks into the soil and water that changes the local pH in surrounding waters (18). This change in water and soil pH increases the mobility of the uranium and promotes it to move into the aqueous phase (17). This method also allows the particulates to runoff into the surface water and move toward larger bodies of water up to 5.6km away (23).

The next most concerning mode for contamination is from the mining of uranium ore. The mining of uranium is typically done through open pit mines, underground mines, in-situ leaching, and recovery from mining by-products, such as the previously mentioned leaching of mill tailings (17,19,22). The in-situ leaching is a contamination concern because of the formation of soluble uranium compounds and the acid contamination that reduces the pH and increases the mobility of uranium in water and soil (18).

Underground mines raise many concerns for workers' safety being that they were constantly breathing in particles of uranium and decay products. This led to the installation of ventilation ducts to move the contaminated air out of the mines. This ventilation is where the contamination concerns began because they were meant to let air pass both ways. Though this brought clean air to the workers, it also allowed the air containing uranium out into the environment (21). Many of the underground mines were later sealed, but they still pose a risk today. They are now areas where erosion, in conjunction with instabilities in the rock walls from mining, could result in a collapse. This would not only be detrimental to the surface, but a collapse would release more uranium into the environment. There is also concern that these areas interact with the atmosphere, and the minerals can oxidize more easily which can lead to contaminated acidic mine drainage (22).

Another concerning method of mining is open pit mining. Open pit mines have the most interactions with the atmosphere, allowing rainwater to fall directly in them, and in some cases, fill them, as shown in Figure 2.1.



Figure 2.1: The Quinta do Bispo uranium mine filled with effluent (17).

Figure 2.1 shows an open pit uranium mine that constantly contains water. This water is at a lower pH, but is not sequestered to the site and can easily contaminate the surrounding soil and runoff waters. The water limits the air contamination from uranium particulates that were a large concern during the operation of this type of mine, but it does not eliminate the contamination altogether (17,21).

Characterization of sites and levels of contamination

The characterization of mining and milling sites were performed by both in-situ and laboratory measurements. The in-situ measurements were performed with an ionization chamber to find the dose rate at specific locations around the sites. The ionization chamber measurements are taken by positioning the chamber 1m above the ground in various locations around the sites to identify high levels of radiation (18). In the analysis it was assumed that dose rate is proportional to uranium concentration. The data collected by the ionization measurements were used to identify location where heaps of tails were left behind or area where the piles were spread

thin over the ground (18). After the areas of interest were identified, samples were taken for further testing in a laboratory setting.

The laboratory samples were selected based on the field measurements, and additional samples were taken from areas where contamination is more concerning such as surface water and nearby water sources. To preserve the samples, the soil samples were collected and sealed before leaving the site, and the water samples were preserved by reducing the pH to 2 and keeping them in containers to reduce evaporation. In the laboratory, the soil samples were dried and put through a sieve to remove any large pieces. Then the samples were sealed and stored until each sample reached radioactive equilibrium. Next, the containers were measured using an HPGe gamma detector. These measurements were used to identify the activity of the samples and the radionuclides present at the site. The isotopes that were found were ^{238}U , ^{235}U , ^{234}U , ^{232}Th , ^{230}Th , ^{226}Ra , ^{210}Pb , ^{210}Po , ^{208}Tl , and ^{212}Pb (17–19,22). The alpha spectroscopy measurements were performed with ion implanted silicon detector on both the small particle and the larger particle waste from the soil samples. These samples were prepared by sieving them to separate the particles by size and then electroplating them onto the discs to place in the detector and limit attenuation. The water samples were also measured using alpha spectroscopy by electroplating the precipitates onto the discs for detection (18). In addition to these methods that rely on detection of ionizing radiation, there are developments in other methods to specifically identify uranium compounds and uranium concentrations using fluorescent spectroscopy both in the field and laboratory settings (3,20,25).

Using the aforementioned methods, mining and milling sites in Portugal were characterized, and the activity and dose rates were measured. The uranium mining and milling sites are shown on the map in Figure 2.2.

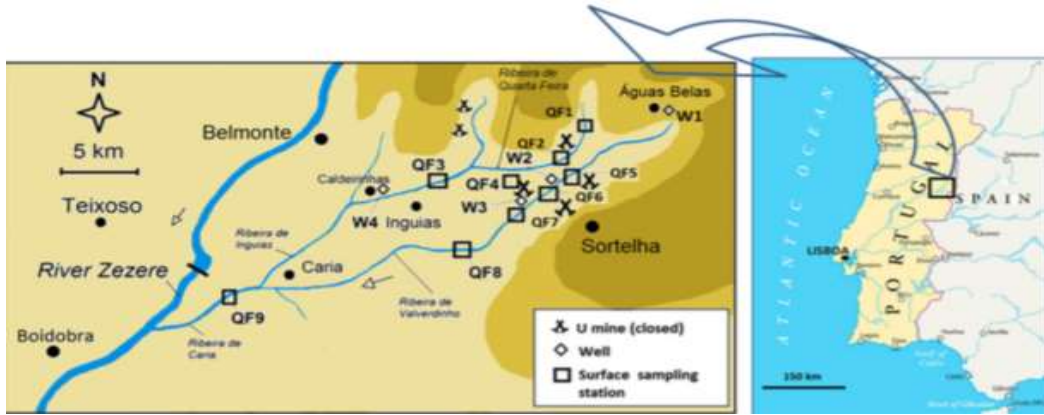


Figure 2.2: Map of uranium mining and milling sites in Portugal (3).

The samples were collected from waste heaps, soil, tailings, neutralization ponds, river bed sediments, surface water particulates, dissolved phases, irrigation wells, and horticulture products(17–19). For the area shown in Figure 2.2, the samples were taken at upstream and downstream locations. The results are shown in Table 2.1 below.

Table 2.1: Concentrations of radionuclides dissolved in surface water and mine discharges ($\mu\text{g/L} \pm 1 \text{ SD}$) (19).

Sampling Site	^{238}U	^{235}U	^{234}U
QF1, Rib. Quarta-Feira	1.66±0.05	0.012±0.001	0.00009±0.000003
QF2, Rib. Quarta-Feira	2.14±0.8	0.015±0.001	0.00012±0.000003
QF3, Rib. Quarta-Feira	1.72±0.6	0.013±0.001	0.00010±0.000003
QF4, Mine Discharge	12.05±3	0.089±0.003	0.00067±0.000013
QF5, Rib. Valerquinho	1.004±0.4	0.008±0.0007	0.00005±0.0000003
QF6, Treated Water Discharge	165.5±8	1.2±0.06	0.00864±0.000022
QF7, Rib, Valverquinho	2.68±0.9	0.018±0.001	0.00015±0.0000004
QF8, Rib, das Enguias	1.31±0.5	0.011±0.001	0.00007±0.0000003

Table 2.1 shows the concentration at the locations on the map depicted by QF1 through QF8.

The water upstream from the mine had an average radioactivity concentration of $1.9\mu\text{g/L}$, but at

the Carrasca mine discharge, the activity increased to 12.05µg/L (19). Table 2.1 also shows that the treated water being discharged from the Bica Mine has a concentration of 165.5µg/L, and this is being discharge into the environment at a high concentration when compared to the natural level of 1.9µg/L (19). In addition to the elevated levels of ²³⁸U, Table 2.1 shows the same trend for ²³⁵U and ²³⁴U. These levels in the water in the surrounding area can lead to concerns of how this contamination will affect the local populations. In addition to evaluating the contamination levels in the water on and near the Portugal nuclear sites, the water that was further away was evaluated. The results of testing the irrigation wells of farms that are located downstream from the nuclear sites are shown in Table 2.2.

Table 2.2: Concentrations of radionuclides in the dissolved phase and particulates in irrigation wells (3).

Sampling Site	²³⁸ U	²³⁵ U	²³⁴ U
Dissolved phase (µg/L ± 1SD)			
W1, Well Águas Belas	9.16±0.24	0.063±0.0025	0.00048±0.000009
W2, Well Quarta-Feira	5.95±0.16	0.041±0.0025	0.00032±0.000009
W3, Well near the Bica mine	24.58±0.72	0.2±0.0125	0.00131±0.000035
W4, Well Caldeirinhas	1.61±0.08	0.011±0.0006	0.00008±0.000004
Particulate Phase (mg/kg ± 1SD)			
W1, Well Águas Belas	113.28±3.21	0.837±0.07	0.00616±0.00017
W2, Well Quarta-Feira	531.05±15.26	3.625±0.37	0.02938±0.00087
W3, Well near the Bica mine	268.74±8.03	1.75±0.19	0.01463±0.00043
W4, Well Caldeirinhas	0.18±0.00015	0.001±0.0002	0.00001±0.0000004

W1 is located in Águas Belas, which is located at a higher elevation than the uranium mines. W4, located in Caldeirinhas Village in the valley, is located far enough away from the mine to be used for a control group (19). When looking at the level of W2 and W3 that were located near the mining site, the relative contamination level of the radionuclides is significantly higher than W1 or W4 showing that these irrigation wells have been directly affected by the mining activities

in the area (19). In order to test how the contamination of irrigation wells could affect the local populous, the plants that were being irrigated with this water were tested for contamination. The contamination levels in the plants from the Quarta-Feira Valley are shown in Table 2.3.

Table 2.3: Concentrations of radionuclides in crops from the Quarta-Feira Valley ($\mu\text{g}/\text{kg}$)(19).

Product, area	^{238}U	^{235}U	^{234}U
Lettuce, QF1	23.54 \pm 1.21	0.1012 \pm 0.03	0.001215 \pm 0.000065
Carrot, QF1	12.37 \pm 0.64	0.1075 \pm 0.02	0.000603 \pm 0.00003
Tomato, QF1	1.12 \pm 0.16	0.0087 \pm 0.01	0.00007 \pm 0.000009
Lettuce, QF2	8.84 \pm 0.40	0.0675 \pm 0.01	0.000447 \pm 0.000017
Tomato, QF2	0.72 \pm 0.06	0.0054 \pm 0.0022	0.000047 \pm 0.000004
Onion, QF2	1.08 \pm 0.07	0.0029 \pm 0.0019	0.00007 \pm 0.000004
Water Cress, QF2	491.68 \pm 23.3	3.1248 \pm 0.31	0.025564 \pm 0.001215
Apple, QF3	0.52 \pm 0.04	0.0045 \pm 0.0015	0.000027 \pm 0.000002
Pear, QF3	0.15 \pm 0.02	0.0023 \pm 0.0012	0.000008 \pm 0.000001
Lettuce, QF4	1.76 \pm 0.08	0.0079 \pm 0.0027	0.00001 \pm 0.000004
Apple, QF4	5.95 \pm 0.16	0.0425 \pm 0.0037	0.000326 \pm 0.000009
Lettuce, QF5	4.74 \pm 0.24	0.02 \pm 0.01	0.000239 \pm 0.000013
Tomato, QF5	0.35 \pm 0.02	0.0046 \pm 0.0017	0.00002 \pm 0.000002
Apple, QF5	0.13 \pm 0.02	0.0004 \pm 0.0002	0.000004 \pm 0.0000004

Table 2.3 measurements are consistent with Table 2.1 in that the two controls have different values with the mountains (QF1) having higher concentration than the valley (QF5), and Quarta-Feira (QF2) being the highest out of the sites in both tables. Table 2.3 shows that the vegetables that were affected most by the contamination were lettuce, carrot, and watercress. The highest levels of contamination were found to be from ^{226}Ra and ^{210}Pb . The produce that accumulated radium and lead the most were the leafy vegetables, which shows that the contamination was caused by exposure to the contaminated water more than the contaminated soils. It has also been shown the contamination can accumulate in livestock tissues as another avenue for contamination to enter the human body (19).

Impacts to human health and the environment

The EPA has set a limit for the level of uranium that can be present before it is considered to be detrimental to human health at $30\mu\text{g/L}$ in water (4). Being that the water contamination near uranium mining sites has been measured to be as high as $1035\mu\text{g/L}$, there could be significant health problem associated with consuming that level of uranium (17).

The human health impact of uranium contamination is related to the potential for internal exposure. This internal exposure can occur through inhalation, ingestion, or absorption (23). Inhalation could be caused by uranium interacting with the atmosphere and releasing particulates into the air (22). Ingestion could be caused by the consumption of contaminated water, plants, or meat from contaminated livestock (19). Absorption can be caused by exposing cuts or openings in/on the body to the contaminated soil or water. Once the radionuclides are inside the body, the ionizing radiation exposure from the alpha, gamma, and beta particles becomes damaging (23). Alpha particles are typically not concerning in normal external cases of radiation exposure because they are easily shielded; however, if they are inside the human body, they deliver the greatest dose of radiation due to their high radiation weighting factor for biological damage and relatively high particle energy. Alpha emitting radionuclides are known as carcinogens because they produce a large number of double-strand DNA breaks which is difficult for the human body to recover from (23). This DNA damage has specifically been seen as a problem in the people living near the previously mentioned mines in Portugal. In those subjects, it was seen that the DNA integrity and content in white blood cells decreased. Individuals that were less than 40 years old exhibited a decrease in NK and T lymphocytes which indicates damage to the hematopoietic organs that produce immune cells (17).

Beta particles and gamma rays have high penetrating power, so they are also external radiation hazards; however, they cause less damage (23). These particles can still deposit high doses when they are present in large concentrations such as individuals inside mines and close to mill tailings. This dose will lead to the ionizing of atoms that can lead to the death of the cells into which they are contained (23). If the cell does survive the radiation, the DNA of that cell could have been damaged, and those cells could initiate cancer. In addition to the radiation from the consumption of radionuclides, the consumption of heavy metals can cause damage to the liver and kidneys (23). Therefore, contamination is potentially a significant problem to humans in the areas surrounding uranium facilities. When contamination is present, it is important to know the dose rate, time of exposure, and the area of exposure to determine the potential level of damage that could occur.

In addition to the impact on human health, radiation can also damage the environment. One major impact on the environment is the decrease in pH in the water to a range of 4.2-6.2 (17). This change in pH can negatively affect the crops that are being irrigated with the acidic water and it will affect the aquatic life in the streams (22,23). The radiation has also negatively impacted the wildlife in locations with uranium mines, include all levels of the food chain. These effects are cause by the animals lower in the food chain consuming contaminated water and plant life and then being eaten by predators higher up in the food chain (22). Once the radioactive material is consumed it affect those living organisms in the same ways as humans.

Radiation being emitted from the uranium can cause significant damage to the humans and the environment, so remediation of nuclear sites is needed to reduce the contamination in the surrounding areas.

Remediation of contaminated sites

The main goals for the remediation of nuclear sites are to: 1) sequester the radioactive waste, 2) protect the surrounding areas and waters from contamination, 3) neutralize the radiological and chemical waste, 4) minimize the physical risk caused by mines, tunnels and other structures, and 5) develop new uses for the land (17,21,26). In order to achieve these goals, the first step of any remediation project is to collect all of the waste from the contaminated area. Once all of the waste has been collected, it must be stored in a location that does not allow any more contamination to occur. In the case of the Urgeirica mine in Portugal, the waste was gathered and deposited in a location that was sealed with clay, screen, geotextiles, gravel, and humus (17). In addition to this treatment of the solid waste, the surface waters were diverged away from the waste storage. This treatment achieved the goals of reducing the radiation dose and limiting the spread of contamination (17). Other locations have used chemical stabilizers and wet scrubbers on the waste before the burial process (21). To reduce the physical risk on the old mine site, open pit mines have been used as waste storage after they were sealed and then filled in (17,21). The underground mines have been grouted to seal ore seams to reduce water contact, improve structure stability, and prevent erosion to reduce the risk of collapse (17,21). To solve the problem of reduction of the contamination of the water, there have been systems put in place to collect the drainage and seepage waters and treat them (17,21). In addition to simply trying to prevent contamination and reduce current contamination levels, locations are also attempting to use natural materials to perform the correction such as using limestone as a pH buffer and clay as a sealant (17,21). These measures have worked so well in previous sites that it is common to build houses or commercial facilities on old mining and milling sites (24).

Once the remediation measures are all in place, the project is not over; there must be long term monitoring of the site. There are monitoring systems that assess water quality, soil contamination, and radiation dose on the remediated sites (17,21,27,28). In order to measure different layers within the sealed waste storage sites, there are probes that are placed at six points in the pile that measure radon concentration and radioactivity (17). For sites that are near houses, there were dosimeters and dust monitors put in place to monitor any potential waste movement (17,27,28).

Conclusions

The environmental contamination of mine sites started in the 1930s with mining of uranium for radium. This contamination was caused by the uranium milling tails being left unprotected from the elements, uranium mines being exposed to the elements, and waste from chemical leaching being in contact with surface waters. The contamination left behind high levels of radionuclides in the soil and water on and around nuclear sites. This contamination is measured in multiple ways, including in-situ ionization chambers and gamma and alpha spectroscopy in a laboratory setting. These methods are used to classify what the dose is at specific location and what isotopes are present. Using these technique, it has been found that there is a significant problem with contamination around mining and milling sites with excess radionuclide concentration in the soil on the site, soil surrounding the site, surface water of the site, ground water on the site, and water from nearby wells and streams. This contamination has a negative impact on the health of the people living in the surrounding areas because these types of contamination lead to internal radiation exposure. This is also the case for animals in the area, so it negatively affects the ecosystem. To lower the contamination and prevent future contamination, the nuclear sites need to be properly decommissioned using the correct remediation measures for each location. Once

that remediation is complete, there should be a set of detectors to monitor potential contamination levels.

2.3 Current Methods of Uranium Detection in Water.

Uranium can be detected in several ways, but the most common method is measuring the high-energy radioactive decay products. This is usually performed by either gross alpha detection or alpha spectroscopy. Unfortunately, at low concentration levels, uranium radioactivity signals are weak and attenuated and, therefore, difficult to measure outside of a laboratory. Uranium is a known alpha particle emitter, so the current initial detection method is a gross alpha test.

The gross alpha test is used if there is a significant amount of alpha emitting radionuclides present in the water. Gross alpha tests require a natural water sample of 1 liter that must be preserved with HCl to maintain a pH of 2 when it is collected. This method begins with the addition of HCl, and then the sample is boiled to eliminate the carbonate and bicarbonate ions that are naturally present and keep the uranium in solution. The boiling of the acidic solutions precipitates the uranium along with ferric hydroxide. Then the uranium is separated using HCl to dissolve the other precipitates through an anion exchange column. This process will produce uranium in its nitrate form. Then the samples will be dried and the alpha particles activity will be counted with an alpha scintillator detector (29). This method can be contaminated with protactinium-231 that can also make it through the chemical processes, but this is a rare case being that protactinium-231 is a decay product of uranium-235, which has a very low natural abundance (30). The problem with this test is that it cannot determine the origin of the alpha particle, so it cannot provide any definitive information about the uranium concentration because there are other alpha particle emitters commonly found in water such as radium. Additionally, once the results are interpreted

from the gross alpha test to show elevated levels of alpha radiation, another testing method must be used to determine the origin of the radiation and the concentration of the radionuclide (31).

If the results of the gross alpha test are positive for elevated level of radiation, a second test must be performed. The tests that can be used to determine is the elevation alpha radiation is coming from uranium are alpha-spectrometry, inductively coupled plasma mass spectrometry, and fluorimetry.

Alpha-spectrometry is a method of radiation detection that can determine the source of the alpha particles based on the energy of the incident particle(s). The alpha spectra of uranium has three specific peaks, and each peak is made by the different isotopes: U-238, U-235, and U-234. The procedure for alpha-spectrometry begins with the purification of the uranium sample. To purify, uranium must be precipitated with aluminum phosphate from the aqueous solution under weakly acidic conditions. The precipitate is then dissolved using acid to be further extracted into ethyl acetate using magnesium nitrate as the salting agent. The extracted layer is then evaporated to dryness, and the residue is taken up with HCL and placed on an anion exchange column to remove any remaining contaminants such as thorium. After the anion exchange, the uranium is eluted with HCL and evaporated near dryness and taken up with low pH (2.6-3.0) NH_4Cl to prepare for electroplating. The acidic solution will ensure a uniform electrodeposition of U_3O_8 onto the cathode. The cathode used for the best resolution is a small diameter titanium plate. Once the sample is prepared, it will be placed in the alpha spectrometer's vacuum chamber and counts will be detected for 1000 minutes (32,33). Alpha spectroscopy is an effective detection method for determining the concentration of uranium in water but only within a laboratory setting. Alpha spectroscopy is not feasible as a field detector because the extensive sample preparation needed before the uranium concentration can be determined. This preparation must be performed in a

laboratory. Additionally, the equipment needed has multiple large components like a computer and vacuum chamber that will need large power supplies to operate properly. The 1000 minutes for producing a reading is unacceptable for rapid detection of uranium concentration.

Inductively coupled mass spectrometry is a very sensitive method of elemental analysis that produces the best resolution on the order of ng/L. While this resolution is very high, this is not the normal operating condition of the mass spectrometer because the low level settings cause high levels of interference (16,34). The volume of the water samples for ICP is 10mL. The collected water samples must be preserved using HCl as in alpha spectrometry. However, there is no extensive purification process with ICP. The procedure for using the mass spectrometer begins with igniting the plasma and allowing the instrument to equilibrate for 30 minutes. Then the forward voltage, plasma flow, auxiliary flow, and nebulizer flow must be set and the lenses must be focused. Next, the sample needs to be monitored for 2s and repeated 5 times for each measurement (22). This method is limited by the equipment needed to perform a measurement. The equipment would be very difficult to downsize enough to allow the transportation to a natural water source. In addition to the size and amount of equipment, the power needed for this process would increase this difficulty. While the time of the actual reading is short, the set up and warm up of the equipment is too slow for rapid detection.

Fluorimetry is a technique of uranium detection that employs as UV excitation source to induce fluorescent emission from the molecule. Commonly, the UV excitation sources used are lasers or UV lamps. Laser induced fluorimetry of uranium uses a nitrogen laser that emits very intense light for a very short amount of time (7ns). The nitrogen laser emits light with a wavelength of 337.1nm (12). The fluorescence detected using this method has a linear relationship to the uranium concentration in the water. Even with the high output from the laser, a chemical

fluorescent enhancer is needed to achieve a detection limit of 0.2ppb. This limit was achieved by Bhangare et al. testing filtered natural water samples and using time gated detection to eliminate any remaining contaminants (12). UV Lamps are commonly used for higher concentration sample that will fluorescence without the high excitation energy provided by a laser. This method can be modified to create a field instrument, but high power consuming components have to be eliminated, including the computer and the laser. The fluorescent enhancement will need to be simplified to allow it to be easily used in the field. The detection limit will also need to be addressed to match or exceed the detection limits of the other methods.

This section shows that the current methods used to detect uranium in water are sufficiently sensitive, but could not be used as field testing instruments as they currently operate. Each of the previously mentioned method have many steps, including chemical processing, and equipment set up that prevents these methods from being used for rapid field detection.

2.3 Uranium Fluorescence

The green fluorescence of uranium was known to be used as a decorative feature in glass dating back to 79AD (35). Not until 1833 was this distinctive fluorescence associated with the uranyl ion (36–38). Multiple spectral emission bands make up the unique characteristics of the uranyl fluorescence. The uranyl optical emission signature can have as many as six peaks at wavelengths ranging from 345-600nm, depending on factors such as pH, temperature, and associated compounds (39,40). Each of these peaks is due to the vibrational modes of the two smaller oxygen atoms vibrating around the much larger uranium atom; this causes vibrational levels in the ground state of the uranyl ion (1,2,41,42). These vibrational modes are caused by the symmetric stretching of the linear $(\text{O}=\text{U}=\text{O})^{2+}$ (43,44). The stretching leads to a vibronic emission that is characterize by the fundamental transition energy, which is the emission line with the highest energy and the

change in energy between each emission line(43). The spectrum has been shown to have two excited states and a minimum of five vibrational ground states as depicted in Figure 2.3 (42,45).

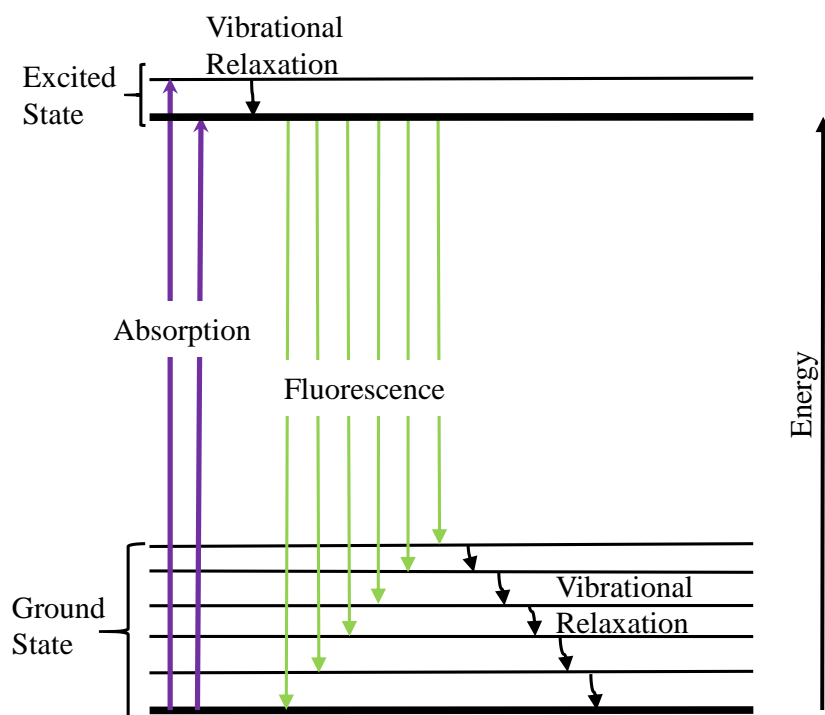


Figure 2.3: Jablonski Diagram for Uranyl in aqueous solutions(42)

The pH of the solution affects the hydrolysis of the uranyl ion, which changes the fluorescent output because there are different species that are created at different pH levels. At some of these pH levels, there is no fluorescence, but at other pH levels, the species do fluoresce (2,46). In the pH range from 1-3, the uranyl does not hydrolyze, so the stand alone UO_2 produces a weak fluorescence. The uranyl begins to hydrolyze at a pH of 3, and this is when the fluorescence will increase dramatically, moving into the neutral pH range, then decreasing at the higher pH ranges (2,46). The decrease in the higher pH ranges is caused by the binding of uranyl with a carbonate, which creates a non-fluorescent compound. The optimal pH range has been found to be 5 to 5.5(2,46). This optimal range is when the uranyl is bound to a hydroxide, which is a fluorescent compound. The studies on pH have also shown that the spectral peaks will shift slightly; low pH

causes a blue shift, and higher pH causes a red shift (2). There are many different compounds of uranyl that can be found in nature that exhibit fluorescence when excited with ultraviolet light such as uranyl acetate, uranyl nitrate, uranyl oxalate, uranyl phosphate, uranyl sulfate, and zinc uranyl acetate. Since the vibrational bands of the uranyl spectra is caused by the structure of the UO_2 , the emission for all of the compounds listed are essentially the same. There are small differences in the wavelength between the compounds, but the significant differences are the intensities at each band wavelength (39). Other compounds of uranyl exist, such as uranyl calcite, and other carbonate species, that will not fluoresce at room temperatures, but they will exhibit the normal fluorescent behavior at very low temperatures (39,47). Other uranium compounds will not fluoresce at all, such as uranyl formate and U_3O_8 (46).

Even though not all compounds can be detected, fluorescence emitted from the uranyl ion has long been used as a method for determining the presence and concentration of uranyl in water (48–50). However, water molecules quench the optical emission making detection at trace concentration levels challenging (36). Multiple methods have been used to enhance the fluorescence of uranyl in water. These methods are main focus on the manipulation of the pH and temperature of the solution in order to control the hydrolysis of the uranyl ion. One method uses phosphoric acid or sulfuric acid to decrease the pH, which in turn increases the creation of uranyl hydroxide (51). Another method uses cryogenic cooling to allow compounds that are not fluorescent at room temperature to fluoresce (14,39,49,50). The most promising method of uranyl enhancement, and the method chosen in this paper, is using silica gel.

2.4 Silica Gel Synthesis and Characterization

Silica gel is typically created using the sol-gel process, which is a process known for creating optically transparent glasses (52,53). The sol-gel process is consecutive hydrolysis and

polycondensation of alkoxy silicon materials in aqueous solution with additional cosolvents (52,54–56). The sol is a colloidal suspension of a solid in a liquid that is converted into a gel by polycondensation. The sol creates a porous matrix in the liquid and then the solvents are removed (53,54). Common silicon precursors that are used to create porous silica are Tetramethylorthosilicate, Tetramethoxysilane (TMOS), Tetraethoxysilane (TEOS), Methyltriethoxysilane (MTES), and polyethoxydisiloxane (PEDS) (52–57). Each precursor creates a different final structure that can be hydrophobic or hydrophilic (54,55). Once a precursor is selected, the next step is to prepare the sol by dissolving the precursor in a water or alcohol based solution that will create the gel (52,54). The pH, as well as other experimental parameters, can be controlled to produce different final structures such as various pore structures or spheres (53,54,56). In addition to controlling the structure with the solvents and precursors, it is common to use additives to produce specific pore structures, mechanical properties, or functional groups (55). The common materials that are used to modify pore size and mechanical properties are glycerol, 1-butyl-3-methyl-imidazolium-tetrafluoroborate, and polyethyleneglycol (PEG) (54,57). PEG is a porogen that is used to create through-pores and is a solubilizer of the silane that is present in most precursors (54). In order to control the permeability of the silica gel, the solution is aged. The ageing process can include washing with water and ethanol, ageing in siloxane solution, ageing in TEOS solution, or aging in ethanol solution. These aging methods also have been reported to strengthen the silica gel matrix (54). The aging process causes more siloxane groups to form, and various strengthening materials are used to promote more siloxane groups to form (52). The last step is to dry the gel to produce the final product. The drying process is governed by capillary pressure. The capillary pressure in the pores causes the volume of the gel to shrink and potentially crack (53,54,56). The drying procedure is typically performed

by either evaporation, using hypercritical conditions for the solvents, or the addition of chemicals to produce a reaction that will dry but not damage the silica left behind (52–54,56).

Once silica gel is synthesized through the sol-gel process, the next step is to characterize the final product. Silica gel is typically classified by pore size, specific surface area, and particle size. The common method for evaluation the pore size and specific surface area is gas adsorption, which can be performed with oxygen, argon, carbon monoxide, carbon dioxide, sulfur dioxide, butane, and most commonly nitrogen (58–60). In order to measure the surface area using gas adsorption, the Brunauer-Emmett-Teller (BET) method was developed and has since become the standard (57–59). The BET method is typically applied using the linear for of the BET equation (59).

$$\frac{p}{n^a (p^o - p)} = \frac{1}{n^a C} + \frac{(C - 1)p}{n_m^a C p^o}$$

Where p^o is the saturation pressure of the absorptive at the temperature the measurement is performed, p is the saturation pressure at the critical temperature of the absorptive, n^a is the amount adsorbed at the relative pressure of $\frac{p}{p^o}$, and n_m^a is the single-layer capacity (59). C is related to the enthalpy of adsorption but is not a quantitative measure of enthalpy, so it is accepted that it is an indication of the magnitude of the adsorbent-adsorbate interaction energy (59). Once the BET equation is used to solve for n_m^a , the surface area and specific surface areas can be calculated.

$$A_s = n_m^a N_A a_m$$

Where A_s is the surface area and specific surface area is A_s divided by the mass of the adsorbent, N_A is Avogadro's number and a_m is the molecular cross sectional area (59).

For the pore size measurement there are multiple methods that have been used. The commonality between these methods is that they are based on the Kelvin equation (58). The Kelvin equation relates pore size to capillary evaporation and condensation (58,60).

$$\frac{1}{r_1} + \frac{1}{r_2} = -\frac{RT}{\sigma v} \ln\left(\frac{p}{p^o}\right)$$

Where r_1 and r_2 are principal radii of the liquid meniscus in the pore, σ is the surface tension of the liquid condensate, and v is the molar volume of the condensate (59). Then with the assumptions of the cylindrical pore and the curvature of the meniscus is related to the pore size the equation becomes

$$r_k = \frac{2\sigma v}{RT \ln\left(\frac{p}{p^o}\right)}$$

Where r_k is the kelvin radius (58,59). To account for the thickness of the adsorbed layer, the pore size is calculated with

$$d_p = r_k + 2t$$

Where t is the thickness of the adsorber layer which is typically found by performing the gas adsorption of a non-porous sample of the same adsorbent (58,59,61).

The Barrett-Joyner-Halenda (BJH) method for pore size distribution calculation still used the kelvin equation with an added a correction from the adsorbed film thickness, which allows for a more accurate calculation of pore size assuming a cylindrical pore (58). In addition to assuming the pore shape, it is assumed the there are no micropores present, and the pore size distribution does not extend into the macro pore range(59). The pore sizes are typically broken down in the three size ranges; micropores($d < 2\text{nm}$), mesopores ($2\text{nm} < d < 50\text{nm}$), and macropores ($d > 50\text{nm}$)(58,59).

2.5 Silica Gel Fluorescent Enhancement of Uranyl

Silica gel is hydrophilic and has been used for applications such as chromatography, removal of ions in solution, and desiccant refrigeration (62,63). Studies of silica in the presence of metal ions have shown that silica has a high adsorption capacity and selectivity, especially when used with uranyl (62). The selectivity towards uranyl ions is caused by the negatively charged sites on the silica surface, to which the uranyl ions attach in conjunction with uranyl's high affinity for oxygen (48). Two important parameters need to be considered when using silica to enhance uranyl fluorescence: the equilibrium capacity and the kinetics of the adsorption process (62). The equilibrium capacity refers to the total number of silica surface sites available to adsorb a uranyl ion, while the kinetics of adsorption is the time required to fill those sites. Study of equilibrium capacity has focused on maximizing the capacity for removing ions from aqueous solutions (46,64–66). The maximization of the equilibrium capacity was achieved by adding functional groups such as amidoxime, carboxyl, dihydroimidazole, and hydroxyquinoline to the surface of the silica gel particles (64–68). The kinetics have been studied for various solutions and with different methods such as in a static or stirred fluid (62). The tests show that in a static or stirred fluid, the time required for uranyl to reach equilibrium capacity can be on the order of hours (62), which is too slow for most measurement applications.

Complexation with silica is the most compelling method for enhancing the fluorescence of uranyl because it is most promising for rapid detection in water outside of a laboratory setting. Silica has been used to enhance many fluorescent compounds such as $\text{La}_4\text{Ti}_9\text{O}_{24}$ and Eu^{3+} (48,69). The silica enhancement method has been used with colloidal silica, and in this project, porous silica gel was used. Silica gel is a three-dimensional network of colloidal silica that is created by the formation of siloxane bonds (48). This three-dimensional network allows the silica to easily

trap the uranyl and increase the local uranyl concentration inside the sample to an easily detectable level. When the uranyl is trapped in the silica gel, it binds to the negatively charged sites on the silica surface. When the uranyl is bound to the silica gel, its fluorescent lifetime will change significantly; it changes from a simple decay to a biexponential decay. This biexponential decay shows two separate lifetimes, a major lifetime of 240 μ s and a minor of 55 μ s (48). This lifetime is significant increase from uranyl in acidic solution (48). The decay lifetime can be used to eliminate fluorescent contaminants that could be found in natural water sources. In addition to extending the life time, the silica also increases the emission intensity. The increase in life time is caused by the uranyl binding to the silica gel, which eliminates the optical quenching from the surrounding water (2,48). Silica gel enhancement can also be affected by pH, both in the same way as previously mentioned, as well an additional way. The additional way the silica gel enhancement is affect is at elevated pH levels, where the fluorescence will drop-off because the silica gel decomposes (2). The silica gel method of fluorescent enhancement is ideal for a field instrument because of the large increase in intensity and extended lifetime and the sample preparation can be performed before collecting the water samples.

Chapter 3: Flow Enhanced Kinetics of Uranyl (UO₂) transport nano-porous silica gel

Previous work has been performed on using silica gel to extract water from soil in order to detect the uranium levels in the soil. This work focuses on the silica gel's ability to enhance the fluorescence of uranium to a level that would be easily detectable.

3.1 Introduction

Uranyl transport into nanoporous silica gel is limited in a static aqueous solution by slow natural diffusion to the open bonding sites. In order to make this process faster, the diffusion dependence was eliminated using pressure driven fluid flow. Uranyl transport and adsorption within nanoporous silica gel was measured using time-dependent fluorescent measurements in an aqueous solution. The transport kinetics were measured under two different conditions: static solution in a standard cuvette and flowing solution through the silica gel.

3.2 Spectra testing with Silica gel and Fluorescent Enhancement

Sample Preparation

Silica gel was purchased from Sigma-Aldrich and Acros Organics with nominal pore sizes ranging from 2.2 nm to 10 nm and particle sizes from 40 μm to 650 μm as reported by the manufacturer. The specific properties of each silica gel used in this study (referred to here as SG-1 through SG-5) are shown in Table 3.1.

Table 3.1: Physical properties of silica gel

Item No.	Company	Pore Size (nm)	Particle size (μm)	Surface Area (m^2/g)
SG-1	Sigma-Aldrich	2.2	75-650	800
SG-2	Sigma-Aldrich	3.0	75-150	480
SG-3	Acros Organics	4.0	40-60	750
SG-4	Acros Organics	6.0	40-60	550
SG-5	Sigma-Aldrich	10.0	63-200	300

The silica gel particles were packed together in custom-made 1-inch square bags made of a monofilament nylon mesh with an opening size of 28 μm purchased from McMaster-Carr. The bags were made by melting the edges together with a small flame. Using a Fisher-Scientific accurate 124 balance, 250 mg of silica was measured and transferred into the nylon bags, which were then sealed. A filled nylon bag and a 20x optical microscope image of the mesh pores are shown in Figure 3.1a and 3.1b. Figure 3.1 also includes an optical image of SG-3 and Scanning electron microscope (SEM) images of SG-1, SG-3, and SG-5.

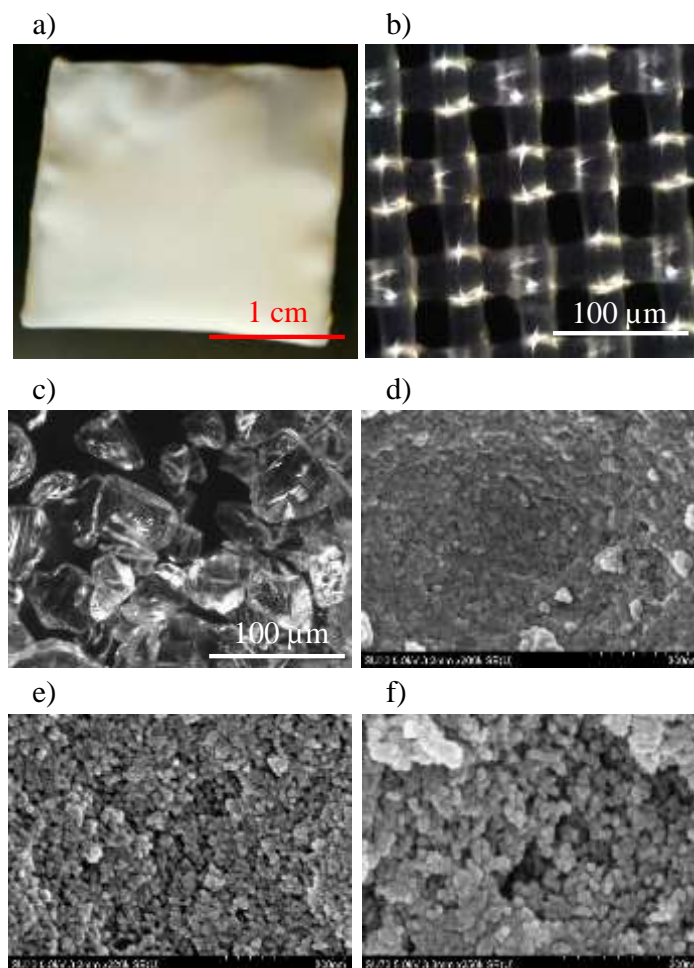


Figure 3.1: a) Silica-filled nylon bag; b) 20x optical image of the nylon mesh; c) optical image of SG-3; d) SEM image of SG-1; e) SEM image of SG-3; and f) SEM image of SG-5.

It can be seen that silica gel consists of an assembly of bonded silica nanoparticles, and there are open pores between the nanoparticles, similar to a granular bed. A 0.01 M aqueous uranyl solution was used in all of the experiments discussed in this portion of the paper and was prepared from a uranyl nitrate salt and 10 MΩ-cm pure deionized water.

Full Spectra Measurements

The fluorescence emission of the uranyl was performed using a QuantMaster-3 Spectrofluorometer with a Xenon Flash lamp excitation source and a photomultiplier tube detector. The parameters used to obtain the steady state emission scan are shown in Table 3.2.

Table 3.2: Parameters for static fluid scans

Parameter	Value	Unit
Excitation	310	nm
Emission	400-600	nm
Step Size	0.5	nm
Delay 1	108	μ s
Int. Time	0.3	μ s
Averages	5	
Shots	10	
Frequency	200	Hz

The nylon bags containing the silica gel were folded and placed into a quartz UV transparent cuvette, and 3 ml of the 0.01 M uranyl solution was added to submerge the sample. The cuvette was placed in the sample holder inside the chamber of the spectrometer with the slits set to the values shown in Table 3.3, and emission spectra were obtained for each sample in Table 3.1.

Table 3.3: Spectrometer slit settings

Slit Name	Actual value (mm)	Bandpass
excitation entrance	3	12
excitation exit	1.25	5
emission entrance	1.25	5
emission exit	1.5	6

Steady-State Emission Spectra

The emission spectra for each silica gel in Table 3.1 are shown in Figure 3.2.

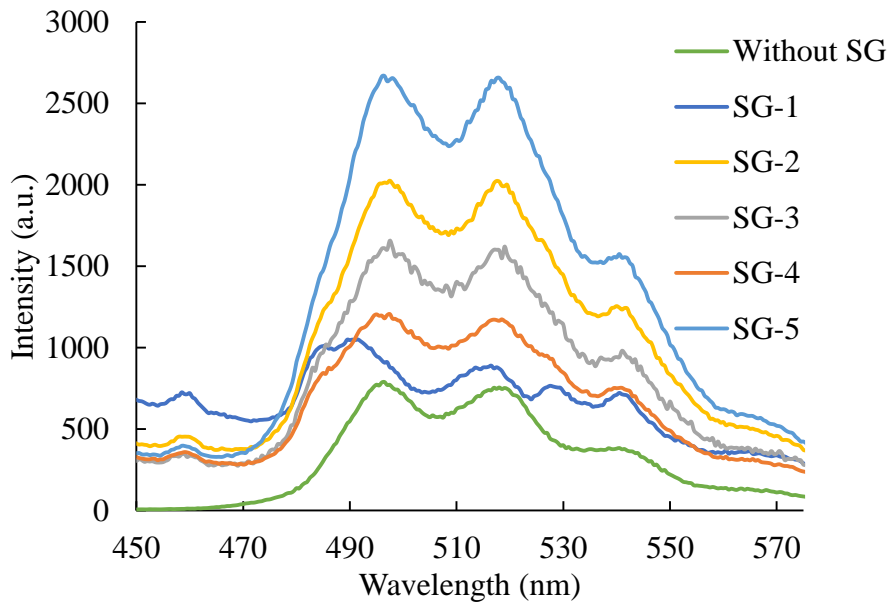


Figure 3.2: Fluorescent spectrum of uranyl for silica gels and without silica gel present.

These spectra were used to determine the peak emission wavelength for the time based scans. Silica gels SG-2 through SG-5 showed three main peaks with the most intense peak at 496 nm. Silica gel SG-1 showed four peaks with the most intense at 491 nm; this resulted in a change of the peak emission wavelength used in the time based scans for this sample. The cause of this small blue shift in the emission spectra for the silica gel with the smallest pore size will be discussed at a later date. Figure 3.2 also shows the large enhancement caused by the addition of the silica gel. When comparing the solution without silica gel to the SG-5 sample, the fluorescent intensity produced is improved by greater than 300%.

3.3 Static Fluid Time Constant

Table 3.4 shows the spectrometer settings used to measure the kinetics of uranyl transport into the silica gel samples under static fluid conditions.

Table 3.4: Parameters for static fluid scans.

Parameter	Value	Unit
Excitation	310	nm
Emission	496	nm
Duration	3600	s
Delay	108	μ s
Int. Time	0.3	μ s
Shots	10	
Frequency	2	Hz

Each silica bag sample was placed into a quartz cuvette containing the 3 ml of the 0.01 M solution. The peak emission wavelength was measured at a frequency of 2 Hz until the intensity reached steady state. A normalized example of this scan is shown below.

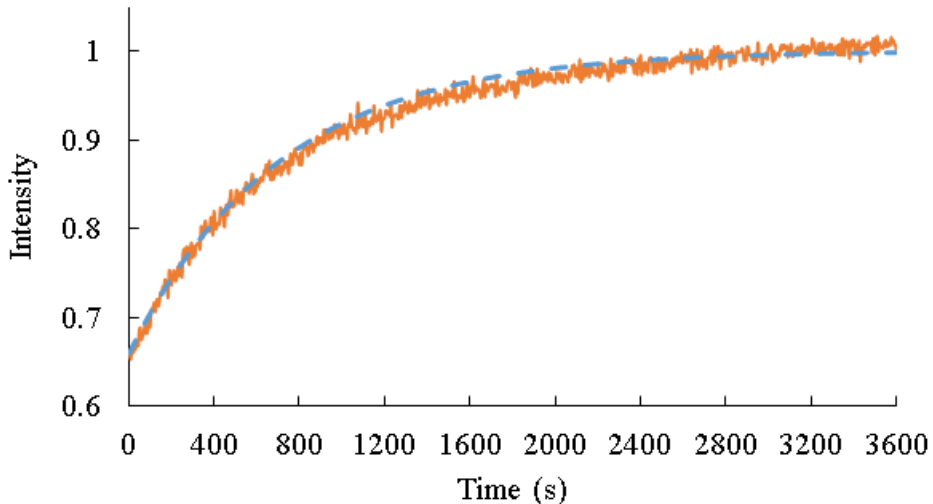


Figure 3.3: Normalized florescent intensity vs. time obtained for SG-4 in a quiescent solution. The scan above shows the raw data collected, displayed with the solid line, and the curve fit, displayed with the dashed line. The fluorescence emission intensity increased with time in a manner that can be modeled using a single exponential as shown in Equation 1

$$I(t) = I_f + (I_o - I_f)e^{\frac{-t}{\tau}} \quad (1)$$

where I_f is the final intensity, I_o is the initial intensity, and τ is the time constant. The data of Figure 3.3 shows a large (approximately 50%) enhancement in the uranyl fluorescence intensity caused by the transport and adsorption within the nanoporous silica gel; however, Figure 3.3 also shows that it takes a relatively long period of time for this signal enhancement to occur (about 40 minutes to reach steady state). This is the time it takes for the silica to initially wick the water into the pore and for the concentration gradient driven diffusion to reach a steady state. This long time constant is unacceptable for applications requiring rapid detection.

Figure 3.4 is a plot of the time constant versus the pore size in the static fluid. This figure shows that as the pore size increases, the time constant for transport and adsorption from a static fluid decreases.

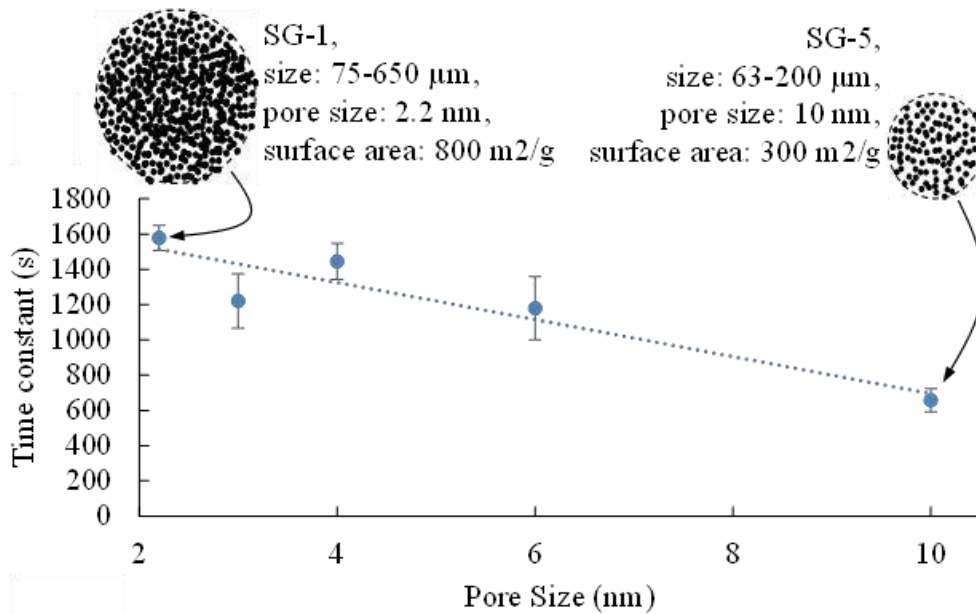


Figure 3.4: Time constant in static fluid versus silica gel pore size.

A least square linear fit is obtained for the data in Figure 3.4 and is given in Equation 2. Here τ is the time constant and d_p is the nominal pore size of the silica gels. The coefficient of determination R^2 was found to be 0.86.

$$\tau = -105d_p + 1745 \quad (2)$$

The trend observed in this figure can be justified noting that the silica gels with greater nominal pore size (SG-5) have the lowest specific surface area, perhaps leading to the highest permeability to water. Greater permeability allows the water to penetrate more easily, which carries the uranyl in at a faster rate. The faster penetration causes the uranyl to reach and fill the available bonding sites faster, reducing the time constant.

3.4 Flow Enhanced Time Constant

The flow system shown schematically in Figure 3.5a was used to measure the kinetics of uranyl transport into the silica gel samples under flow conditions.

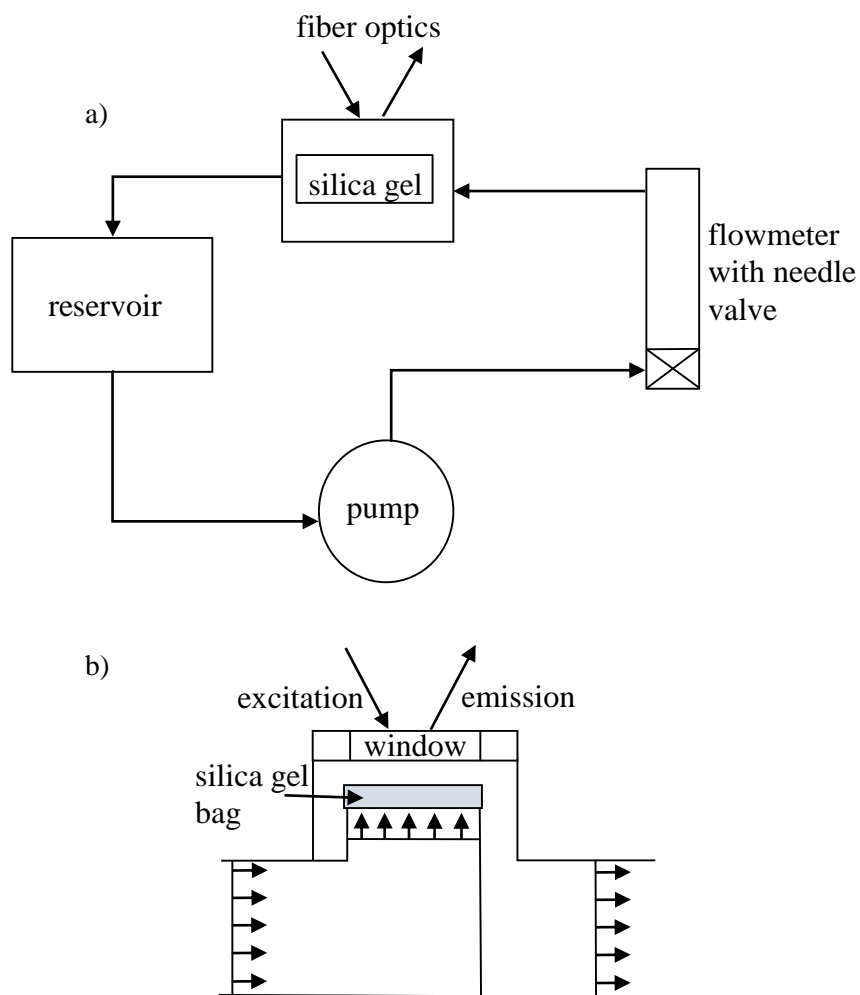


Figure 3.5: a) Schematic of flow system; and b) internal geometry of the silica strainer.

Fiber optic cables were used to connect the flow system to the spectrofluorometer, and the slits were opened to the values shown in Table 3.5 to compensate for the signal attenuation caused by the fiber optic connections.

Table 3.5: Spectrometer slit settings for flow enhanced scans.

Slit Name	Actual value (mm)	Bandpass
excitation entrance	7	28
excitation exit	7	28
emission entrance	5.5	22
emission exit	3.25	13

The flow system used ½” ID R-3603 Tygon tubing, a Danner model 7 utility pump, and a king flow meter with a scale from 0 to 3 gph. The fiber optics were aligned perpendicular to the sample as the 0.01 M solution flowed through the silica gel. The silica was held in place by a custom-designed insert that is placed inside of a commercially available in-line strainer and sealed with teflon tape. The insert holds also replaced the normal cap on the strainer and houses a quartz window to allow the excitation and detection to take place. The first design of the strainer insert is shown in Figure 3.6.

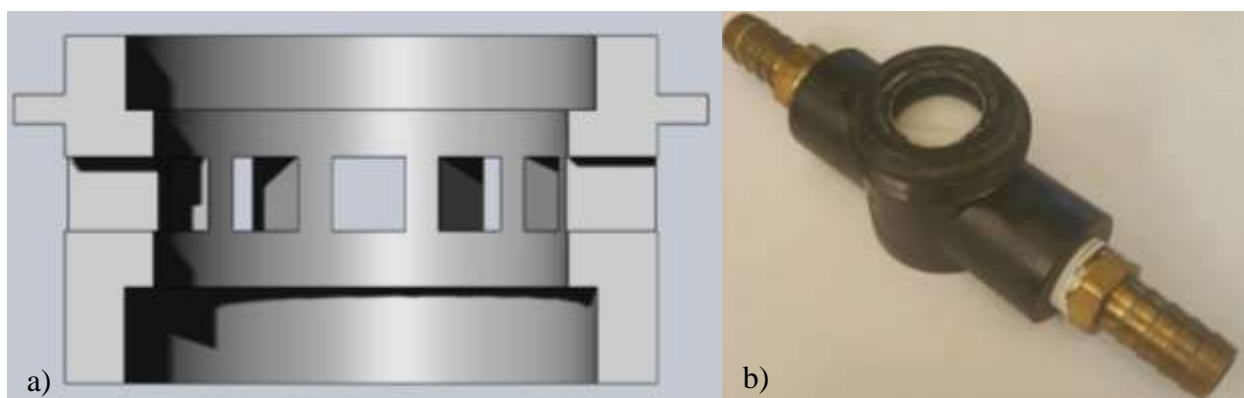


Figure 3.6: a) Section view of the first strainer insert, b) Picture the assembled strainer with insert.

The first design worked well in terms of allowing light to pass through and holding the silica bag in place. The down fall of this design came in allowing the water to flow through the side holes and down to the exit. The sides of the lower portion were so close to the edges of the inside of the strainer that it increased the pressure drop across the device and also caused leaks. The second version of the strainer had an additional slot that went down the sides of the main tube to provide large flow channels down to the exit of the strainer. The second design can be seen below.



Figure 3.7: Section view of the second version of the strainer insert.

The second version of the insert allowed the water to flow more easily through the strainer. The seal of the insert still needed to be improved, and it was noticed that the bottom of the insert was contacting the inlet tube of the strainer. This contact made the insert tilt to one side, which left a small gap in the seal. The final version of the insert focused on improving the seal. This was achieved by making the insert shorter to prevent tilting. Additionally, the ledge where the quartz window rest was enlarged to allow for a larger seal; this also increased the ledge that held the silica gel bag in place.

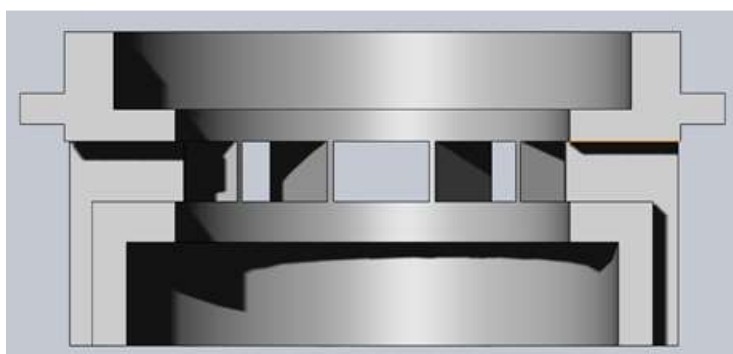


Figure 3.8: Section view of the final version of the strainer insert.

The flow-enhanced scans were performed with the same solution concentration as the static scans, but the duration, integration time, and frequency of the emission intensity measurements were changed to 150 s, 0.3 s, and 200 Hz respectively because of the much faster adsorption

kinetics. The reservoir was filled with 700 mL of solution. The solution was pumped through the silica sample, and the fluorescence intensity was measured as a function of time. The scan began when the pump was turned on, but the zero point for the time constant determination occurred when the leading edge of the water solution first touched the bag. Therefore, this method measured the kinetics of uranyl transport into a dry silica gel to a fully saturated state from the time the solution began to flow through the bag containing the silica gel.

3.5 Results and Discussion

Time Constant Results

Figure 3.9a is a normalized plot of the peak emission wavelength intensity as a function of time for silica gel SG-4 in the static uranyl solution.

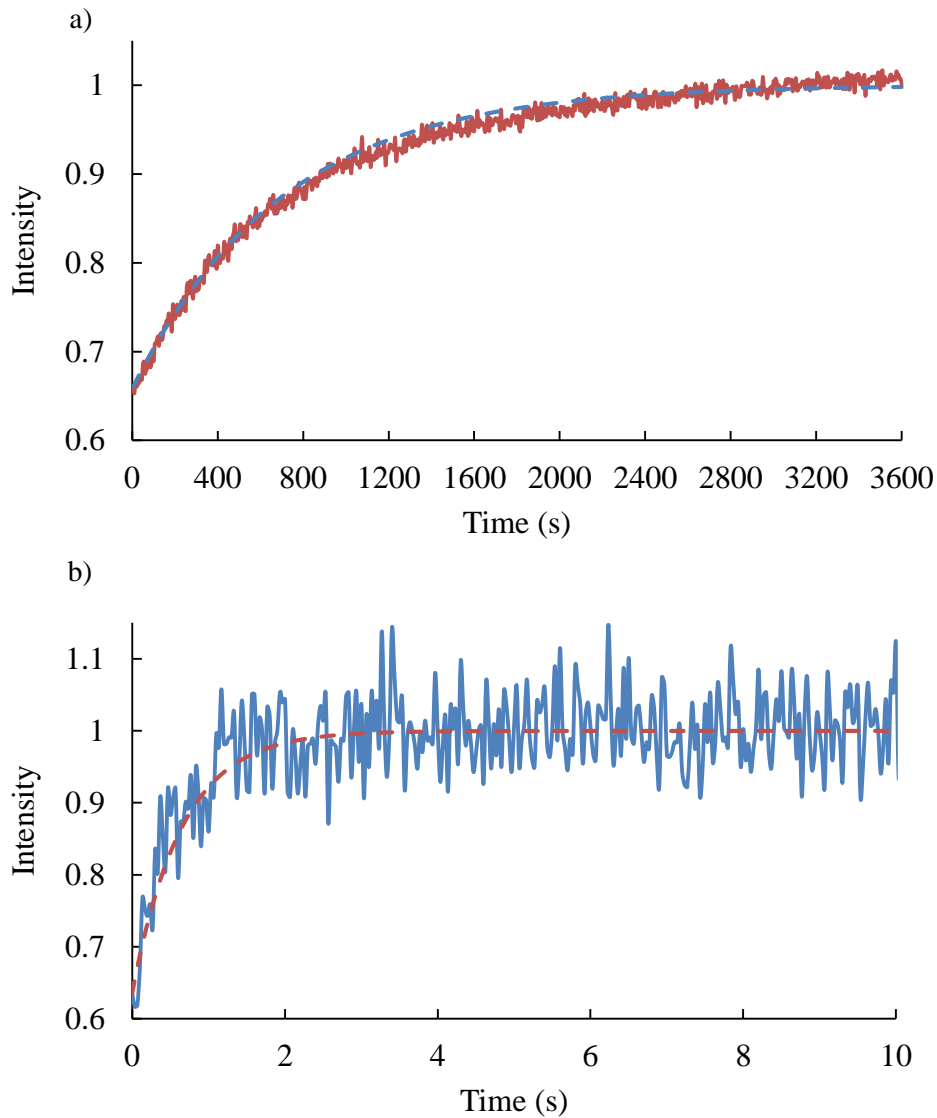


Figure 3.9: a) Normalized florescent intensity vs. time obtained for SG-4 in a quiescent solution as seen in Figure 3.3 above; b) Normalized florescent intensity vs. time obtained for SG-3 at 1 gph

Figure 3.9b is a normalized plot of the peak emission wavelength intensity as a function of time under flow conditions using SG-3. The magnitude of the fluorescence enhancement under flow conditions was similar (approximately 55%) to the signal enhancement under static conditions, but the time constant is dramatically smaller. By comparing Figures 3.9a and 3.9b, it can be seen that

the fluid flow significantly lowers the time needed for the uranyl fluorescence intensity to reach a plateau. We speculate that the slow saturation rate in the case of quiescent solution is due to the shortage of uranyl in the interstitial fluid inside the silica bags, as shown schematically in Figure 3.10a.

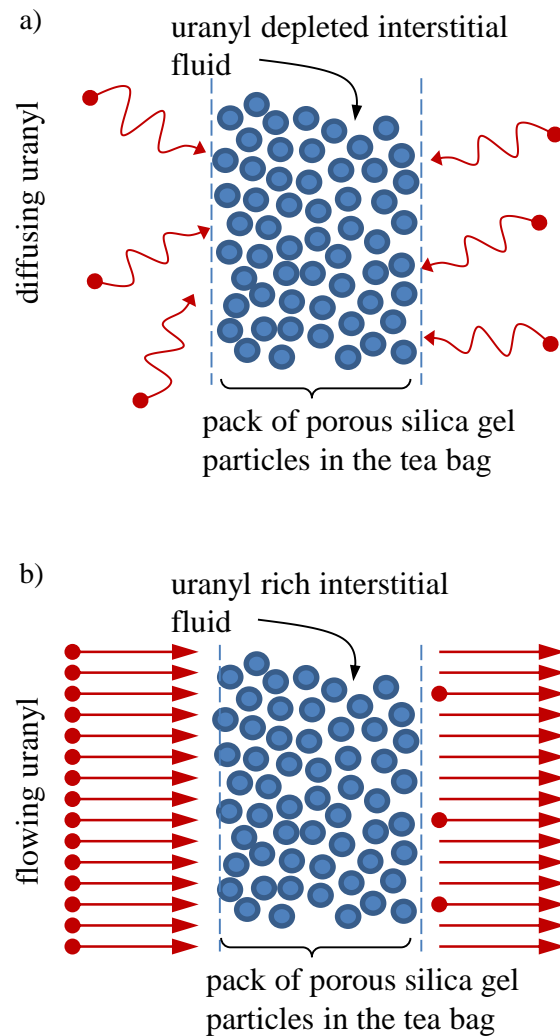


Figure 3.10: a) Schematic representation of uranyl transport into silica gel pack beds in quiescent solution and b) in presence of flow.

In the absence of flow, the uranyl transport mechanism is solely due to diffusion in a static fluid driven by the concentration gradient from the bulk concentration to the surface concentration of

the silica (Fick's Law). The surface concentration of uranyl is depleted by the uranyl bonding to the silica gel, which forces slow diffusion to take place from the bulk fluid to the surface and then into the pores. The rapid decrease in the saturation time in the presence of flow seems to occur because the flowing fluid maintains a constant uranyl concentration around the bed of silica gel particles and eliminates the time delay caused by diffusion (see Figure 3.10b).

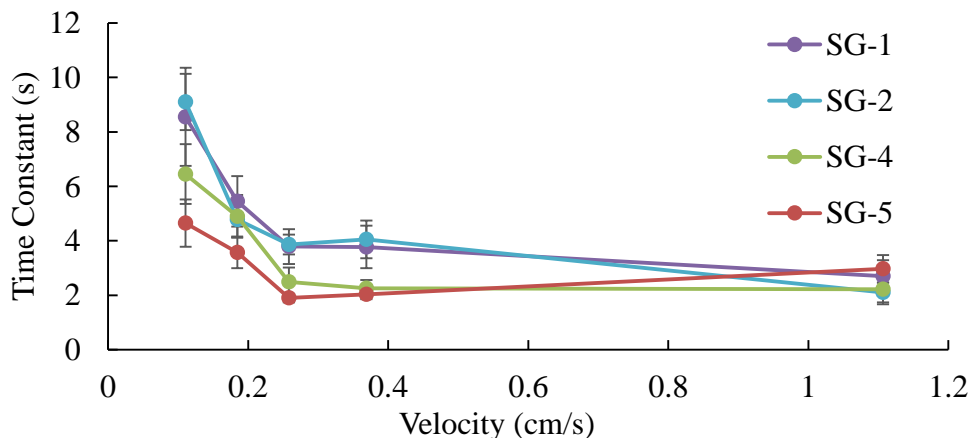


Figure 3.11: Time constant in presence of flow.

For flow velocities from 0.36 cm/s down to 0.18 cm/s, the time constant does not appear to have any dependence on the pore size (see Figure 3.11). For the 0.11 cm/s velocity (corresponding to the lowest flow rate used in this study), the time constant does decrease with increasing pore size above 4.0 nm, similar to the trend shown for the static fluid. Because the silica is initially dry, the water is first wicked into the pores until it becomes saturated. The silica's hydrophilic surface allows the water to rapidly fill the pores compared to the much slower diffusion of the uranyl. The larger pore sizes cause this diffusion to take place at a faster rate. This occurs because the uranyl is removed faster as it reaches the open sites within the pores due to the increased permeability. When the uranyl solution flows through the silica gel particles, some fluid moves around the particles while some fluid flows into the pores. The pores that are connected like a regular granular bed will allow the solution to flow to all sites within the particle. The forced flow through the

pores overcomes both the diffusion and permeability affects, which allows the time constant to be reduced by orders of magnitude. Figure 3.11 also shows that there is a critical velocity at approximately 0.36 cm/s. Above the critical velocity, the time constant levels off and becomes independent of velocity; while below the critical velocity, the time constant increases rapidly toward the static value. The static time constant value at zero velocity is not shown in Figure 3.11 as it is orders of magnitude above the scale of that figure. The critical velocity required to achieve the optimum enhancement in adsorption kinetics is approximately the same for all of the pore sizes. The critical velocity is the same for all pore sizes because it is the velocity at which the uranyl transport is no longer being limited by diffusion but is being driven by the fluid flowing into and around the pores. The pore size does have an effect on the kinetics of the uranyl transport from the static fluid.

3.6 Conclusions

In a static fluid, the transport of uranyl ions into nanoporous silica gel takes on the order of one hour to reach saturation as determined by measuring the fluorescence emission intensity as a function of time. In a moving fluid, however, the transport kinetics increase significantly, and the time required to reach saturation is reduced to approximately 2s at a flow velocity greater than or equal to 0.36 cm/s. Above 0.36 cm/s, the time constant did not depend on the velocity, but at velocities lower than 0.36 cm/s, the time constant increased toward the static fluid case. In a static fluid, the time constant decreased linearly with pore size, but this trend was not observed in a moving fluid at velocities greater than 0.11 cm/s. In a moving fluid, the process of uranyl transport into the pores is no longer controlled by diffusion and permeability. Uranyl transport seems to be dominated by the pressure-driven fluid flow similar to flow through a granular filter. The results indicate that rapid detection and measurement of trace levels of uranyl in water can be achieved

by using fluid flow to enhance the transport and adsorption of uranyl onto the available bonding sites within nanoporous silica gel.

Chapter 4: Table Top Instrument Development

The development of the instrument begins with creating a top table assembly of the components needed for accurate detection of uranyl in aqueous solutions. The main components need in the final instrument will be a small pump, flow cell, photomultiplier tube (PMT), ultraviolet light emitting diode (UVLED), and a micro controller. The small pump will be used to pump the uranium solution from the water source into the flow cell that contains a silica gel packet and will have a quartz window to allow for excitation and emission detection. The UVLED will have a wavelength near the maximum absorbance of uranyl to achieve the maximum fluorescent output. The PMT will be used to detect the fluorescent output of the uranyl and relay an analog signal to the microcontroller for processing. The Arduino microcontroller is also being used to control the gating of the excitation.

4.1 Flow cell design

The flow cell was designed to be similar to the flow cell in the initial flow enhanced kinetics experiment setup but much smaller in overall size. The size was reduced to accommodate the final goal of having a hand-held device. Initially, the design was four pieces that were printed using the MakerBot Replicator 2. This printing used PLA filament and had a low resolution, but it was sufficient for the prototyping purpose at this point in the development. The four pieces were two barb hose fittings, one top, and one base. The barb hose fitting were printed because tapping the printed PLA pieces to use brass fittings would be difficult, and printing them as part of the base produced very poor fittings. The initial design are shown below.

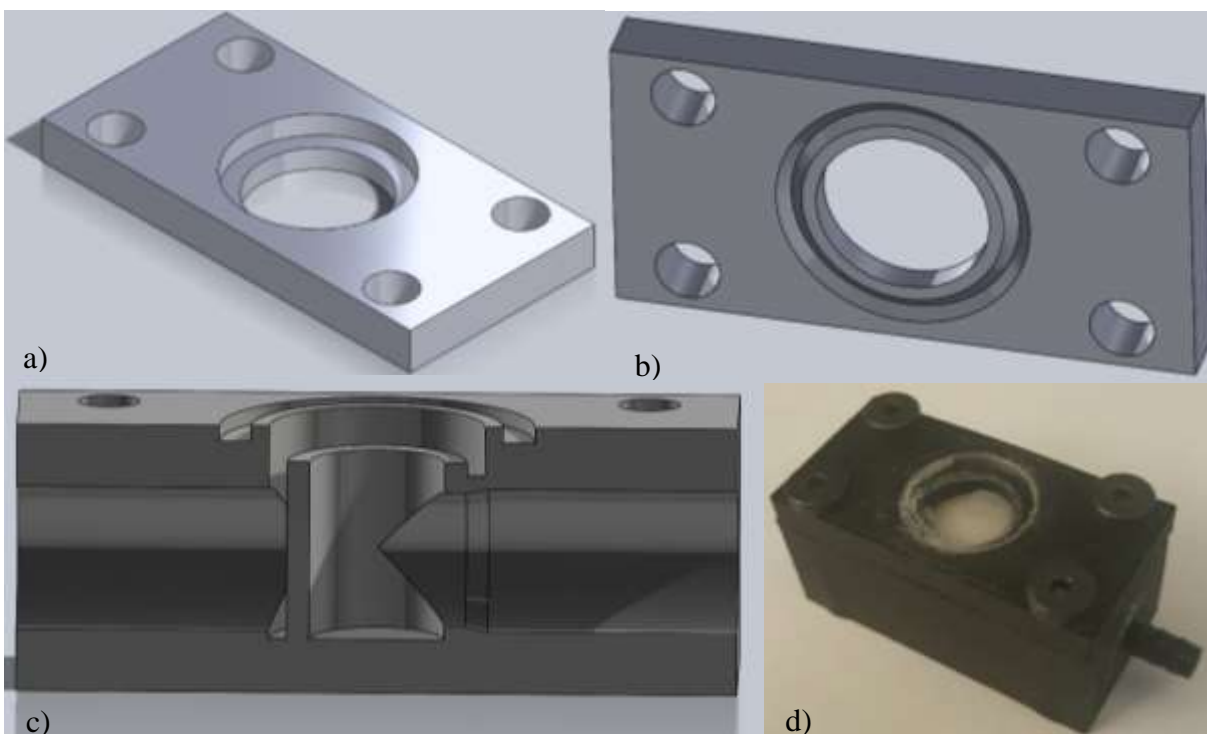


Figure 4.1: a) The top view of the flow cell lid, b) the bottom view of the flow cell lid, c) the section view of the flow cell base without barbed hose fitting installed, d) fully assembled flow cell.

Once these pieces were printed, the quartz window was glued into the top piece. The holes in the base were tapped to fit 8-32 threaded screws, while the holes in the top were designed as pass-through holes. To complete the seal of the sample chamber, an o-ring was placed in the slot around the sample chamber, which compresses when the top is tightened.

The silica gel bag was placed in the sample chamber, so that the uranium solution could flow up through the bottom of the bag, down over the edge of the center tube, and exit the chamber to be recirculated. This design flow pattern was effective with large concentrations (ppm range) of uranyl, where during the pumping time, the bag became completely saturated with uranyl. When the silica bag becomes completely saturated, the fluorescence can be measured on both the top and bottom of the bag. When the concentration was decreased to the parts per billion (ppb)

range, the fluorescence was no longer detected. This was due to the silica gel bags not becoming fully saturated within the time the measurements were taking place. The incomplete saturation could be seen by removing the silica bag; the bottom side of the bag would fluoresce, but the top side would not. Only the bottom side of the bag fluoresced because initially, the solution entered through the bottom of the flow cell and the uranyl deposited onto the silica it encountered first. The uranyl deposition on the bottom of the bag was problematic because the fluorescent detection window is at the top of the flow cell. The design was then modified to have the solution flow through the top of the bag and move down to the exit. This modified design used the same top piece as before, but the flow pattern was changed. The revised section view is shown below.

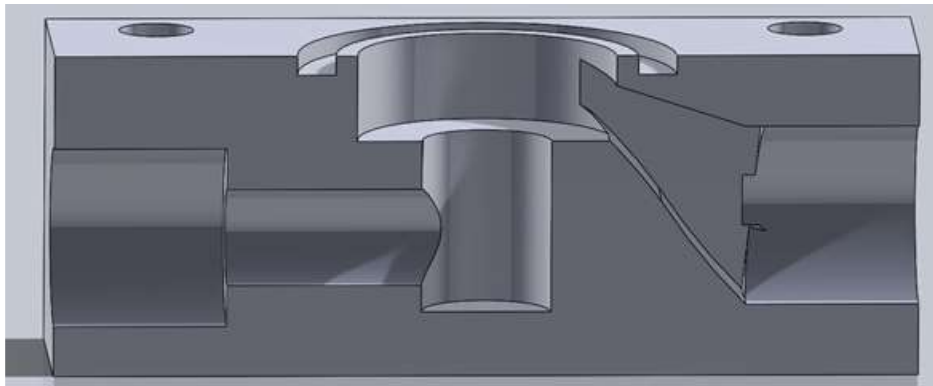


Figure 4.2: The second flow cell design section view.

The second flow cell design succeeded in the deposition of the uranyl on the top side of the bag, but it was inconsistent in maintaining this top side first flow pattern. The flow had a tendency to pick up the bag and keep the bag against the quartz window while allowing the solution to flow underneath the bag to the exit. This causes the bag to be ineffective in collecting the uranyl from the solution.

The third flow cell was able to fix the aforementioned problem. The cross section of the third version of the flow cell is shown below.

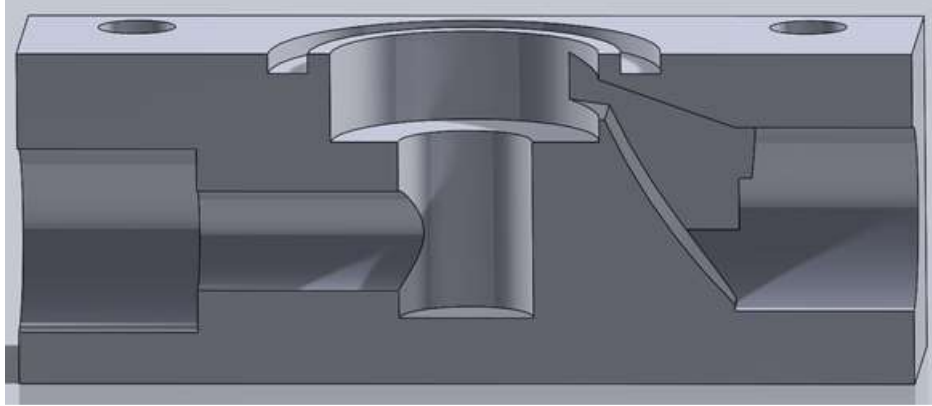


Figure 4.3: The third flow cell design section view.

A lip was added to the sample chamber so that the edge of the silica gel bag could rest below the water entry level; therefore, the bag could not be lifted and allow the water to flow underneath. This model has not shown any other problems except for some leaking issues, which are caused by the use of the PLA and MakerBot Replicator 2 printer not producing 100% water tight pieces. The final version of the flow cell will be printed on the EDEN260VS printer which will produce water tight components and allow for better quality prints. This printer is also capable of printing the barb fitting on the base. The final model is shown below.

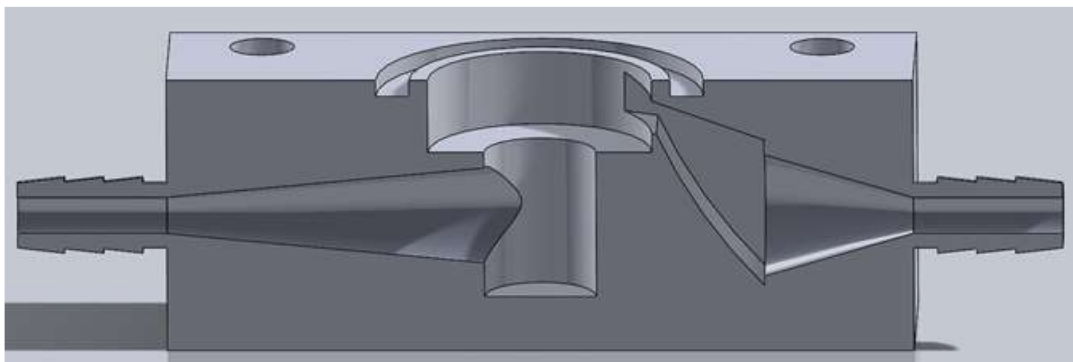


Figure 4.4: The section view of the final flow cell.

4.2 Hardware Holder Design

The hardware holder was designed to hold the PMT module, UVLED, and the flow cell in place in order to allow for the proper excitation and emission detection. The initial design is shown below with the PMT module hole located on the left and the UVLED hole located on the right.

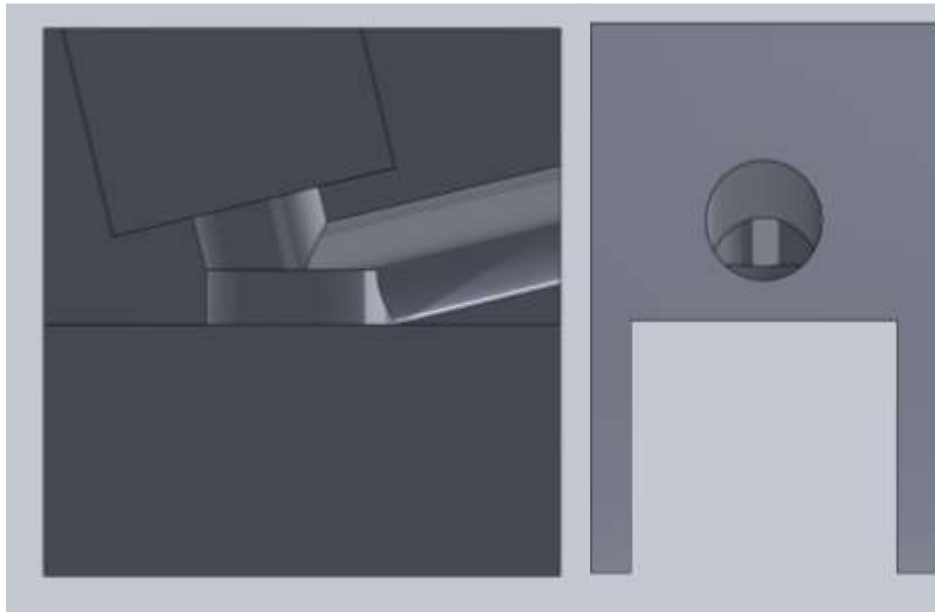


Figure 4.5: Hardware holder section view and right side view.

The initial hardware holder had a problem with light contamination because the screws that were used to hold the lid on the flow cell allowed light to pass between them into the detection area. In order to combat this problem, the next design has recessed areas for the screw heads to rest and the lid of the flow cell was flush with the bottom of the detection area as seen below.

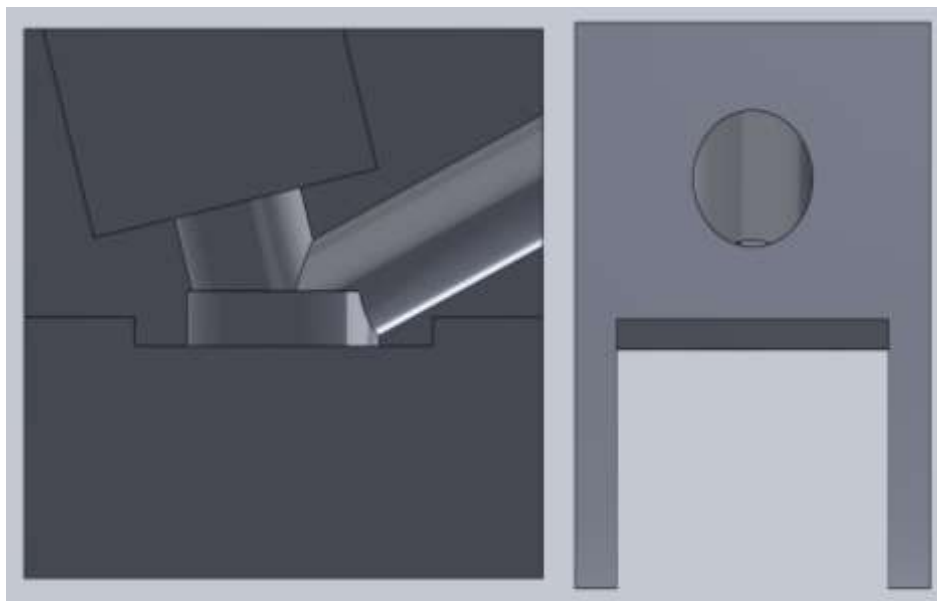


Figure 4.6: Second revised hardware holder section and right side view.

The hardware holder at this point was designed with the gated excitation in mind; however, the letdown time of the UVLED was too long to allow proper detection within the fluorescent lifetime of uranyl. The addition of a narrow bandwidth filter would eliminate most common forms of light contamination, including the UVLED, with a full width half max of 20nm. The third revision of the hardware holder allows for a 15mm narrow bandwidth filter to be placed with the flow cell and UVLED on one side and the entrance to the PMT on the other side. Additionally, the second revision did not mate with the flow cell easily, so the screw head recessions were modified. The third revision of the hardware holder is shown below.

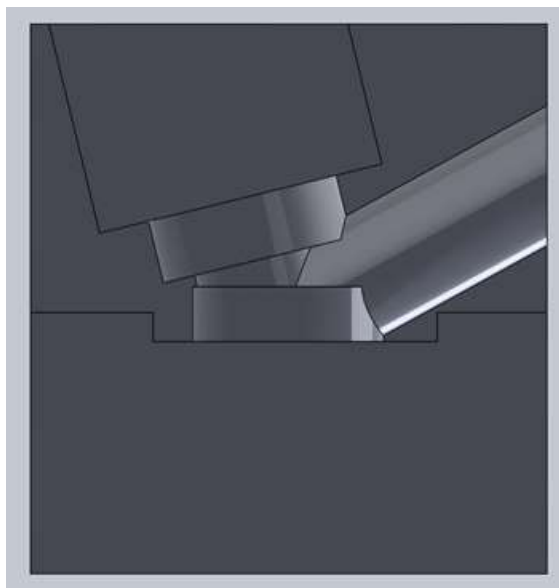


Figure 4.7: Third revision hardware holder revision section view.

Figure 4.7 shows that the two recessions for the screw heads are now different widths; this allows for one alignment point, making installation of the flow cell easier.

In the final form of the prototype holder, a cooling mechanism must be added for the UVLED because the hot LED is capable of melting the 3d printed parts.

4.3 Circuit and Program Development

The circuitry for the table top instrument was developed using the Arduino platform, including the Arduino UNO microcontroller board and the Arduino IDE software. The circuit powers the UVLED; it also powers and controls the sensitivity of the PMT.

LED Selection and Performance

The UVLED selection was based on the LEDs commercially available through the vendor Digi-Key electronics, who provided a wide range of wavelength, viewing angles, and price points. Knowing that uranyl has a maximum absorbance wavelength of 300nm (as seen below), the UVLEDs used in this work had wavelengths of 365nm, 325nm, 310nm, and 280nm.

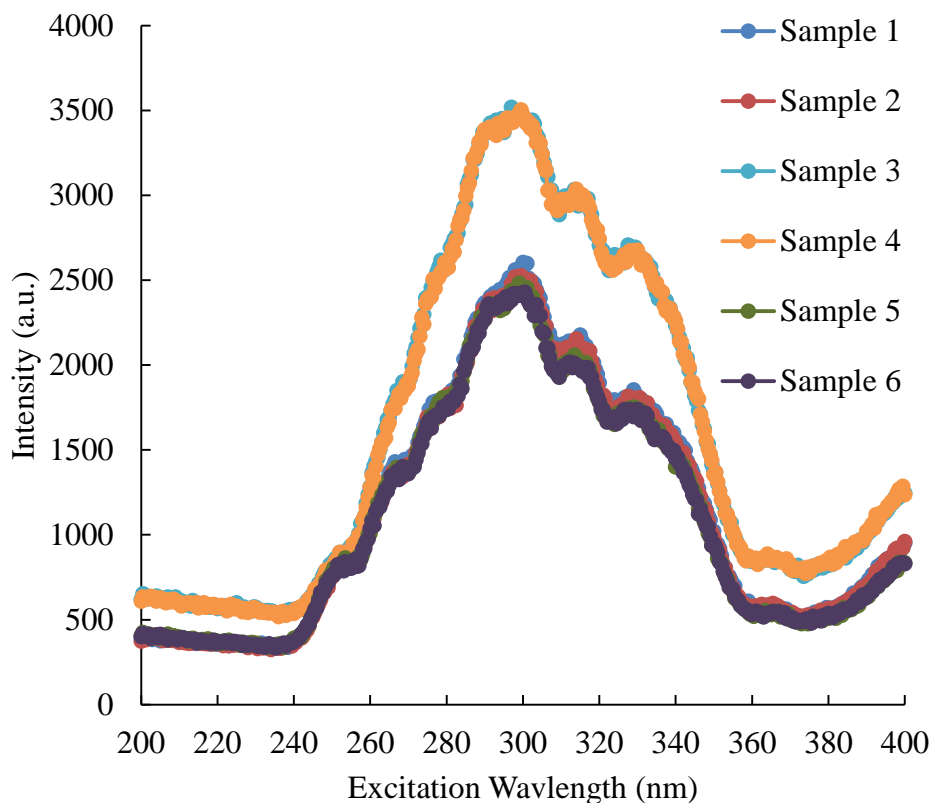


Figure 4.8: Excitation scan of Uranyl Nitrate in silica gel.

Each of the UVLEDs listed above had different forward voltage and current requirements, as seen in the table below.

Wavelength (nm)	Current (mA)	Voltage (V)
280	7	40
310	6.5	40
325	5	40
365	3.5	15

Each UVLED was initially tested to see which produced the most fluorescent output from the uranyl, using the aforementioned specifications. The UVLEDs were turned on and left at full output for the duration of the scan. Fiber optic connections to the spectrometer were used to detect the emission of the uranyl coming from a presoaked silica gel bag that was placed under the UVLED. The results of these tests are shown below.

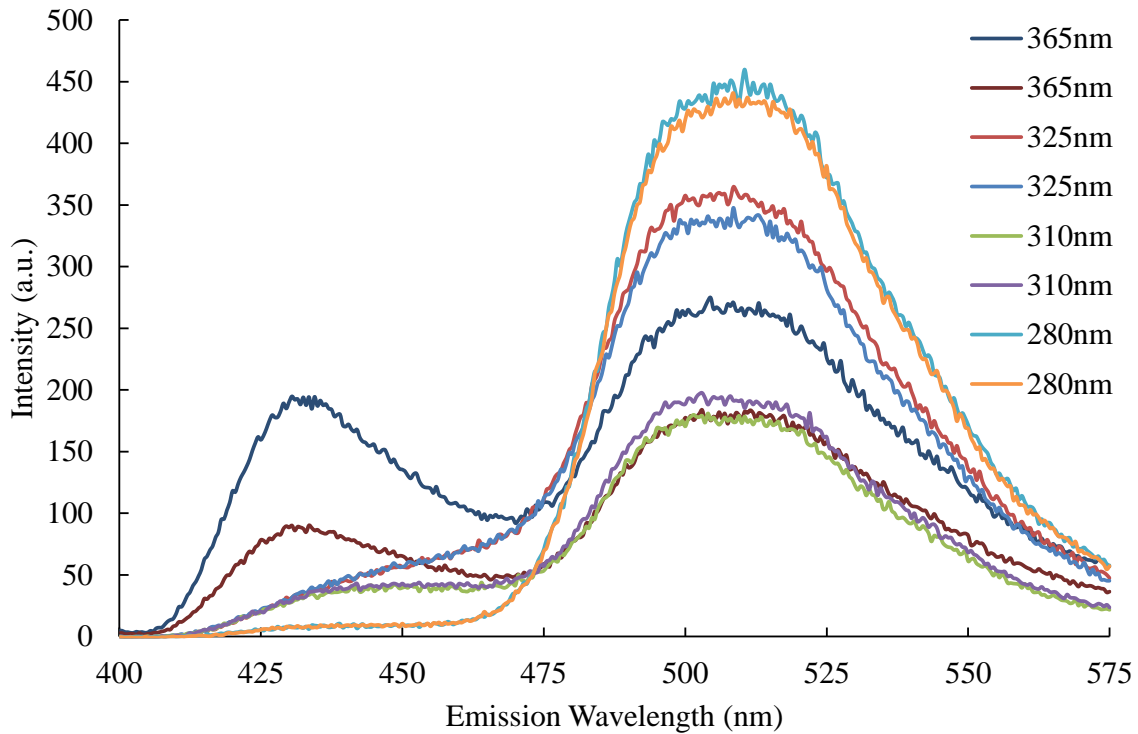


Figure 4.9: Uranyl emission with different excitation UVLEDs.

The use of the fiber optics for emission detection and a constant excitation source resulted in the spectra in Figure 4.9, as opposed to the normal signature of uranyl. The figure shows that the highest intensity of light was created by the 280nm UVLEDs, with 325nm as the second best. In addition to testing the fluorescent output by using the UVLEDs as excitation sources, the output of each UVLED was tested to check how closely they matched the manufacturer's specifications. The outputs were tested inside the spectrometers chamber to produce the best possible results. The spectra for the UVLEDs are shown below, where each spectrum line is from a different UVLED. Each wavelength is shown in a separate graph.

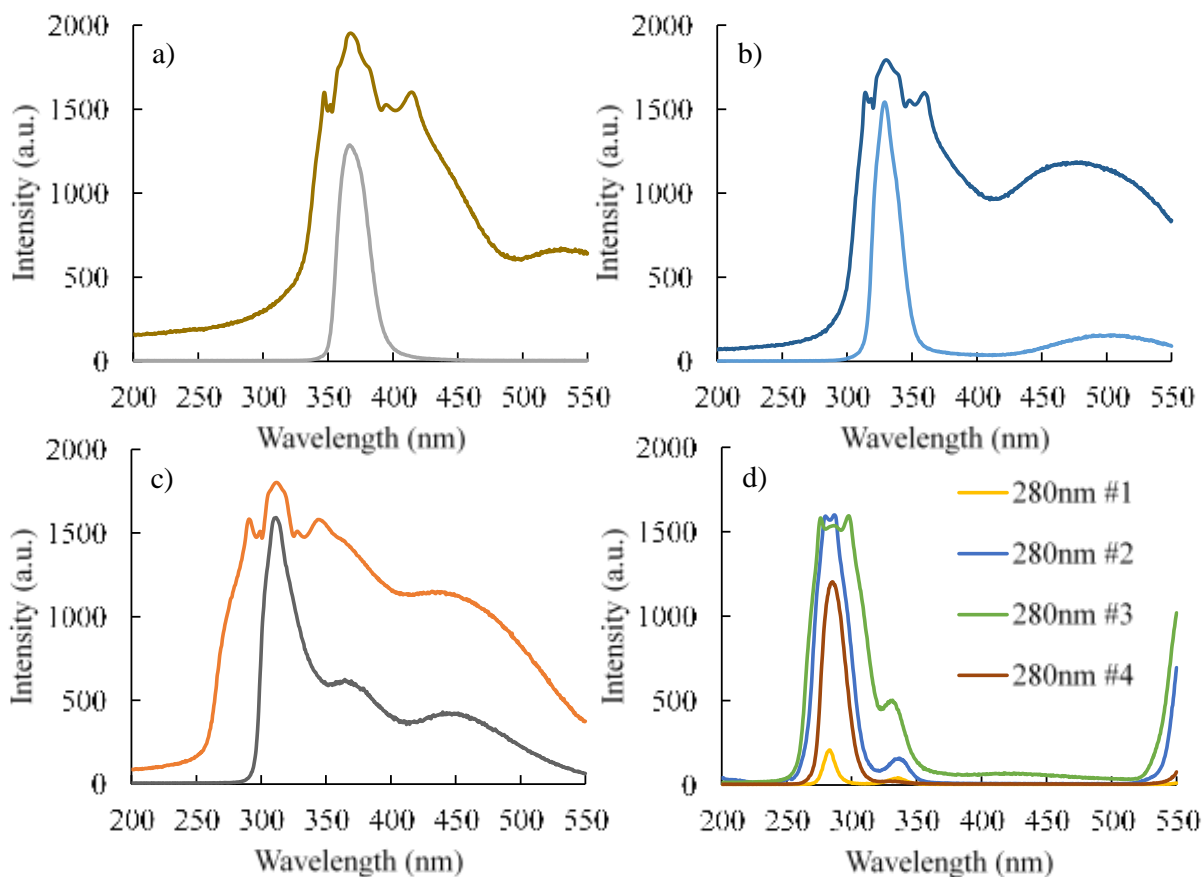


Figure 4.10: UVLED output by wavelength: a) 365nm, b) 325nm, c)310nm, d) 280nm to include 114° (1,2) and 24° (3,4) viewing angle.

The figure above shows that the commercially purchased UVLEDs are not all the same, even if they are supposed to have the same wavelength. Taking into account the study of the fluorescent output and the UV spectra, the LED chosen for the future sensitivity measurements was the 280nm #4. This LED has a viewing angle of 24°; this LED will be more focused on the sample, whereas the 114° projected too much light onto the filter.

Circuit Development

The circuit used for the table top instrument powers the UVLED, peristaltic pump, and the PMT. The UVLED that was selected for the excitation source needs 7V for the optimal output of light to produce the most intense fluorescence, but the controlled pins on the Arduino UNO board

operate at 5V. In order to produce the 7V needed, a non-inverting operational amplifier (opamp) was setup. The gain for a non-inverting opamp setup is given by the equation

$$Gain = \left(1 + \frac{R_2}{R_1}\right)$$

where R_1 and R_2 are the resistances of the resistor in the voltage divider. Using standard resistor of $R_1 = 10k\Omega$ and $R_2 = 3.9k\Omega$, the gain produced was 1.39. This in turn produces an output voltage of 6.95. The circuit schematic for the UVLED portion is shown below.

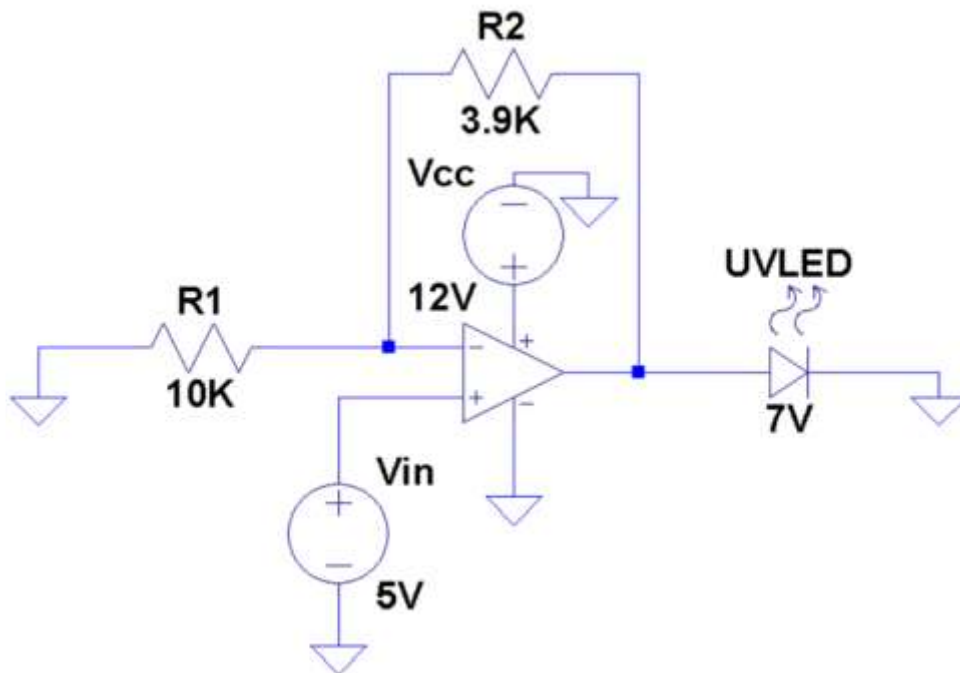


Figure 4.11: Circuit schematic for the UVLED portion of the table top instrument.

The schematic is shown without the Arduino UNO board, but the board controls the voltage supply to the circuit. The 5V V_{in} supply comes from pin 9, and the Vcc 12V comes from the V_{in} port on the Arduino board.

The PMT needs four different voltages to operate. Three of the four voltages needed are supplied by an external power supply. Those three voltages are the positive and negative 5V inputs and the 1.2V reference voltage. The fourth voltage is the $V_{control}$ input voltage. The control voltage

is the voltage that determines the gain of the PMT. This voltage needs to be between 0.5V and 1.1V in order to make this a variable voltage of 10K potentiometer (T103). The potentiometer allows the gain to be adjusted while doing sensitivity testing. Once the sensitivity limit has been reached, the potentiometer can be replaced with a resistor to take away the adjustability in the final design. In order to connect this potentiometer, three connections are made: one is the 5V input from pin 13, one is ground, and the last is the output to the Vcontrol wire to the PMT. The peristaltic pump needs 12V to run at maximum output, but voltage is also a way to control the speed of the pump. The voltage can be controlled by an external method similar to the potentiometer used for the control voltage of the PMT or a programmable analog signal. The programmable analog signal was used in this case because there is no need for on-the-fly changes to the pump speed. This analog signal is controlled through the Adafruit Motor/Stepper/Servo shield for Arduino. This motor shield has screw-down terminal blocks for easy confection, and it is 12V input compatible.

Program Development

The program for the table set up controls the UVLED, peristaltic pump, PMT, and the reading from the PMT. This program has been written in the Arduino IDE. Using the LED in combination with the basic Arduino IDE functions `analogwrite()` and `digitalwrite()` to flash the LED for the gated excitation brought a new challenge to the table top instrument. The challenge was the fall time, the time it takes the LED to go from maximum light output to zero output, was significantly longer than expected. This problem was discovered by measuring a sequence of light flashes using the spectrometer. The spectrometer was set to 300Hz for a 10 second time based emission scan to capture at the fastest possible rate. An example of the scan is shown below.

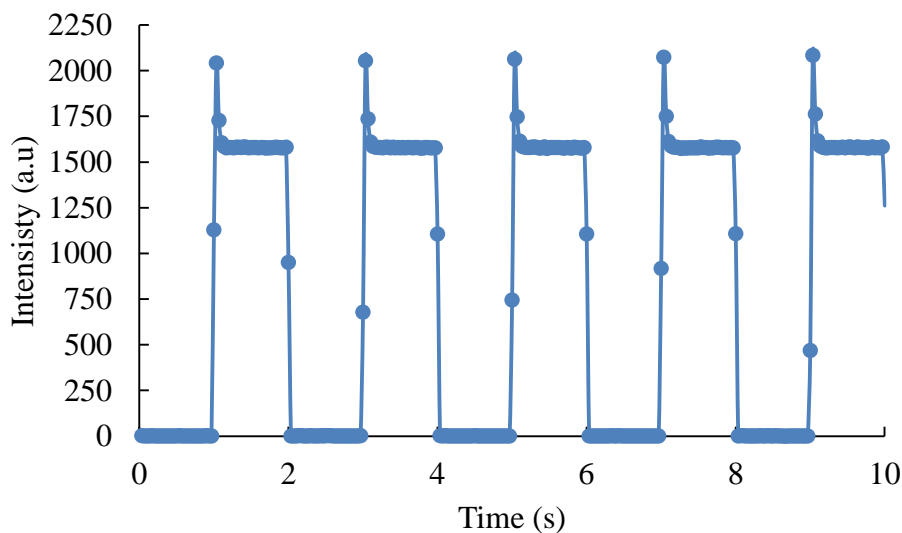


Figure 4.12: Time based emission scan of 280nm 24viewing angle UVLED.

The scan above shows that there are data points in the fall time, which means that the fall time takes longer than the time between measurements: 0.0333 seconds. The fluorescent lifetime of uranyl is $240\mu\text{s}$, so the fall time of 0.0333 seconds is insufficient for a gated excitation (32).

Originally, this was thought to be a problem with the UVLED, but all of the LEDs performed the same. When the program was further investigated, it was realized that the Arduino board was capable of much faster speeds than at which it was currently running, so the speed was changed from 9600bps to 115200bps. After changing the Arduino board speed, the speed at which the loop was running was also investigated. It was found that the built-in functions in the Arduino IDE are very low; in order to simplify the programming, the function have to run full “c” programmed routines to perform basic functions. In order to make functions including the on/off of the UVLED perform as fast as possible, the conventional Arduino functions were eliminated from the code and replaced with direct port control using “c” programing segments within the Arduino code. Switching to the “c” language allowed the Arduino to perform the same tasks without having to run sub-routines. The increase in speed can be seen in the time based scan below that was created using the same 280nm UVLED as the previous scan.

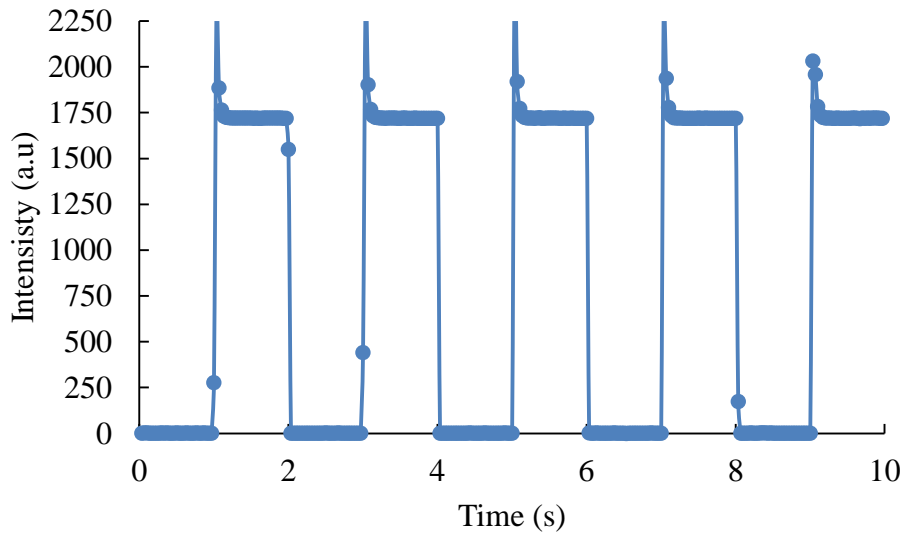


Figure 4.13: Time based emission scan of 280nm 24viewing angle UVLED using port control programing.

The figure above shows that on the fall of cycles two and three, the UVLED fall time was faster than the speed of the spectrometer. The other cycles do not show this pattern because the timing of the spectrometer and Arduino were controlled separately.

The program for the PMT portion performs two tasks: first, it turns the PMT on and off through the Vcontrol wire, and second, it reads the analog signal. The on and off task is controlled in the direct port control; it is controlled in the same method as the UVLED: using pin13. Pin13 is the pin that goes through the potentiometer. Using direct port control of pin13 will allow the PMT to turn on immediately after the UVLED turns off. The immediate switch allows for a reading to be taken before the fluorescent lifetime of the uranyl times out.

In terms of the second function of the PMT program, the analogread() function was used to measure the output of the PMT. The PMT had an output between 0 and 4V. The analogread() function reads voltages between 0 to 5V, but it is interpreted as numbers between 0 and 1023.

The relationship between the 0 to 5V and the 0 to 1023 was tested to show that the relationship was linear, as shown in the equation below. This equation had an R^2 value equal to 1.

$$Signal = 207.5(input) - 1$$

The maximum safe output of the PMT is 4V, so using the equation above, the displayed number is 829. If the PMT outputs above 4V, there is an addition IF loop after the signal is taken that will print “HIGH VOLTAGE” and turn the PMT off.

The program for controlling the peristaltic pump uses the Adafruit_Motorshield library that is recommended to be used with the motor shield. This library has specific built-in functions for controlling DC motor, steppers, and servos. The only functions currently used in this experiment are specifically for the DC motors. The main functions used for the motor are the run and setSpeed functions. The run function can be used to control the direction of rotation of the motor, and the setSpeed function allows the use of a variable analog signal to set the speed of the motor. The pump control section of the program, which is outside the main loop, controls the pump to initially turn on and then continuously pump water until the testing is complete.

4.4 Current Status

The current status of this instrument is promising. The recent time-based method of detection limit has not been reached. Theoretically, the time-based method is limited by the amount of water in the source. The time-based method allowed for a reduction in the $V_{control}$ from the 0.77V used in direct detection to 0.63V. The $V_{control}$ has a maximum of 1.1V which leaves a large amount of improvement if necessary. The increase in $V_{control}$ will cause a recalibration of the constants for the time-based detection method, but it would allow a reduction in the time to detect very low concentrations of uranium in water. This performance has given enough

information for an international patent to be filed for this technology, which currently has multiple accepted claims.

In addition to changing the PMT setting, efforts will be made to improve the signal-to-noise ratio by refining the gated excitation and filtration of the UVLED. Once the signal-to-noise ratio has improved, the flow cell will be modified to run multiple samples before having to remove the flow cell. Then this entire system will be consolidated into a hand-held battery-powered device used for field testing of natural waters.

4.5 Develop a final hand-held design for the instrument.

The development of a hand-held device is the ultimate goal of this project. In order to design this final hand-held device, a touch screen will need to be developed in order to control the device and to display the output of the detected concentration. The device will contain all of the components from objective 2, but it will also have to have some additional components that will be needed to perform field testing. The biggest change from the current table top design will be to the flow cell design. The flow cell will have to be modified to allow multiple samples to be taken without having to remove the samples from the device. This could be achieved by having a cartridge that houses multiple samples or having multiple flow cells to which the water could be directed. The main additional component will be a power supply that must be light weight and output 12V. The 12V requirement is needed to power the peristaltic pump and the op amp for the UVLED. Another major improvement that could be made is switching the PMT and optical filters with a spectrometer. There are many options for this that include a small spectrometer that can be controlled and operated with a Raspberry Pi computer and powered by a lithium ion battery. This would allow for full spectral analysis to be used to eliminate possible contaminants and even expand the capabilities to detect other fluorescent materials. Another additional

component may be a filter that could be placed at the water inlet to block all large contaminants from making their way into the device and blocking water flow of the light path to or from the sample. The most important design will be the robust waterproof housing that will hold all of the electrical components in place during transportation and use. This device will then be used for field testing for uranium concentrations in water.

Chapter 5: Uranyl Adsorption Kinetics within Silica Gel:

Dependence on Flow Velocity and Concentration

5.1 Introduction

Uranium is a radioactive element and uranium compounds are naturally occurring in water. Increased uranium concentrations in the environment have been associated with uranium ore mining, soil fertilization and nuclear fuel manufacturing and disposal(1–3,70). Measuring the natural concentration and deviations from that concentration is necessary for national security, non-proliferation, and water quality assessment (4,5). The traditional method of measuring uranium is based on the detection of high-energy particles that result from radioactive decay. However, detecting trace amounts of uranium compounds in water is challenging because the radiation signals are weak and attenuated.

The most common form of uranium in nature is uranyl, which is the oxidized ionic form. Uranyl is the +6 oxidation state with the chemical formula of UO_2^{2+} (13,14). Uranyl compounds can be water soluble and exhibit a distinct green fluorescent emission when excited with an ultraviolet light (36). The green emission can have up to six peaks with wavelengths in the range of 345-600nm. Various environmental factors, such as pH and temperature, can affect the wavelength(s) of the emission (39). The distinct peaks in the emission signature are caused by the vibrational modes of the two smaller oxygen atoms bound to the large uranium central atom (1,2,41,70).

Fluorescence has been used to detect the presence and concentration of uranyl in water for many years (48–50). The detection of uranyl in water at trace levels still presents challenges because water molecules quench the optical emission mode (36). This challenge has given rise to multiple methods of uranyl fluorescent enhancement. These methods include manipulation of the solution's pH, reducing the solution temperature, and immobilizing the uranyl on the surface of silica (14,39,49,50). In this work, porous silica gel is used to both accumulate and enhance the fluorescence of the uranyl. Silica has also been used to enhance the fluorescence of other materials such as Eu^{3+} , $\text{La}_4\text{Ti}_9\text{O}_{24}$, Rhodamine B, and alpha fetoprotein (48,69,71,72).

Silica gel is a hydrophilic material that is commonly used for chromatography, desiccant refrigeration, immobilization of cells and enzymes, and in this case, ion removal and fluorescence enhancement (62,63,73,74). In previous studies of silica gel on metal ion removal, it was shown that silica has a high adsorption capacity and affinity for uranyl (62). This attraction between the silica and the uranyl is caused by the negatively charged surface sites on the silica attaching to the positively charged uranyl cation (48). The amount of uranyl that can be adsorbed into these negatively charged sites is known as the equilibrium capacity. The equilibrium capacity has been studied with the objective of maximizing the capacity. This has been achieved by adding functional groups to the silica gel surface (46,64,65,68). The equilibrium capacity, while not the focus of this work, is still critical to the function of this method. The ability to store the uranyl entering the silica gel allows the uranyl to accumulate to a level that is easily detectable, which allows for a lower threshold of detection. This mechanism can be employed in very low concentration solutions, and we have shown that the solution concentration can be correlated with the amount of time needed to reach the detection threshold.

The time needed to reach the detection threshold is related to the kinetics of adsorption. The kinetics of adsorption has been studied in different scenarios such as static fluid, stirred fluid, and pressure driven flow (62,70). These studies showed that there was little improvement in stirring the fluid when compared to a static fluid; both studies had the time to reach equilibrium on the order of an hour, because of the slow rate of diffusion into the nanopores. However, when the fluid is forced through the silica gel using pressurized flow, the time is reduced to the order of seconds (62,70). In this paper, we establish the relationship between uranyl concentration and the kinetics of adsorption in nanoporous silica gel.

5.2 Experimental Methodology

Sample Preparation

Silica gel was purchased from Sigma-Aldrich with a nominal pore size of 10nm, particle size range of 63-200 μm , and specific surface area of 300 m^2/g . Two experimental systems were used to investigate the uranyl adsorption kinetics in silica gel over a wide range of concentrations. The silica gel particles were placed in 12mm diameter porous mesh bags for the low velocity system and 1-inch square bags for the high velocity system. The bags were made of nylon mesh with 28 μm openings from McMaster-Carr. The small bags were formed by melting the edges of two circles of mesh together and the large were formed by folding a rectangle in half and melting the edges. Using a Fisher-Scientific accu-124 balance, 50mg of silica gel was placed into each bag for the low velocity system and 250mg for the high velocity system. The two different sized nylon bags are shown in Figure 5.1.

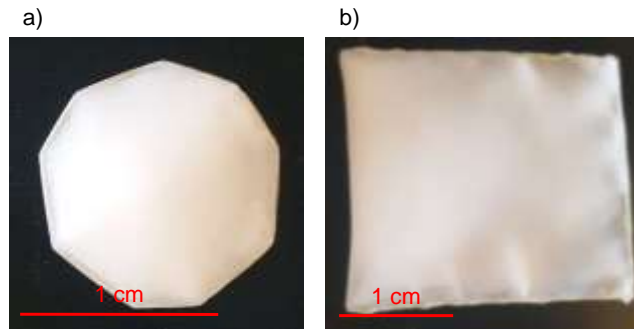


Figure 5.1: a) Low velocity system bag, b) high velocity system bag

The Uranyl Nitrate was purchased from American Master Tech and was weighed using the Fisher-Scientific accu-124 balance to make a stock solution of 39.4 mg/L. The stock solution was then diluted to create the solutions used in this study.

Time Constant Measurement with the Low Velocity System

The response time used in this study refers to the time required for the fluorescence signal from the uranyl deposited within the silica gel to produce a preselected photo multiplier tube (PMT) output voltage. This measurement was performed using a custom-made instrument that is schematically shown below.

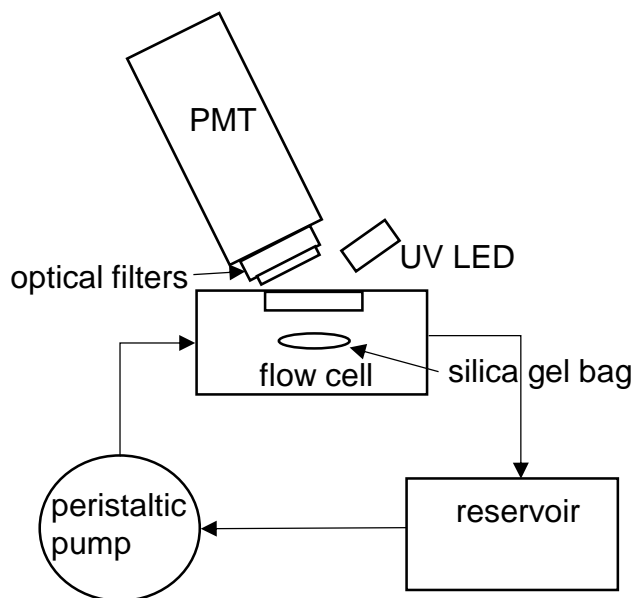


Figure 5.2: Schematic of the custom flow system

This system included a 280nm wavelength LED for excitation, a UV band pass filter, a notch pass visible light filter, a custom flow cell, Adafruit Industries peristaltic pump, and a solution reservoir. The flow cell, UV LED, optical filters, and PMT were all held in place using a custom 3D-printed piece that maintains a constant geometric relationship between all optical components. The UV band pass filter was used to limit the amount of UV light reaching the entrance of the PMT, and the notch pass filter was used to block all visible light outside of the maximum peak of the uranyl emission spectra. All flow components were connected with $\frac{1}{8}$ " ID rubber tubing. All of the components were controlled, and the signal was obtained, using a micro controller. This micro controller also was used to adjust the gain of the PMT through the V_{control} wire which was set to 0.58V.

The low velocity measurements were performed by pumping the solution through the silica gel sample at an average flow velocity of 3.14cm/s while the fluorescence intensity was monitored as a function of time. Flow velocity through the silica gel, rather than liquid flow rate, was used in order to compare the results from the two different sized silica gel bags. Signal monitoring

started when the pump was turned on, but the initial time for establishing the response time was set to when the water front reached the silica gel sample. Signal monitoring continued until the threshold PMT output voltage was reached. The solution was added to the system just before each scan and replaced for each measurement. Once the measurement was complete, the entire system was deconstructed and all flow components were cleaned and dried.

Time Constant Measurement with the High Velocity System

The high velocity system is a modification of the low velocity system to accommodate a larger pump, flow cell, reservoir, and a flow meter with a needle valve to control flow rate. The only additional component for this system was the flow meter with the needle valve. All of the components were connected using ½" ID R-3603 Tygon tubing. The flow cell used in this system is a vacuum strainer that had an additional custom piece which held the silica gel bag in place and allowed the water to flow through the bag. The silica gel bag size was increased to a 1-inch square bag to cover the cross section of the larger flow cell compartment, and the mass of the silica gel in the bag was increased to 250mg. The piece that holds all of the instrumentation was modified to contain the larger flow cell. This modification resulted in a small increase in the PMT gain, where the V_{control} was set to 0.63V. This setting change reproduced the same initial signal as the low velocity system. The average flow velocity in this system was determined to be 5.53cm/s.

5.3 Results and Discussion

Time Constant Results

In our previous studies of the kinetics of uranyl transport into silica gel, the fluorescence intensity verses time curve was fit using equation 1. This equation was used to find the saturation time constant as shown in Figure 3a. The maximum signal (e.g. saturation), I_f in equation 1, is

the point where all of the bonding sites in the silica gel have been filled, and the silica gel cannot hold anymore uranyl. In Figure 5.3a it can be seen that the initial increase is linear until the bonding sites begin to saturate and then the exponential curve takes over.

$$I(t) = I_f + (I_o - I_f)e^{-\frac{t}{\tau}} \quad (1)$$

where I_f is the final intensity, I_o is the initial intensity, and τ is the time constant (3).

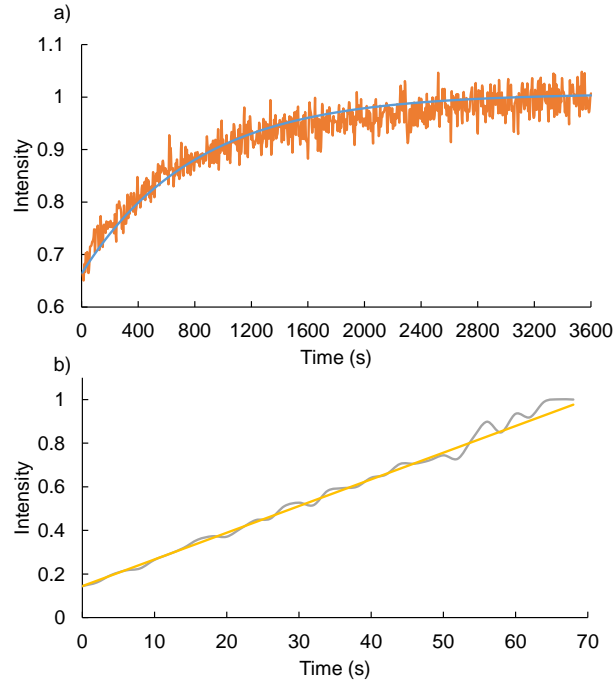


Figure 5.3: a) Normalized florescent intensity vs. time with silica gel saturation; b) Normalized florescent intensity vs. time in the linear region

For measurement times that are short compared to the time required to saturate the silica gel, the output signal intensity versus time is approximately linear as shown in Figure 5.3b. In this case, the time constant can be determined from the following linear equation, and a response time can be defined as the time required to reach a particular output signal.

$$I(t) = I_o - \frac{(I_o - I_f)t}{\tau} \quad (2)$$

In this study, a particular output voltage from the PMT was selected as a fixed threshold, and the time required to reach this threshold was determined at four concentrations and two liquid flow velocities. A response time was determined at each of the following concentrations and at both flow velocities: 3940 $\mu\text{g/L}$, 2000 $\mu\text{g/L}$, 1000 $\mu\text{g/L}$, and 394 $\mu\text{g/L}$. Figure 5.4 shows response time (time constant) at the high and low velocities as a function of the uranyl concentration.

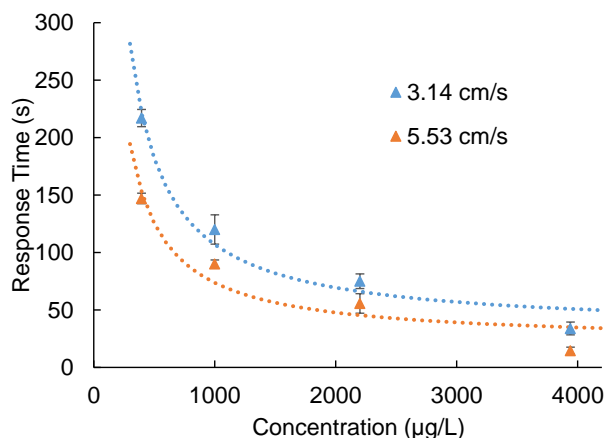


Figure 5.4: Concentration as a function of response time.

Figure 5.4 is a plot of the response time versus the uranyl concentration and the dotted line curve fits show that the response time is inversely proportional to the solution concentration.

The response time dependence on concentration is not unexpected and is because a dilute solution will take longer to deposit a particular number of uranyl ions within the silica gel. Thus, as the concentration is decreased, the time required to accumulate a particular amount of uranyl will increase because more solution will need to pass through the silica to provide that amount of uranyl. Figure 5.4 also shows that the response time decreases with increasing fluid velocity as would be expected. Increasing the average fluid velocity into the silica gel from 3.14 cm/s to 5.53 cm/s decreases the time constant by 65 percent on average with the largest decrease occurring at the lowest concentration.

The trend lines shown in Figure 5.4 were created using the equation below and the constants in Table 5.1.

$$t = t_0 + \frac{g^*}{VAC}$$

Table 5.1: Experimental Constants

Velocity (m/s)	t ₀ (s)	A (m ²)	g* (μg)
0.0314	31.8936	2.827E-05	66.53252
0.0553	21.8285	0.000285	816.1008

where C is the uranyl concentration, t_0 is the offset time, V is the fluid velocity, A is the cross sectional area of the silica gel bag in the flow channel, g^* is the amount of uranyl deposited in the silica gel and t is the response time. Using the constants in Table 5.1, the R^2 were found to be 0.9691 and 0.9122 for the velocities of 3.14cm/s and 5.53cm/s respectively. The constants shown in Table 1 are used when calculating the concentration in $\mu\text{g}/\text{m}^3$. g^* represents the amount of uranyl deposited in the silica gel bag in order to reach the specified threshold setting of the PMT. This is a constant that was found to be significantly higher in the high velocity system due to the much larger mass of silica gel.

The trend lines were used to perform an uncertainty analysis. This uncertainty analysis was performed using the statistical error of the response time measurements and then using the trend line equation to incorporate the uncertainty propagation. The uncertainty propagation was incorporated by multiplying the statistical error by the derivative of the curve-fit equation evaluated at each of the respective points. The calculated uncertainty at the lowest concentration in the study was $\pm 9\mu\text{g}/\text{L}$, but on average for all of the concentrations measured, the uncertainty gives an interval of ± 2.57 percent.

5.4 Conclusions

The time constant of uranyl transport into nanoporous silica gel under fluid flow conditions shows an inverse relationship with the concentration of uranyl in the solution. The relationship shows that as the concentration of uranyl decreases, the time required to reach a particular output

signal level will increase. Any fixed output signal level can be used as a threshold and reducing the threshold will reduce the measurement time to allow for measurements at extremely low concentrations. The results also indicate that increasing the fluid velocity will also reduce the time necessary to determine the uranium concentration. The results show that trace levels of uranium in solution can be measured in a short period of time and with a relatively high level of accuracy using this method.

Chapter 6: Uranyl Fluorescence Lifetime in Nanoporous Silica Gel: The Influence of Pore Size, pH and Water

6.1 Introduction

Uranium is a natural radioactive element found in mineral deposits and ground water. Elevated levels in water can be associated with industrial agriculture, mining and nuclear fuel manufacturing and disposal (1–3,75). Uranium in drinking water can pose a threat to human health but is challenging to detect in the field (4). This has prompted a drive to develop new field measurement methods that will be able to rapidly detect uranium in water at low concentrations. The most common and bioavailable form of uranium found in water is the uranium dioxide ion known as uranyl UO_2^{2+} (13,14,75). The bond length between the uranium and oxygen has been reported to be in the range on 1.5\AA - 2\AA with the common values between 1.7\AA - 1.8\AA (76,77). Uranyl has been known for its unique visible green emission for over 150 years (36,37,78). This visible emission, with wavelengths ranging from 345nm-600nm, has distinct peaks associated with the vibrational harmonics of the oxygen atoms vibrating around the uranium atom (1,2,39,41). The intensity of the fluorescent emission has been used as a method to determine the uranium concentration in water samples (48–50,70). However, at low concentrations, the fluorescence is difficult to detect, particularly in an aqueous environment, since water can both quench and attenuate the uranyl fluorescence (36). In order to improve the uranyl detection threshold in water, many strategies have been employed such as optimizing the pH and

temperature and through chemical complexation. Silica has been used to enhance the fluorescence of uranyl and other compounds including Rhodamine B, Eu^{3+} , $\text{La}_4\text{Ti}_9\text{O}_{24}$, and alpha fetoprotein (48,69,71,73). In this paper, nanoporous silica gel is used to collect, concentrate and enhance the fluorescence intensity and increase the fluorescence lifetime of uranyl in water samples.

Hydrophilic, nanoporous silica gel has a very high surface area and can collect and accumulate uranyl ions because the positively charged ions bind to the negatively charged surface sites of the silica. These properties of silica gel have been used for ion removal and desiccant refrigeration (48,62,63). Silica gel also increases the fluorescent lifetime of the uranyl ion. The lifetime of uranyl in water is about $14\mu\text{s}$, but when adsorbed onto the surface of silica, the lifetime can be increased by more than an order of magnitude (79). Increasing the fluorescence lifetime is useful for detection and identification, because most natural fluorophores have a very short lifetime, and can, therefore, be rejected using time gating techniques. It has been shown that different uranyl complexes are predominant at different pH values, resulting in a variation in fluorescence lifetime with pH (79). Gabriel et al showed that at low pH (4.01-6.7) uranyl in complex with silica will form UO_2SiO_2 with a lifetime of $170\mu\text{s}$ whereas $\text{UO}_2\text{SiO}_2\text{OH}$ is formed at higher pH (7.35-8.87) with a lifetime of $360\mu\text{s}$ (79). Leung et al showed that the fluorescence lifetime increases with temperature from 4K to 293K (80). In this paper, we investigate the effect of silica gel pore size on the fluorescence lifetime of uranyl attached to the silica surface in both an acidic and neutral pH. We also investigate the influence of water within the nanopores by measuring the lifetime after removal and reintroduction of the water. Our results show that the presence of water within the silica gel increases the fluorescence lifetime of uranyl-silica compounds by as much as $40\mu\text{s}$ and that very small pores can further enhance the lifetime by as much as $20\mu\text{s}$. We

also report a blue shift in the emission spectrum for the smallest pore size and hypothesize that the shift could be the result of quantum confinement and a corresponding adjustment of the energy levels for emission.

6.2 Experimental Methodology

Sample Preparation

The silica gel was acquired from Sigma Aldrich and Acros Organics with pore sizes ranging from 22Å to 100Å, particle sizes from 40µm to 650µm, and surface areas from 800m²/g to 300 m²/g as reported by the manufacturer. The complete list of physical properties for the silica gels used in this work are shown in Table 6.1.

Table 6.1 Physical properties of silica gels

Item	Company	Pore Size (Å)	Particle Size (µm)	Surface Area (m ² /g)
1	Sigma-Aldrich	100	63-200	300
2	Acros Organics	60	40-60	550
3	Acros Organics	40	40-60	750
4	Sigma-Aldrich	30	75-150	480
5	Sigma-Aldrich	22	75-650	800

The silica gel was placed in custom-made 1-inch square mesh packets made of nylon fiber mesh that was purchased from McMaster-Carr. The mesh had 28 µm size openings with equivalent fiber diameters. Using a Fisher-Scientific accu-124 balance, 250 mg of silica was measured and transferred to the nylon packets. The solution used in this project was 0.01M aqueous uranyl nitrate in pure deionized water. The uranyl nitrate was purchased from American Master Tech.

Full Spectra Measurements

Baseline fluorescence emission measurements were performed using a QuantaMaster-3 Spectrofluorometer with a Xenon flash lamp excitation source. The spectrometer settings for the spectral scans are shown in Table 6.2.

Table 6.2: Spectrometer settings from spectral scans

Parameter	Value	Unit
Excitation	310	nm
Emission	470-575	nm
Step Size	0.25	nm
Delay 1	108	μs
Int. Time	0.3	μs
Averages	10	
Shots	10	
Frequency	200	Hz

All measurements were performed in the spectrometer chamber using quartz UV transparent cuvettes into which the silica gel packets were folded and placed.

Fluorescence Lifetime Measurements

The fluorescence lifetime measurements were performed using the QuantaMaster-3 Spectrofluorometer. The lifetime calculation was performed using the single exponential fit in the Felix 32 software. One example of this fit is shown in Figure 6.1 below.

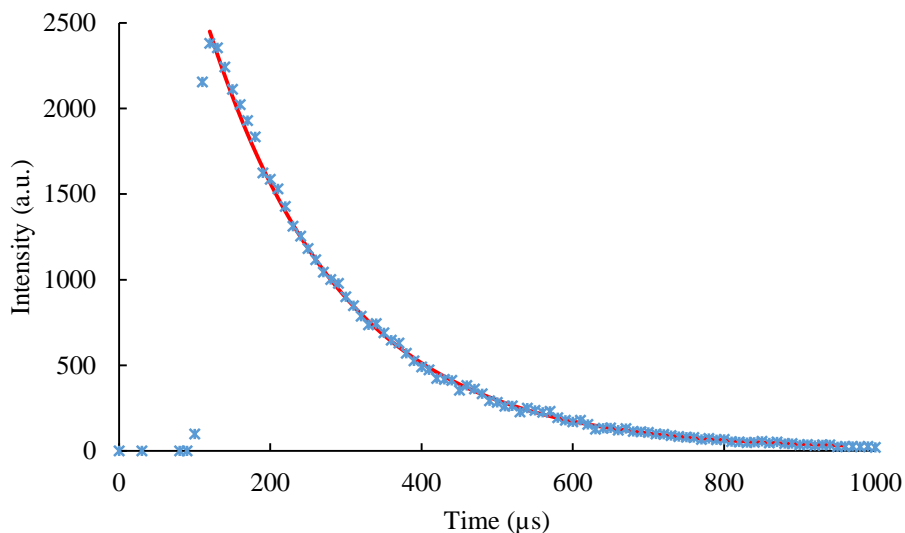


Figure 6.1: Figure 1: Lifetime measurement scan.

The spectrometer setting for the lifetime scan are shown in Table 6.3.

Table 6.3: Spectrometer settings from lifetime scans

Parameter	Value	Unit
Excitation	310	nm
Emission	496	nm
Start Delay	0	μs
End Delay	1000	μs
Channels	100	
Int Time	0.3	μs
Averages	1	
Shots	5	
Frequency	200	Hz

Silica gel samples at five different pore sizes were immersed in 50mL 0.01M uranyl nitrate solutions for three days to allow the uranyl cations to saturate the negatively charged surface sites of the silica gel. The uranyl nitrate solution was acidic with a pH of 3.96. The fluorescence lifetime of the uranyl within the silica gel was measured and the process and lifetime measurements were repeated for ten samples at each pore size. Each silica gel sample was then removed from the uranyl nitrate solution and placed in DI water for 3 days and the lifetime measurements were repeated at each pore size. The DI water environment increased the pH from 3.96 to near neutral (6.59) allowing a comparison of the lifetime at acidic and neutral conditions. The silica gel samples from both the 3.96 and 6.59 pH environments were then allowed to completely dry and the fluorescence lifetime was measured again for each sample to determine the effect of water on the lifetime. The fluorescence lifetime of the samples prepared from the 6.59 pH solution and dried were measured again after being re-immersed in DI water.

6.3 Results and Discussion

Emission Spectra

The emission spectra of the uranyl when adsorbed into each of the silica gel samples are shown in Figure 6.2.

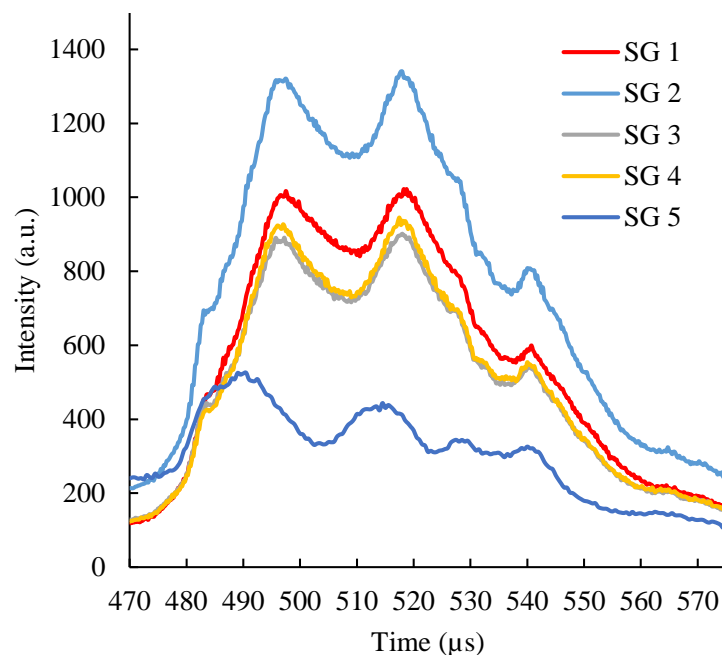


Figure 6.2: Fluorescent spectra for uranyl adsorbed in silica

These spectra were utilized to determine the optimum wavelength to measure the fluorescence lifetime. In these silica gels the specific peaks are always seen but the relative intensities of the peaks can be affected by the ratio of silica to uranyl (20). Silica gels 1 through 4 have the same spectral peaks at 496nm, 518nm and 540nm. Silica gel 5 has a slightly different spectra with peaks at 491nm, 515nm and 540nm. We believe that this small blue shift is indicative of a quantum confinement effect that is caused by the uranyl ion being constrained within the 22Å pores of the silica gel. Quantum confinement of the uranyl ion has been exhibited by cadmium sulfide quantum dots with particle sizes of 2.2nm and 1.88nm, which is very similar in size the pores of silica gel 5 (75). This reinforces the idea that the small pore size is causing the spectral shift. However, a full analysis of the effect of quantum confinement on uranyl fluorescence is beyond the scope of this paper.

Fluorescence Lifetime

Figure 6.3 is a plot of the fluorescence lifetime versus silica gel pore size for the acidic and neutral aqueous environments both before and after drying.

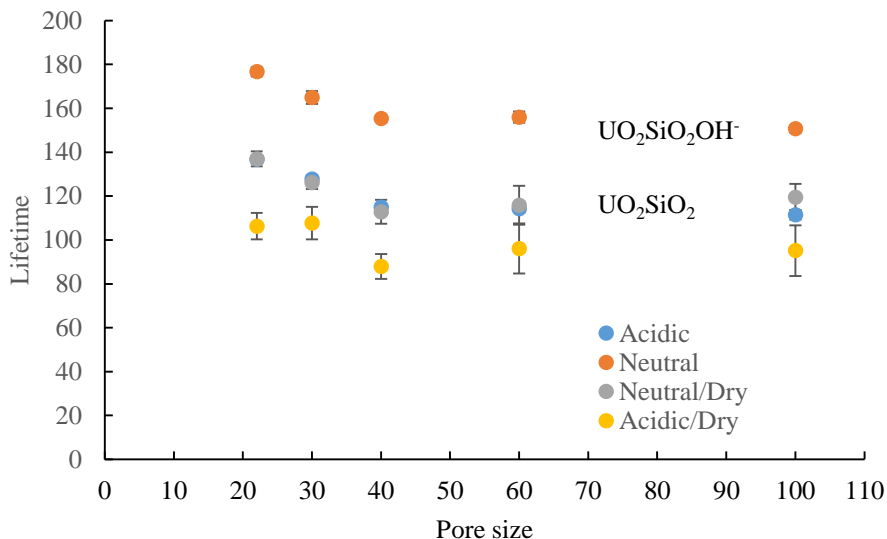


Figure 6.3: Lifetime as a function of pore size

Figure 6.3 shows that the fluorescence lifetime is relatively independent on pore size above 40Å and for all four environments (acidic, neutral and dry/acidic, dry/neutral). However, below 40Å the fluorescence lifetime increases with decreasing pore size for all four environments. The amount of increase is approximately 20μs over the 18Å decrease in pore size and the trend is relatively independent of the pH or water content.

In addition to the pore size trend, Figure 6.3 shows that the solution pH has a strong effect on the lifetime and is approximately 40μs longer for the neutral solution in comparison to the acidic solution at all pore sizes. This increase in lifetime with solution pH is caused by the addition of a hydroxyl group to the uranyl-silica gel surface complex. The most abundant complex formed at the 3.96 pH solution is UO_2SiO_2 which has a significantly shorter fluorescent lifetime than the $\text{UO}_2\text{SiO}_2\text{OH}^-$ molecule, which becomes more prevalent with increasing pH. While the effect of

pH on uranyl lifetime has been previously reported in solution, this data shows that similar hydrolysis reactions occur for the surface complexes within the silica gel nanopores.

Figure 6.3 also shows that the presence of water within the nanopores significantly impacts the lifetime of the uranyl. The lifetime decreases when the water is removed from both the acidic and neutral environments and the magnitude of the decrease is larger for the neutral solution at all pore sizes. As we show below, the removal of the water causes the uranyl to form an additional bond to the silica surface, which reduces the fluorescent lifetime. Figure 6.4 shows that the process is reversible and that the lifetime can be increased by adding water to the dry samples.

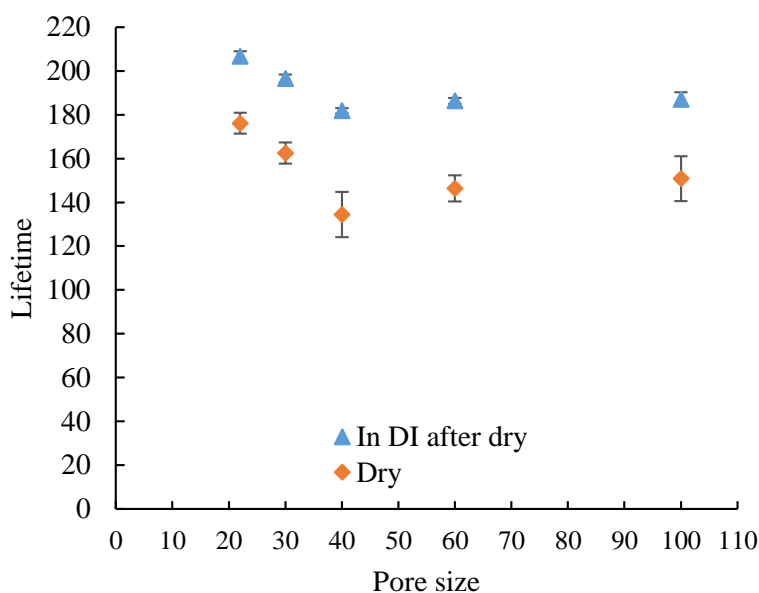


Figure 6.4: Lifetimes after the samples remained dry for 204 days.

Figure 6.4 also shows that the fluorescence lifetime increased during the 204 day drying period. We do not currently have an explanation for this increase, but because silica gel is extremely hydrophilic, we suspect that humidity caused some additional hydrolysis of the uranyl within the silica gel pores resulting in a longer lifetime in the aged sample.

Figure 6.5 shows the fluorescence spectra of a dry sample of silica gel and a spectra of the same sample in DI water.

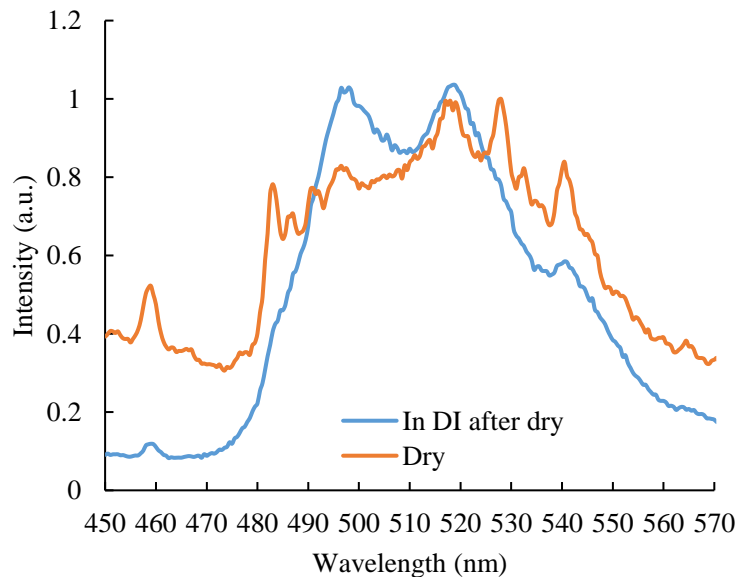


Figure 6.5: Spectra of a uranyl silica samples after drying for 204 day and when resubmerged in DI water

Figure 6.5 shows that the three main spectra peaks seen in the samples in the DI water are still observed in the dry samples, but a new peak at 528nm is very prominent in the dry samples. This peak is not seen in the original spectra and does not match with the 22nm spacing between the main peaks of the spectra when the sample is wet. This spacing is associated with the harmonic frequencies of the oxygen atoms around the uranium atom which created those wavelength emission, but the 528nm is distinctly different and is associated with a different emission transition. That is, when surrounded by water the uranyl complex is partially solubilized while still anchored to the silica surface. The removal of the water causes the uranyl complex to form an additional uranyl silicate bond that reduces the fluorescent lifetime and cause a new emission peak at 528nm. The 528nm peaks has been associated the uranyl silicate in a previous study

performed on silica rich soil samples from the Hanford site. This peak was found to be an emission of the $(\text{UO}_2)_2\text{SiO}_4$ found in the soil samples by Wang et al (20).

6.4 Conclusions

The fluorescence lifetime of uranyl bound within nanoporous silica gel is dependent on factors such as pore size, pH and water content. The lifetime increases monotonically as the pore size decreases below 40\AA and, at the smallest pore size studied in this project (22\AA), a blue shift in the emission spectra was observed and is believed to be caused by quantum confinement. The lifetime increased by about $20\mu\text{s}$ as the pore size decreased from 40\AA to 22\AA . The lifetime increased as the pH was increased from an acidic 3.96 to a neutral 6.59 at all pore sizes due to hydrolysis of the uranyl-silica complex with increasing pH. Specifically, at higher pH values $\text{UO}_2\text{SiO}_2\text{OH}^-$ is formed and has a longer lifetime than UO_2SiO_2 . The removal of water causes a decrease in the lifetime at all pore sizes and this decrease is due to an additional uranyl silicate bond that is formed in the absence of water. The lifetime increases again when water is reintroduced to the sample. This study investigated some of the main parameters that can affect the fluorescence lifetime of uranyl in complex with nanoporous silica gel. This information will be useful in the development of methods to collect, accumulate and detect uranium from water supplies.

Chapter 7: The Effect of Cations on Fluorescence and Kinetics of Uranyl in Nanoporous Silica Gel

7.1 Introduction

Uranium is a naturally occurring radioactive element that can be dangerous if present in high concentrations. Methods to detect trace amounts of uranium have focused on measuring the levels existing in areas where humans can come in contact with it such as in soil and water (1–5,25). There are multiple ways to detect uranium such as gamma spectroscopy, alpha spectroscopy, and fluorescence spectroscopy. Typically, these measurements need to be performed in a laboratory, but there has been a push toward field measurements. All of the spectroscopy detection methods mentioned are viable while uranium is at a high concentration, but as the concentration decreases, so does the viability of alpha and gamma spectroscopy due to attenuation of the signal and low signal intensity. Fluorescence spectroscopy is applied to the most common form of uranium in nature known as uranyl, which is the UO_2^{2+} ion (13,14). Fluorescence is attractive because there are methods to enhance the fluorescence signal that can be implemented to decrease the threshold of detection. These methods include manipulating the pH, changing temperature, and complexation with silica gel (14,39,48,49). These methods are all very effective, but in a field setting, the most promising method is complexation with silica gel because the silica can be prepared beforehand and does not require any further adjustments (1,2,25,70). Silica gel is ideal for field instrumentation because it can be used in conjunction with pressurized flow to accumulate

uranyl quickly for detection of trace levels of uranyl in water (70). The silica gel accumulates uranyl because it has negatively charged surface sites that bind with the positively charged uranyl; this continuously occurs until all the surface sites are full. Some challenges with field detection can still occur when using fluorescence, the most notable being quenching from other materials commonly found in water. The quenchers that are of most concern when using silica gel are other cations because they can reduce the fluorescence intensity and can compete with the adsorption of uranyl into the silica by filling the negatively charged surface sites.

To quantify the influence of competing cations on the fluorescence, the Stern-Volmer equation is used to show how the quenching will change with the concentration of the cation (75,81,82).

$$\frac{I_0}{I} = 1 + K_{sv}C_Q$$

I_0 is the intensity of the fluorophore without a quenching cation present, I is the intensity with the quenching cation present, C_Q is the molar concentration of the quenching cation, and k_{sv} is the Stern-Volmer Quenching coefficient (81,82). The Stern-Volmer quenching coefficient is the measure of the quenching rate of each respective cation. The linear relationship of the equation is ideal to measure deactivations through collisions with the cations (81). The Stern-Volmer equation used in this study is a simplified version of the equation that was used to quantify the quenching from the collision mechanism. This simplified form of the equation neglects static quenching (complexation) because the quenchers being tested were cations that were not expected to form a complex with the uranyl cation(83). The Stern-Volmer equation, while it is used to determine how the concentration of the quencher effects the fluorescence of the fluorophore, does not account for the concentration of the fluorophore itself (84).

The influence of cations on the adsorption kinetics of uranyl into silica gel is determined based on the time it takes to reach complete saturation of the negatively charged surface sites. The time

constant with and without competing cations was measured by monitoring the fluorescence intensity as a function of time as in previous studies (25,70).

For this study, the cations used were Mn^{2+} , Ca^{2+} , Mg^{2+} , Na^+ , K^+ , and Li^+ , which are all commonly found in fresh water. The concentrations used were based on the maximum values published from water samples at 65 locations around the world. The maximum concentrations used in this study are shown in Table 7.1.

Table 7.1: Concentrations of cations found in fresh water(85–91)

Ion	Molarity
Calcium	0.15
Magnesium	0.3
Sodium	1
Potassium	0.1
Lithium	0.002
Manganese	4.00E-05

7.2 Experimental Methodology

Sample Preparation

The silica gel used was purchased from Acros Organics and has a pore size of 60 Å, particle sizes in the range of 40-60 µm, and a specific surface area of 550 m²/g. The silica gel was placed in 1-inch square permeable pouches made from nylon mesh from McMaster-Carr. The edges of the bags were flame sealed to produce a pouch containing 250 mg of silica gel. The ion solutions were made using the chemicals shown in Table 7.2 and pure deionized water.

Table 7.2: Ion Sources

Item	Company	Chemical Name
1	American Master Tech	Uranyl Nitrate
2	FisherChemicals	Sodium Chloride
3	Sigma-Aldrich	Lithium Chloride
4	Sigma-Aldrich	Potassium Chloride
5	Sigma-Aldrich	Magnesium Chloride
6	Sigma-Aldrich	Calcium Chloride
7	Sigma-Aldrich	Manganese(II) Chloride

Once the stock solutions were made, they were diluted to achieve the desired concentrations, and the pH was adjusted to 4 using either 0.1 M HCL or 0.1 M NaOH.

Spectra Measurements

The fluorescent spectra for each sample was measured using a QuantaMaster-3 Spectrofluorometer with a Xenon Flash lamp source. The spectrometer settings from the spectra scans are shown in Table 7.3.

Table 7.3: Spectrofluorometer settings for full spectra scans

Parameter	Value	Unit
Excitation	310	nm
Emission	400-575	nm
Step Size	0.5	nm
Delay	108	μ s
Int. Time	0.3	μ s
Averages	3	
Shots	10	
Frequency	200	Hz

The silica bag samples were placed in the 0.01 M Uranyl solution and allowed to reach complete saturation before being placed in a UV transparent cuvette. Figure 7.1 is the spectra of the silica gel sample in the uranyl solution. The cuvette was then emptied and the uranyl solution was replaced with the respective cation solution, and the measurement was repeated.

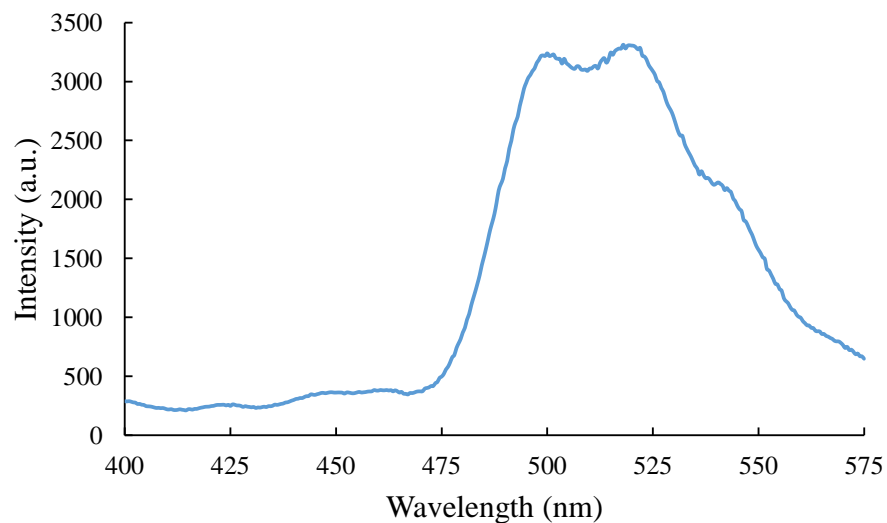


Figure 7.1: Full spectra of Uranyl

Time Constant Measurements

The time constant measurements were performed using the QuantaMaster-3 Spectrofluorometer. The silica gel bag was placed into the quartz cuvette and then a mixture of the uranyl and cation solutions were added. These mixtures were created using a 1:1 volume ratio of the stock uranyl solution and the highest concentration of each cation and deionized water as a control. The time-based scan measures the intensity of the 518 nm emission wavelength over time. The settings from the time-based scans are shown in Table 7.4 below.

Table 7.4: Spectrometer settings from time-based scans

Parameter	Value	Unit
Excitation	310	nm
Emission	518	nm
Points/sec	0.2	
Duration	3600	s
Delay	108	μ s
Int. Time	0.3	μ s
Shots	10	
Frequency	2	Hz

The fluorescence intensity as a function of time curve was then fit with equation 1 in order to find the time constant τ .

$$I(t) = I_f + (I_o - I_f)e^{-\frac{t}{\tau}} \quad (1)$$

One example of this curve fit is shown in Figure 7.2.

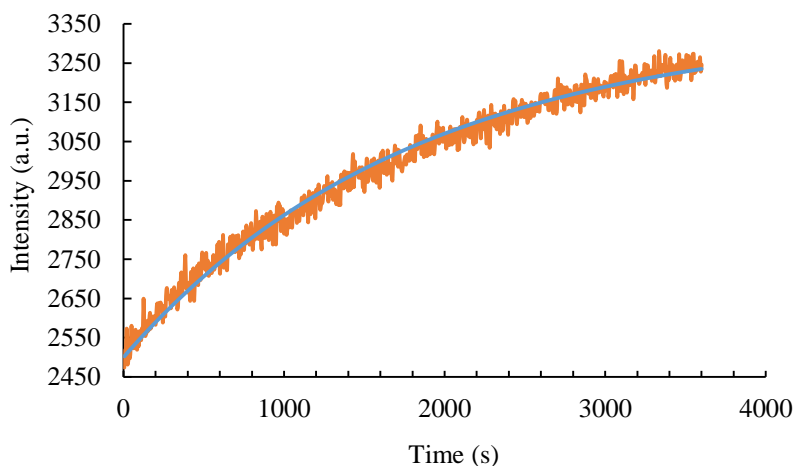


Figure 7.2: Fluorescent intensity as a function of time

Energy-dispersive X-ray Spectroscopy Measurements

Energy-dispersive x-ray spectroscopy (EDS) was used to measure the weight percentage of uranium and the cations in the silica gel samples. EDS analysis was performed using the Hitachi Ultra High-Resolution Analytical FE-SEM SU-70 with EDAX Software. The samples were prepared by spreading the silica gel on carbon tape that covered the top of the SEM mount, and then they were sputtered with carbon to reduce charging of the samples. The silicon peak was allowed to reach 120,000 counts before the peak identification was used, and then the weight percentages were quantified for each element found. One example of the spectrum collected is shown in Figure 7.3.

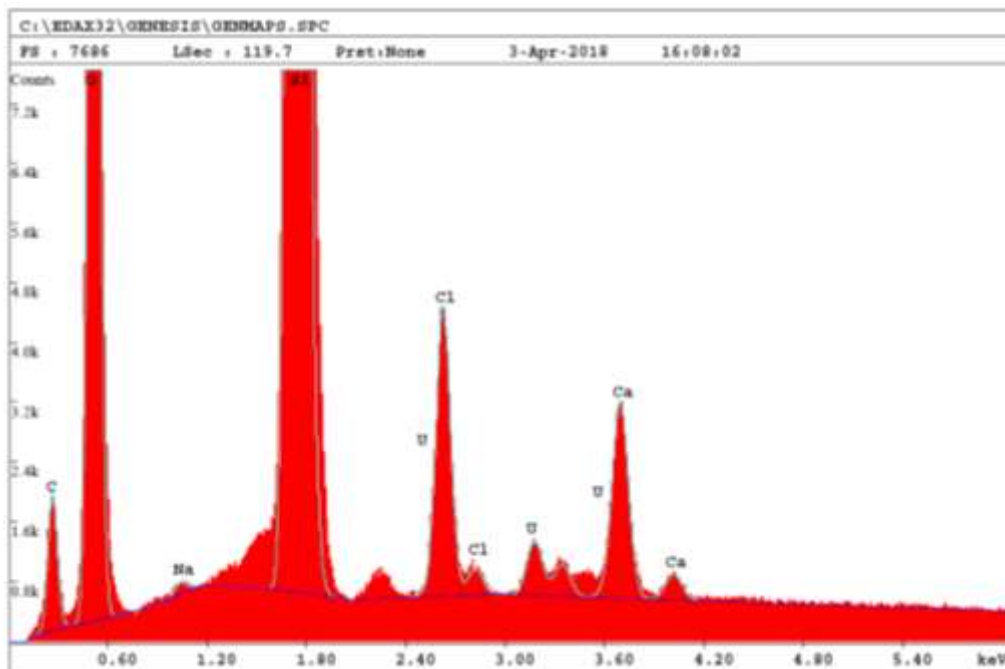


Figure 7.3: EDS Spectrum for the Calcium cation sample

The spectrum in Figure 7.3 shows the carbon from the sputtering, silica and oxygen from the silica gel, sodium and chlorine from the pH adjustment, uranium, and calcium, which was the cation for this sample.

7.3 Results and Discussion

Stern-Volmer Quenching Coefficients

The results from the Mn^{2+} , Ca^{2+} , and Li^+ cations showed that within the concentration levels used in this study, quenching did not occur. Therefore, for natural water, even with the highest levels of Mn^{2+} , Ca^{2+} , and Li^+ , fluorescence is a viable method for detecting trace amounts of uranyl. The ions that did quench the fluorescence within the natural concentrations were Mg^{2+} , Na^+ , and K^+ . Each of the cations were tested at the four concentrations shown in Table 7.5.

Table 7.5: Concentrations of cations tested.

Ion	Concentration (M)			
	Mg ²⁺	0.3	0.15	0.025
Na ⁺	1	0.7	0.3	0.065
K ⁺	0.1	0.075	0.05	0.025

Stern-Volmer plots for Na⁺ and Mg²⁺ are shown in Figure 7.4 below.

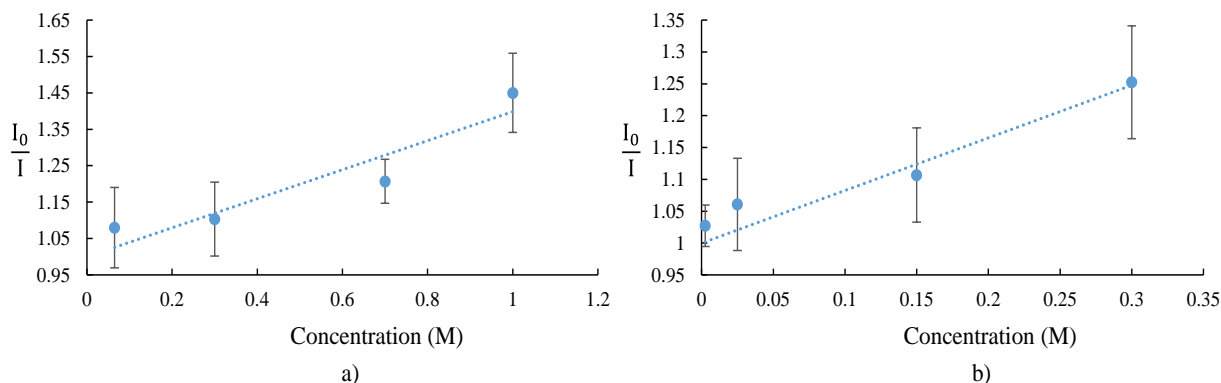


Figure 7.4: a) Stern-Volmer plot for Na⁺, b) Stern-Volmer plot for Mg²⁺

Figure 7.4 shows the linear Stern-Volmer equation as a trend line on each figure. This linear trend suggests that the quenching mechanism is bimolecular quenching. The mechanism is also known as collision quenching because the de-excitation is caused by the excited uranyl ion coming in contact with the other cation, which provides a non-radiative de-excitation mode. The trend line also gives the Stern-Volmer coefficients. Figure 7.4a shows that Na⁺ has the highest quenching with a 45% intensity reduction at the highest concentration. Figure 7.4b shows that Mg²⁺ attenuates the intensity by approximately 25% at the maximum concentration. The Stern-Volmer coefficients are shown in Table 7.6.

Table 7.6: Stern-Volmer Coefficients

Ion	K _{sv}	R ²
Mg ²⁺	0.825	0.9135
Na ⁺	0.3984	0.872
K ⁺	0.9711	0.7277

Table 7.6 shows that even though Na^+ has the largest reduction in the intensity, the quenching rate per mole is much lower than Mg^{2+} and K^+ . Table 7.6 also shows the most effective quencher is the K^+ ion, but it has the lowest natural concentration.

Time Constant Results

The time constant was used to investigate the adsorption kinetics of the uranyl into the nanoporous silica gel. The kinetics of this process is governed by the diffusion of the uranyl driven by the concentration gradient between the bulk solution and the water inside the pores. The process starts by wicking the water containing uranyl into hydrophilic silica gel pores. Once the water penetrates the pores, a concentration gradient is established as the uranyl binds to the negatively charged silica surface. This diffusion process begins quickly because the negatively charged sites are plentiful; however, as the sites begin to fill, the process slows down as the uranyl approaches the equilibrium capacity of the silica gel. This results in the behavior shown in Figure 7.2. The uranyl time constants in the presence of each of the cations is shown in Figure 7.5 in comparison to a DI water control.

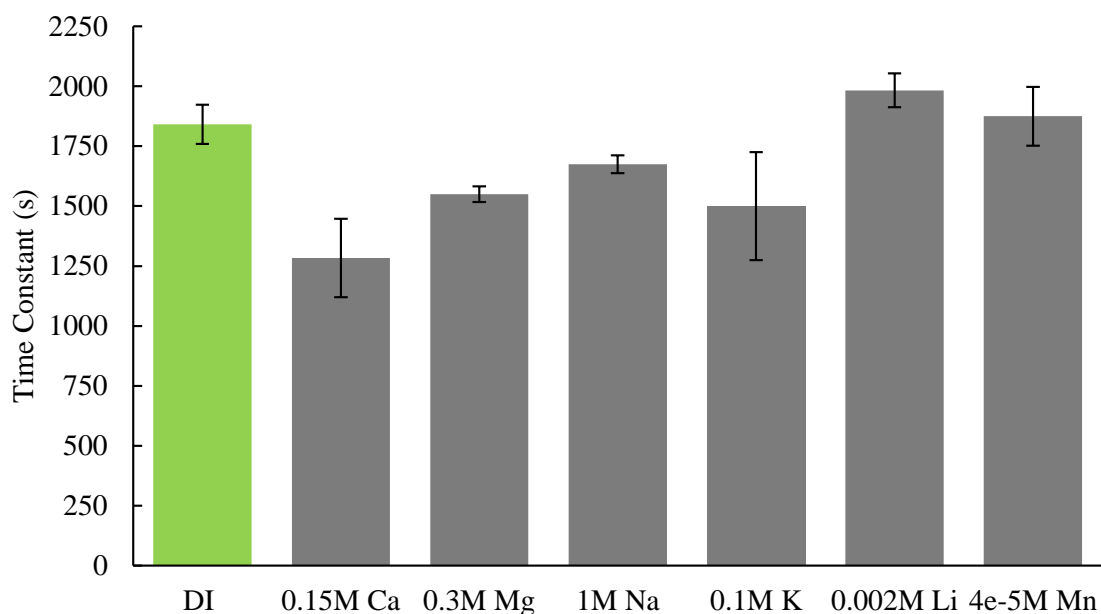


Figure 7.5: Time constant results for each cation

Figure 7.5 shows that Mn^{2+} and Li^+ had negligible effects on the time constants because of their low concentrations, and very little interaction with the uranyl was observed in the quenching study. The remaining four cations reduced the time constant. The largest reduction coming from Ca^{2+} (30.3%). The average reduction from the remaining four cations was 18.4%. This reduction is caused by the cations filling the negatively charged surface sites, reducing the number of surface sites available to the uranyl. The reduction in the number of sites that can be filled results in a lower equilibrium capacity of the silica gel and allows the uranyl to reach the capacity faster.

EDS Results

EDS was used to measure the weight percent of uranium in the silica gel when exposed to each of the cation/uranyl solutions and then compared to the silica that was exposed to only uranyl solution. The weight percentages are shown in Figure 7.6.

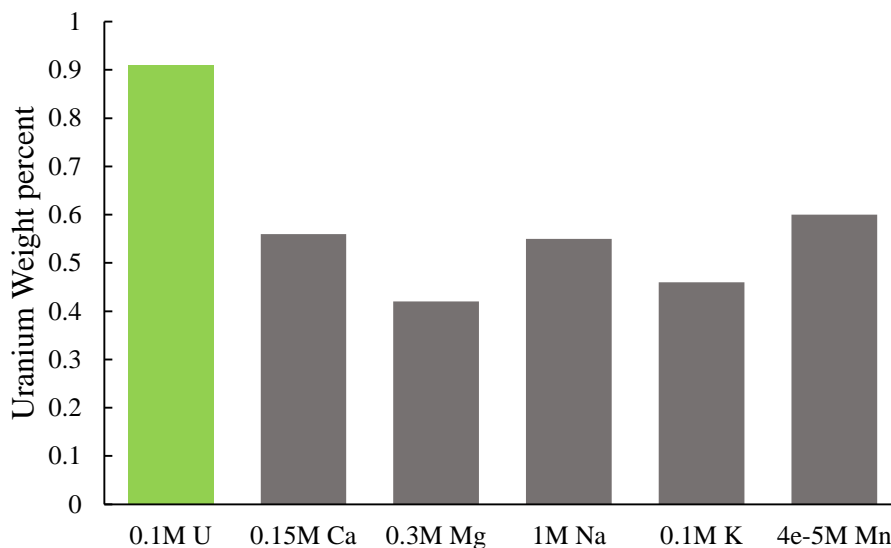


Figure 7.6: Weight percent of uranium measure using EDS

The EDS results show that all of the cations cause a reduction in the weight percent of the uranium by reducing the number of surface sites available to the uranium. The reduction in weight percent of the uranium means the amount of uranium that could be adsorbed by the silica gel was reduced; this led to the decrease in time constant to reach the capacity. The largest reduction in weight percent was seen in the presence of Mg^{2+} . Lithium is not shown in the figure because it cannot be measured using the EDS system.

Further evidence of the reduction in equilibrium capacity can be seen by comparing Figure 7.2 to the previous study on uranyl kinetics performed by this research group (70). The previous study showed a 50% increase in emission intensity over the length of the scan compared to the approximately 25% seen in Figure 7.2. This increase in intensity shows that the uptake of uranyl by the silica gel was less in the presence of competing cations than it was in the previous study without cations, which shows that the cations are occupying a fraction of the surface sites.

7.4 Conclusions

Silica gel is commonly used to enhance fluorescence of uranyl, the most common natural form of uranium. When using silica gel to enhance fluorescence, it is critical to consider competing cations that could exist in natural water systems. The cations that are commonly found in fresh water were tested at concentrations that can be found in fresh water sources around the world. The cations used were Mn^{2+} , Ca^{2+} , Mg^{2+} , Na^+ , K^+ , and Li^+ . We found that the quenching mechanism for these cations is collision quenching, where the cation provides a non-radiative mode for de-excitation of the uranyl ion. This mode of quenching was analyzed using the Stern-Volmer equation, where the slope of the line is the quenching rate. The highest quenching rate was found to be K^+ followed by Mg^{2+} and Na^+ , but, at the concentrations studied in this investigation, there was no quenching found in the case of Mn^{2+} , Ca^{2+} , and Li^+ . In addition to the

quenching of fluorescence, the cations also compete for the negatively charged surface sites of the silica gel. This competition was studied by measuring the time constant of the adsorption in the presence of competing cations and EDS. It was seen that Ca^{2+} , Mg^{2+} , Na^+ , and K^+ all decrease the time constant by occupying a fraction of the surface sites and lowering the equilibrium capacity of the silica gel, but the lower concentration ions did not impact the time constant. The presence of a competing cation could lead to a signal reduction as high as 30% in comparison to a water sample containing pure uranyl. The results of this study show that cations present in a particular water sample can influence the fluorescence measurement at very high concentrations.

Chapter 8: Gamma Spectroscopy of Uranium Adsorbed in Nanoporous Silica Gel

8.1 Introduction

Silica gel is a hydrophilic material that is a common desiccant used for applications such as removing moisture from packaging, chromatography, removing ions from solution, refrigeration, and enhancing fluorescence (62,63). Removing ions from solution and enhancing fluorescence are applicable to the detection of uranium because the uranyl (UO_2^{2+}) ion, which is the most common form of uranium in nature, is fluorescent (5,13). The removal of uranyl from solution allows the uranium to be concentrated to an easily detectable level, and fluorescence enhancement also assists in detection (25,48–50). Fluorescence is used to detect uranium because the uranyl ion has a unique emission spectra that is caused by the vibrational modes of the oxygen atoms around the much larger uranium atom (1,2,92). The fluorescence enhancement of silica gel has been previously studied for chemicals such as Eu^{3+} , $\text{La}_4\text{Ti}_9\text{O}_{24}$, and Rhodamine B (69,72). This paper focuses on silica gel's ability to remove the uranyl ion from water. Silica gel removes uranyl ions from solution because it has negatively charged surface sites that form hydrogen bonds with the positively charged ion. When using silica gel to remove ions from solution, one main concern is the equilibrium capacity of the silica, which is the amount of a specific ion that can be trapped in a specific amount of silica gel. There have been methods developed to increase the equilibrium capacity of silica gel by adding various functional group to the silica gel such as amidoxime,

carboxyl, dihydroimidazole, and hydroxyquinoline (64–68). In addition to knowing the capacity, it is also important to understand the kinetics of the uptake of uranyl by the silica gel and the effect of chemical modifications. The kinetics of the uptake have been measured in static, stirred, and pressure driven fluid flow methods (62,70). Once the silica gel has concentrated the uranium, the amount of uranium trapped inside the silica gel should be monitored. The amount of uranium accumulated within the silica gel can be a concern for individuals that are attempting to properly dispose of the silica and uranyl waste. In order to quantify the amount of uranium trapped in the silica, the activity of that uranium can be measured using nondestructive assay methods, such as gamma spectroscopy.

Gamma spectroscopy is a common method to detect and measure radionuclides. This method uses the measurement of the gamma ray spectra to determine the isotopes present and the activities of each isotope. For uranium, the natural isotopes found are ^{238}U (99.275%), ^{235}U (0.720%), and ^{234}U (0.005%). Due to the low abundance and small probability of emitting a gamma ray, ^{234}U is often not used in the analyses. In order to properly measure the activity of ^{235}U , multiple gamma rays emitted from ^{235}U are measured. These gamma ray energies (and their yields) include 143.76keV (10.5%), 163.35keV (4.7%), 185.71keV (54.0%), 202.12keV (1.0%), and 205.31keV (4.7%). The primary reason to use multiple gamma rays in the analyses is to improve statistical accuracy and to account for potential ^{226}Ra content. ^{226}Ra is a daughter of ^{238}U and emits a gamma ray with an energy of 186.21keV, virtually indistinguishable from the primary gamma ray emitted from ^{235}U . The ^{238}U decay chain can be seen in Figure 8.1.

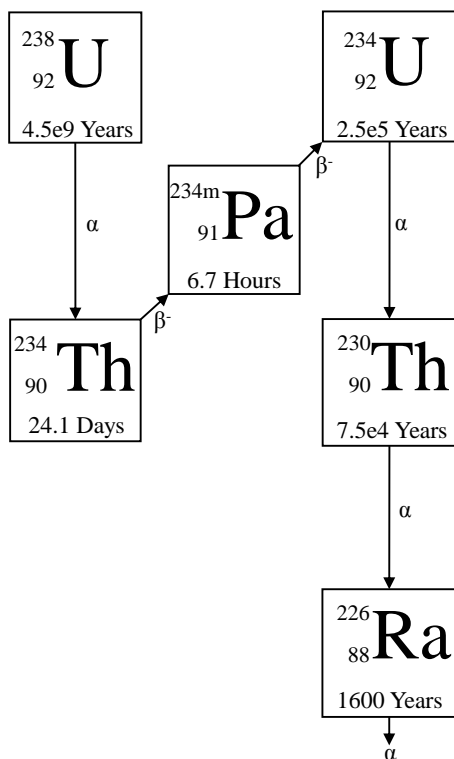


Figure 8.1: ^{238}U decay chain (93)

The activity of a radionuclide is a key quantity in determining its concentration in a sample. A sample's activity, A , can be determined from the detector system total efficiency, ε , yield of the gamma ray of interest, Y , and count rate recorded by the detector system for the gamma ray of interest, C . This relationship is shown in Eq. 1 (94).

$$A = \frac{C}{\varepsilon Y} \quad (1)$$

To improve accuracy, the activity of a radionuclide is determined using a weighted average based on the uncertainty of each measured gamma ray, shown in Eq. 2 and 3 (94).

$$\bar{A} = \frac{\sum_{i=1}^N A_i w_i}{\sum_{i=1}^N w_i} \quad (2)$$

$$w_i = \frac{1}{\sigma_i^2} \quad (3)$$

Where \bar{A} is the weighted average radionuclide activity, A_i is the radionuclide activity estimation from gamma ray i , w_i is the weight of activity A_i , and σ_i is the uncertainty of activity A_i .

To measure the ^{238}U isotope, the 766.4keV and 1001.0keV gamma rays from its daughter $^{234\text{m}}\text{Pa}$ are used. This is done due to the fact that ^{238}U does not directly emit easily detectible gamma rays (95). $^{234\text{m}}\text{Pa}$ comes from ^{238}U decaying through an alpha emission to ^{234}Th with a half-life of 24.1days that then beta decays to $^{234\text{m}}\text{Pa}$ with a half-life of 6.7 hours (93). These measurements are commonly used when determining the enrichment of uranium samples and classifying waste. The knowledge gained from this study will be used to ensure that the silica gel used for optical uranium detection is handled properly while giving more information about how the uranium is deposited within the silica gel.

8.2 Experimental Methodology

Sample Preparation

The silica gel used in this study was purchased from Sigma-Aldrich and Acros Organics with various different physical characteristics. The manufacturer-reported physical characteristics are shown in Table 8.1.

Table 8.1: Manufacturer reported physical characteristics for the silica gel

Item	Company	Pore Size (Å)	Particle Size (µm)	Surface Area (m ² /g)
Silica-1	Sigma-Aldrich	22	75-650	800
Silica-2	Sigma-Aldrich	30	75-150	480
Silica-3	Acros Organics	40	40-60	750
Silica-4	Acros Organics	60	40-60	550
Silica-5	Sigma-Aldrich	100	63-200	300

The silica gel was placed inside a pouch made of 28µm nylon mesh, which was flame sealed to create a pouch that is a 1-inch square. Each pouch was filled with 250mg of silica gel.

Uranyl nitrate salt purchased from American Master Tech was used to create the 0.01M solution with a uranium enrichment below 0.3% ²³⁵U.

The silica gel pouches were then exposed to uranyl in two different ways. The first method used a pump to force the solution through the silica gel that was set up to act as a filter. The silica gel pouch was placed in a flow cell that orients the silica gel pouch perpendicular to the direction of flow. In this configuration the solution was pumped through the pouch at a flow rate of 0.946L/min for 20seconds which is sufficient to deposit a detectable amount of uranyl in the silica based on data from a previous study (5). The second method soaked the silica gel in a static uranyl solution for three days to allow the uranyl to fully saturate the silica gel based on the data from a previous study (19). The two methods were used to test how the uranyl is deposited in the silica under pressure driven flow verses natural diffusion.

Five samples of each silica gel were place in a plastic petri dish that was sealed. Then each petri dish was analyzed using gamma spectroscopy to measure the activity of the samples and calculate the mass of the uranyl accumulated in the silica gel pores. The total mass of silica gel in each petri dish was 1.25g.

Gamma Spectroscopy Measurements

A LabSOCS characterized high-purity germanium (HPGe) detector system was used to assay the silica gel samples. The detector system is a 40% relative efficiency coaxial germanium p-type detector in a Canberra Model 747 four-pi shield. To reduce lead x-ray interference at low gamma ray energies, the shield uses a graded system consisting of 1mm of tin, 1.6mm of copper, and 100mm of lead (96). The HPGe detector used has an energy range of 40keV to 10MeV and an energy resolution of 1.2keV at 186keV and 1.7keV at 1001keV (97) The detector is accompanied by a liquid nitrogen Canberra Cryo-Cycle II, which keeps the detector at an operating temperature around 77K (98). The multichannel analyzer (MCA) used to collect the data was the Canberra DSA 2000. The MCA had an output voltage of 4000V and was set to collect data using 8192 channels. Canberra's Genie 2000 with Lab SOCS software was used to collect and analyze the data (99–101). The course and fine gain settings were adjusted to allow for gamma ray measurement data to be collected over the energy range of 0keV to 4.2MeV, approximately 0.5keV per channel. The detector was energy calibrated using 11 different gamma-ray energies emitted from a ^{152}Eu point source. An efficiency calibration was also done using Canberra's Geometry Composer. The model created matches the geometry of the silica gel samples during the measurements. This geometry consists of a cylinder with height 11mm and diameter 43mm placed 2mm from the HPGe detector surface and aligned with the center of the detector. A 253hour background measurement was acquired with the HPGe detector system which was used to subtract background from the silica gels' spectra. The silica gel samples were individually measured for varying amounts of time depending on the HPGe detector system availability, with most common duration consisting of 15hours. An example detector spectrum is shown in Figure 8.2 for a 26hour

measurement of the silica-5 natural diffusion sample approximately 2 days after being removed from the uranyl.

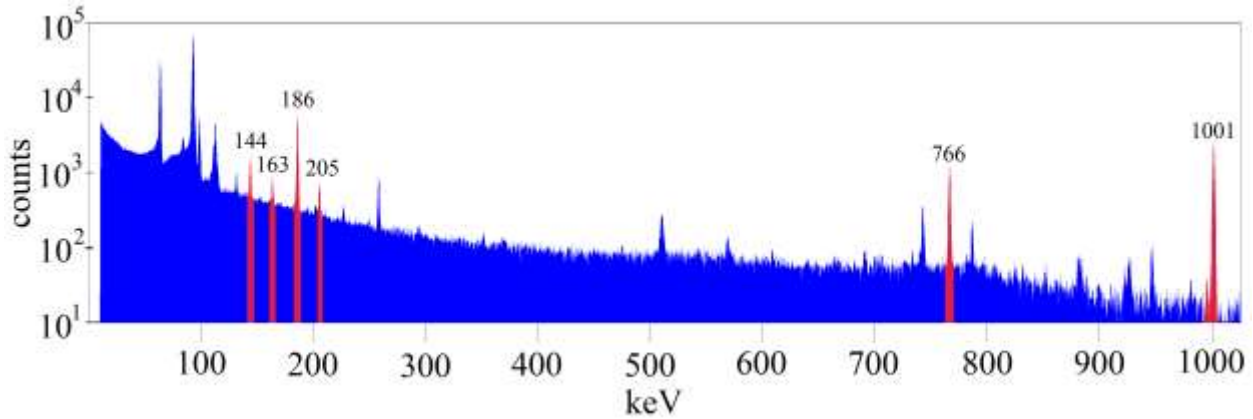


Figure 8.2: Gamma spectra of the silica-5 natural diffusion sample

Data Analysis

The background-subtracted gamma ray spectra were analyzed using Genie 2000 gamma analysis software. The number of counts in each gamma ray peak of interest and radionuclide activity were determined using the software's default peak analysis sequence. The Gaussian fit of each peak was verified for accuracy using the software's interactive peak fit. The modeled geometry was verified using the software's Line Activity Correlation Evaluator which can help identify discrepancies in the modeled sample's density, thickness, and elemental composition. The activity of ²³⁸U in the sample was determined from that of ^{234m}Pa. This is only valid when these two radionuclides are in secular equilibrium and can give the false impression that the ²³⁸U activity is changing with time if they are not in secular equilibrium. The transient activity of ^{234m}Pa, shown in Eq. 5, can be derived from the initial activity equation, Eq. 4. This derivation can be found in most introductory nuclear engineering textbooks as well as at (102).

$$\frac{dN_U}{dt} = \lambda_U N_U \quad (4)$$

$$A_{Pa}(t) = \frac{\lambda_{Pa} A_U^0 (e^{-\lambda_U t} - e^{-\lambda_{Pa} t})}{\lambda_{Pa} - \lambda_U} + A_{Pa}^0 e^{-\lambda_{Pa} t} \quad (5)$$

Where N_U is the number of ^{238}U atoms in the sample, λ_U is the decay constant for ^{238}U , A_U^0 is the initial ^{238}U activity in the sample, λ_{Pa} is the decay constant for $^{234\text{m}}\text{Pa}$, $A_{Pa}(t)$ is the $^{234\text{m}}\text{Pa}$ activity in the sample at time t , A_{Pa}^0 is the initial $^{234\text{m}}\text{Pa}$ activity in the sample, and t is the time since exposing the silica gel to uranyl nitrate.

The mass of ^{235}U and ^{238}U can be calculated in each sample using the fundamental activity equation, Eq. 6, and substituting a derived term, Eq. 7, for the number of radioactive atoms, Eq. 8.

$$A_i = N_i \lambda_i \quad (6)$$

$$N_i = \frac{N_A m_i}{M_i} \quad (7)$$

$$m_i = \frac{A_i M_i}{N_A \lambda_i} \quad (8)$$

Where A_i is the activity in the sample for uranium isotope i , N_i is the number of atoms in the sample for uranium isotope i , λ_i is the decay constant for uranium isotope i , N_A is Avogadro's number, m_i is the mass of uranium in the sample for uranium isotope i , and M_i is the molar mass for uranium isotope i .

The uranium isotopic masses can be partially verified by comparing their measured values to the declared uranium enrichment of the sample, E . This is shown in Eq. 9, assuming the mass of other uranium isotopes is negligible.

$$E = \left(1 + \frac{m_{238}}{m_{235}}\right)^{-1} \quad (9)$$

8.3 Results and Discussion

Secular Equilibrium

The radioactive material being assayed for this project is silica gel containing adsorbed uranium. What is not precisely known is the amount of protactinium that was absorbed in relationship to ^{238}U . Because of this, periodic measurements of the silica gel samples were performed to determine if $^{234\text{m}}\text{Pa}$ and ^{238}U are in secular equilibrium. These measurements span a 160 day period after the silica gel samples were removed from the uranyl solution. The limiting half-life in $^{234\text{m}}\text{Pa}$ - ^{238}U secular equilibrium is that of ^{234}Th at 24.1 days. By measuring the samples 160 days (6.75 half-lives) after uranyl exposure, $^{234\text{m}}\text{Pa}$ - ^{238}U are at least 99.1% within their secular equilibrium activities. This can be seen in Figure 8.3 as the activity of $^{234\text{m}}\text{Pa}$ approaches an asymptotic value with time.

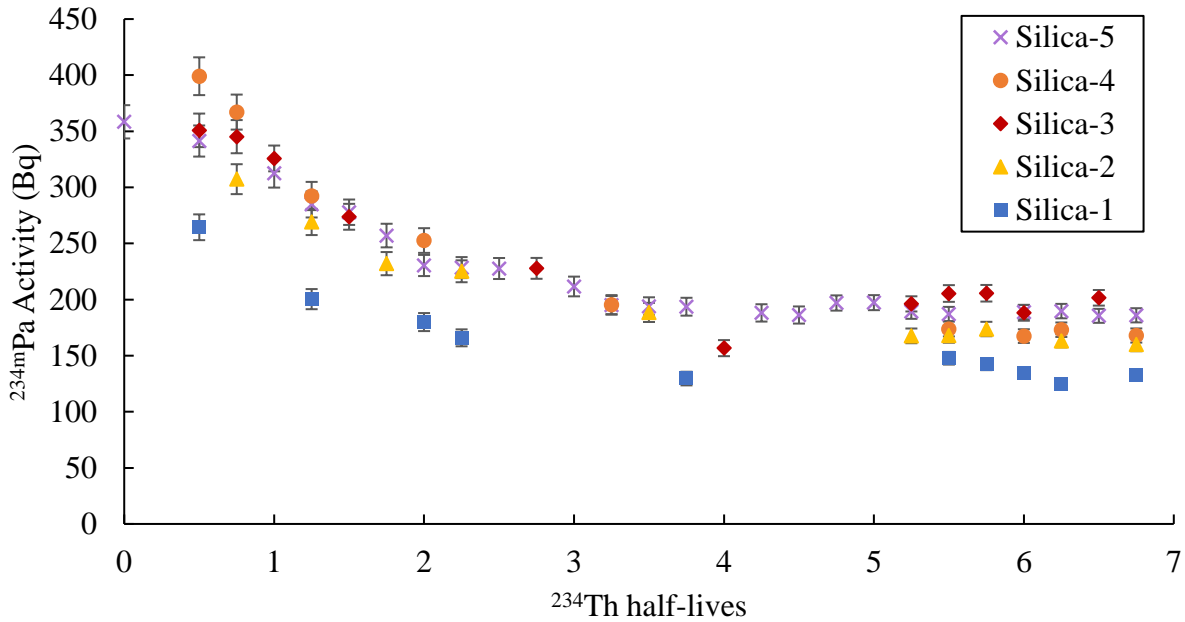


Figure 8.3: Activity as a function of half-life for ^{234m}Pa

Figure 8.3 shows that the initial activity (mass) of ^{234m}Pa was greater than that of its secular equilibrium value. This means that protactinium is more likely to be adsorbed by the silica gel than uranium. As predicted by decay theory, the ^{234m}Pa activity reaches its asymptotic secular equilibrium value within 6.75 half-lives, within measurement uncertainty. Performing a least squares analysis on Eq. 5 with the data shown in Figure 8.3, an estimate of the initial ^{234m}Pa activity in the sample can be made for each silica sample. These results, shown in Table 8.2, indicate that protactinium is approximately twice as likely to be absorbed in silica gel as uranium, regardless of pore size.

Table 8.2: ^{234m}Pa and ^{238}U initial activities based on best fit curves for each silica gel sample

Item	Initial ^{234m}Pa activity (Bq)	Initial ^{238}U activity (Bq)
Silica-1	247	133
Silica-2	375	160
Silica-3	439	202
Silica-4	475	168
Silica-5	390	186

Uranium Enrichment Validation

A validation check can be performed with the measured ^{235}U and ^{238}U activities by comparing the measured uranium enrichment to the declared value. This is shown in Table 8.3 for each silica gel sample. The measured results indicate that the uranium enrichment of each silica gel sample is statistically the same and that the average uranium enrichment is $0.192\% \pm 0.014\%$. This is within the declared value of less than $0.3\% \text{ }^{235}\text{U}$.

Table 8.3: Measured uranium enrichment with uncertainty for each silica sample

Item	Enrichment	Uncertainty
Silica-1	0.193%	0.015%
Silica-2	0.190%	0.015%
Silica-3	0.184%	0.013%
Silica-4	0.200%	0.015%
Silica-5	0.193%	0.013%

Diffusion Samples

The diffusion samples were used to show how much uranyl can be deposited in a specific mass of silica. The theoretical maximum uranium mass that could be deposited in the silica is 197mg from the amount of solution in which the silica gel samples were placed. The total uranium mass in each silica gel sample was determined by taking a weighted average of the ^{235}U and ^{238}U measured data. The results from the diffusion samples are shown in Figure 8.4 below.

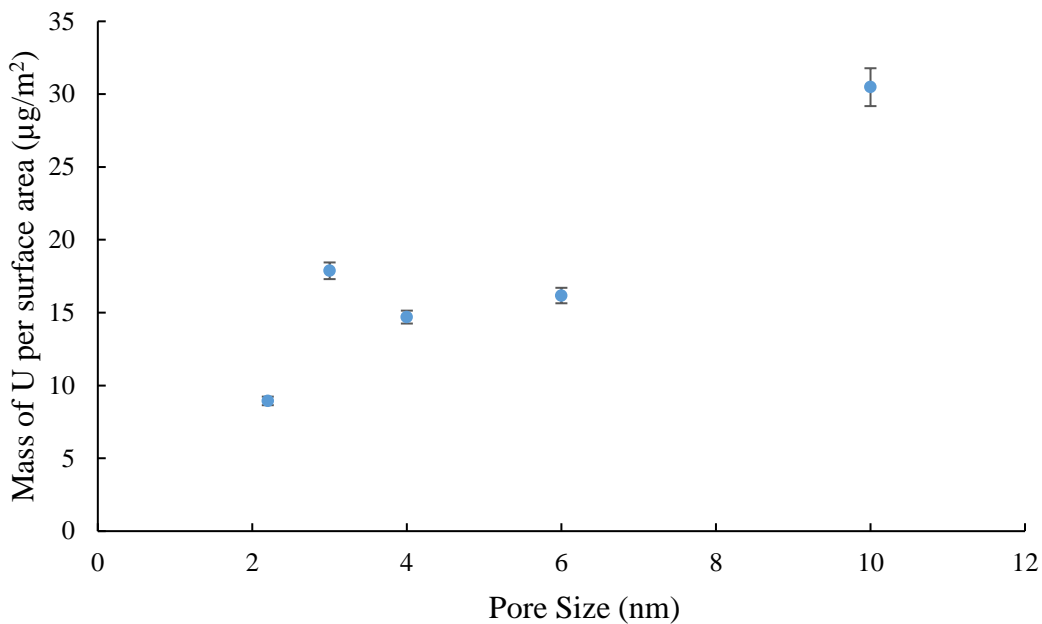


Figure 8.4: Weighted average total uranium mass captured per silica surface area as a function of silica gel pore size

A proportional trend with surface area that was based on the number of negatively charged surface sites was expected, but this was not seen in the results. Figure 8.4 shows an approximate linear increase in accumulated mass per surface area with increase in pore size. This trend shows that the pore size has a significant effect on the surface sites that can be reached by the uranyl. This relationship with permeability is seen because silica gel surface area is measured using nitrogen gas adsorption, but at the lower pore sizes, the uranyl solution cannot reach the same surfaces as the nitrogen gas. The adsorption process is controlled by diffusion of uranyl into the silica gel pores, but it is limited by the permeability of the silica gel.

Filtration Samples

The filtration samples were placed in a flow cell that oriented the silica gel perpendicular to the flow of the solution. This method significantly increased the kinetics of the adsorption. Each

sample was placed in the flow conditions for 20 seconds, which allowed 6.214mg of uranium to pass through the silica gel filter. Unlike the diffusion samples, the uranium mass results from the filtration samples were determined from only the ^{235}U data. This was due to the fact that the measurements of the filtration samples were taken shortly after passing the uranyl nitrate through the silica gel samples. The results from the mass accumulated in the silica gel under these conditions are shown in Figure 8.5.

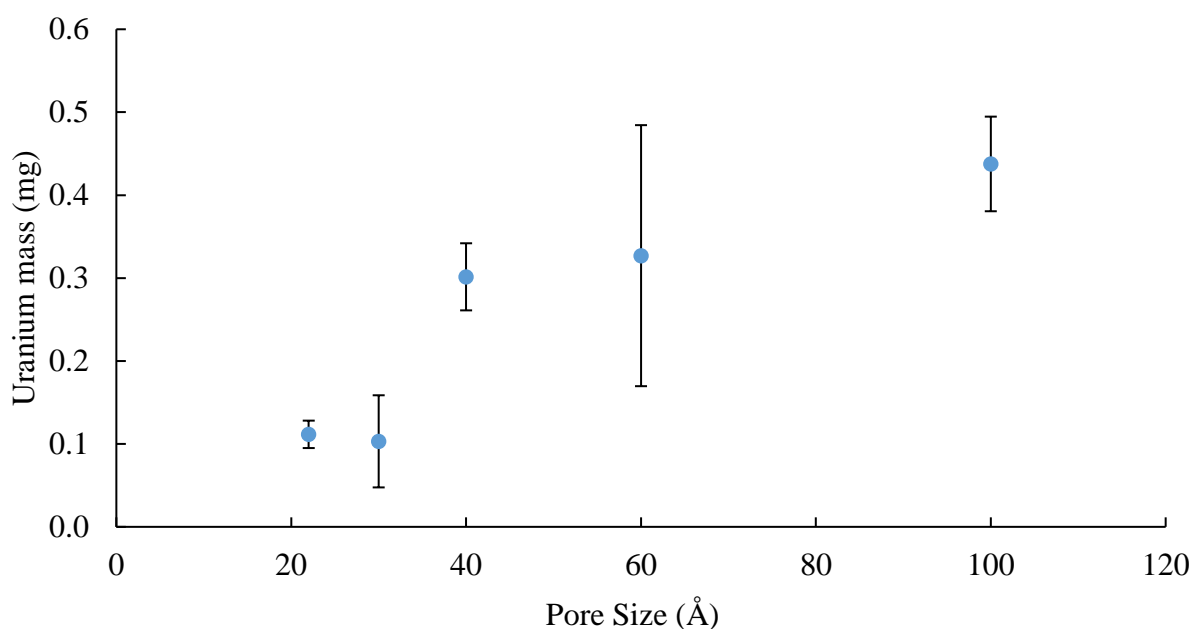


Figure 8.5: Mass of uranium captured as a function of silica gel pore size under flow conditions. Figure 8.5 shows that the uranium captured in the silica gel had an approximate linear trend, within uncertainty, with pore size which matches the permeability trend seen in the previous study. Figure 8.5 also shows that under the flow condition, there was significantly less uranyl deposited than in the diffusion samples. This indicates that when the silica gel does not accumulate enough uranium to limit the number of available surface sites, the deposition of uranyl is likely dependent on pore

size. Based on the amount of uranyl that passed through the silica gel, the filtration efficiency was calculated and is shown in Table 8.4.

Table 8.4: Filtration Efficiency

Item	Efficiency
Silica-1	1.80%
Silica-2	1.66%
Silica-3	4.85%
Silica-4	5.26%
Silica-5	7.04%

The filtration efficiency shows that the silica by itself is not a very effective filter media for removing uranyl ions but is able to accumulate an easily detectable amount of uranium in a short period of time. This filtration efficiency may be improved by the addition of some functional groups that have been added to improve the equilibrium capacity.

8.4 Conclusions

Silica gel is a common material that is used to remove ions from solution, including the uranyl ion. It is used to remove uranyl from solution for fluorescent detection because it also enhances the fluorescence. When removing uranyl from solution, silica gel produces relatively pure uranium that can be removed from the silica gel through basic chemical processes. In the small quantities that are typically found in nature, this would not be a concern, but if a large amount of silica containing uranium is collected the samples could be deemed more than simple chemical waste. The testing to access this possibility led to greater insight into the mechanisms that control the uranyl deposition. In the case of pure diffusion being the driving force, it was seen that the permeability of the silica controlled the deposition until the pore size reached 40Å. Above 40Å, the surface area has a limiting effect because the lower surface area makes it difficult for the uranyl to reach open surface sites. On the other hand, when the silica gel is used as a filter, permeability

is the limiting factor because the surface sites are not near capacity based on the low mass that was deposited. The filtration samples also show that the silica gel is not the most efficient filter media and could be improved by the addition of functional groups that have been used to improve equilibrium capacity. While silica gel is not the most efficient filter, it does accumulate easily detectable levels of uranyl in a short period of time which makes it an excellent candidate to be used as a detection enhancement material.

Chapter 9: Conclusions

When evaluating the adsorption of uranyl into mesoporous silica gel, there were two parameters that needed to be addressed: kinetics of adsorption and the equilibrium capacity. The kinetics of adsorption were tested under various conditions including static fluid, flow conditions, and different concentrations. In the static fluid test, it was determined that the time constant of adsorption was on the order of an hour. The time of adsorption in the static fluid is slow because it is governed by diffusion from the bulk solution into the pore and surfaces of the silica gel. This process in the static fluid is also limited by the permeability of the silica gel which is shown by the reduction of the time constant with the increase in silica gel pore size. The time constant was then evaluated at various fluid velocities. The results showed that there was a critical velocity of 0.36 cm/s at which there was no further reduction in time constant by increasing the fluid velocity. The time constant at the critical velocity reached a minimum of two seconds. This critical velocity was the point at which the supply of uranyl to the surface was equal to the rate of removal of uranyl from the solution by bonding with the silica gel. The critical velocity was dependent on the concentration of the solution which led to the testing of how concentration affects the kinetics. The concentrations were tested by determining the time it took to reach a specific threshold. The threshold was set to be within the linear region of the uptake curve. The response time to reach the threshold point was seen to have an inverse relationship with the concentration. This relationship led to the development of a time-based method to detect trace

amount of uranium in water. The time-based method of detection was incorporated to create a table top instrument for detection of trace amount of uranium in water.

The table top instrument was first used without the time-based detection method to determine the setting needed to detect low concentrations. The baseline settings resulted in a base line detection limit of 3.9 ppb which is one order of magnitude below the EPA MCL for uranium in water. The limit was achieved at the $V_{control}$ setting of 0.77 V. The $V_{control}$ setting of 0.77 V left a large margin for improvement because it can be increased to 1.1 V with the current hardware. Once the time-based detection was implemented, the $V_{control}$ was decrease to 0.63 V and was still able to reach the same limit easily. The true lower limit of detection has yet to be reached using the time-based system. The time-based method has more margin for improvement beyond the $V_{control}$ because the threshold that must be reached can be adjusted as long as the signal-to-noise ratio is maintained. The threshold can be used to set the range of concentrations that can be detected by the instrument and can be adjusted based on the information needed. In addition to designing the hardware, the program was also designed to improve detection by implementing gated detection based on the lifetime of the uranyl fluorescence which can be used to elimination contaminants that have similar spectral characteristics to uranyl.

The use of the fluorescent lifetime to eliminate contaminants lead to further study of how the lifetime could be affected by the environment. The factors that were tested were the pore size of the silica gel, pH of the solution, and the water content in the silica gel. It was seen that at pore sizes below 40 Å, the lifetime increased by as much as 20 μ s between the 40 Å and 22 Å pore sizes. It was also seen that the smallest pore size had a blue spectral shift that, with the extended lifetime, is indicative of quantum confinement. The pH study showed that as the pH increased

from acidic (3.96) to neutral (6.59), the lifetime increased by 40 μs due to the predominate complex formed changing from UO_2SiO_2 to $\text{UO}_2\text{SiO}_2\text{OH}^-$. When $\text{UO}_2\text{SiO}_2\text{OH}^-$ is the predominated complex the lifetime is extended because $\text{UO}_2\text{SiO}_2\text{OH}^-$ has a significantly longer lifetime than the UO_2SiO_2 . The lifetime was also affected by water being present in the silica gel because when the water is removed, $(\text{UO}_2)_2\text{SiO}_4$ is formed. Uranyl silicate was identified by its 528 nm spectral peak, and it caused a decrease in lifetime.

In addition to the study of lifetime to eliminated fluorescent contaminants, additional non-fluorescent contaminants were tested to see how they would affect the detection of uranium. The non-fluorescent contaminants tested were Mn^{2+} , Ca^{2+} , Mg^{2+} , Na^+ , K^+ , and Li^+ . These are quenchers of fluorescence that also affect the adsorption into silica gel because of their positive charges. These cations were selected because they all exist in natural fresh water, and they were each tested at their maximum natural concentrations. To quantify the fluorescent quenching caused by the cations, the Stern-Volmer equation was used to determine the quenching rate as a function of contaminant concentration. It was determined that at the highest natural concentrations, Mn^{2+} , Ca^{2+} , and Li^+ did not cause any quenching. The remaining three contaminants were tested, and it was determined that K^+ was the most effective quencher with the highest quenching rate, but it also has the lowest natural concentration. The Na^+ cation caused the largest reduction in intensity because it has a high natural concentration, but it actually has the lowest quenching rate of the three cations. The reduction in fluorescent intensity could result in an underestimation of the uranium concentration, but the quenching rates could be used to correct for the cations present if the concentration of the contaminants are known. The same cations were tested to see how they affect the kinetics of adsorption by measuring the static fluid time constant in the presence of the cations. Mn^{2+} and Li^+ had negligible effects on the time

constant due to their low natural concentrations. The remaining four cations all caused a decrease in the time constant. This decrease was caused by the contaminant cations taking some of the negatively charge surface sites on the silica gel surface, which caused a reduction in the number of surface sites available to uranyl. The reduction in surface sites decreased the equilibrium capacity for uranyl which lead to the reduction in time. The result was also confirmed with the reduction in the weight percent of uranyl in these samples that was seen in the results from the EDS analysis of the samples. The resulting time constant change could lead to an over estimation of the uranium concentration when using the time-based method of detection. The change in weight percent of uranium present in the silica gel showed that the capacity of the silica gel is critical when additional ions are present.

The capacity of the silica gel was tested using gamma spectroscopy to measure the mass of the uranium accumulated in the silica by diffusion in static fluid and under flow conditions. It was seen that in the static conditions, the permeability still affects the amount of uranium that can be accumulated in the silica gel. The permeability affect is caused by the amount of surface area that can be reached by the water is different than the surface area measured with gas adsorption. Therefore, the largest pore size allows the most uranium to be deposited even through it has a lower surface area. Under flow condition it was seen that very little of the uranium that passes through the silica gel gets adsorbed by the silica gel with a maximum accumulation of only 7%. This shows that the fluid is mostly flowed around the silica gel which further reduced the number of surface sites the uranyl can reach. When under the flow condition, very little of the uranyl is accumulated in the silica gel, but the amount that was accumulated is still enough to reach easily detectable levels in a short period of time.

All of the results from this work will be included in the final prototype of the hand-held device for detection of trace amount of uranium. These results will be incorporated with the addition of a pH probe and a method to input the concentration of common cations. In addition to these corrections, the final prototype will include a spectrometer, a flow cell that can run multiple samples without the need to be replaced, a touch screen display or a method to link to a hand held device, and a portable power supply. The spectrometer will eliminate the need for optical filters and increase the capabilities of the device to potentially detect other fluorophores found in water. The improved flow cell will use the same flow pattern as the optimized version, but the new design will be incorporated to house multiple samples that can be easily changed. The touch screen display will allow the user to input necessary data such as known cations that are present, and it will give a method to display the concentration after detection and monitor the spectrum. These additions will all have to be low power components in order to be incorporated into the portable device that will be battery powered.

List of References

List of References

1. Chen C-C, Pestov D, Nelson JD, Anderson JE, Tepper G. Uranyl Soil Extraction and Fluorescence Enhancement by Nanoporous Silica Gel: pH effects. *Journal of Fluorescence*. 2011 Jan;21(1):119–24.
2. Pestov D, Chen C-C, Nelson JD, Anderson JE, Tepper G. Directed fluorescence sensor element for standoff detection of uranium in soil. *Sensors and Actuators B: Chemical*. 2009 Apr;138(1):134–7.
3. Bernhard G, Geipel G, Brendler V, Nitsche H. Speciation of Uranium in Seepage Waters of a Mine Tailing Pile Studied by Time-Resolved Laser-Induced Fluorescence Spectroscopy (TRLFS). *Radiochimica Acta* [Internet]. 1996;74(1). Available from: <http://www.degruyter.com/view/j/ract.1996.74.issue-s1/ract.1996.74.special-issue.87/ract.1996.74.special-issue.87.xml>
4. US EPA. National Primary Drinking Water Regulations [Internet]. US EPA. 2015. Available from: <https://www.epa.gov/ground-water-and-drinking-water/national-primary-drinking-water-regulations>
5. Riley RG, Zachara JM, Wobber FJ. Chemical Contaminants on DOE Lands and Selection of Contaminant Mixtures for Subsurface Science Research.
6. Vicente-Vicente L, Quiros Y, Pérez-Barriocanal F, López-Novoa JM, López-Hernández FJ, Morales AI. Nephrotoxicity of Uranium: Pathophysiological, Diagnostic and Therapeutic Perspectives. *Toxicological Sciences*. 2010 Dec;118(2):324–47.
7. Nolan J, Weber KA. Natural Uranium Contamination in Major U.S. Aquifers Linked to Nitrate. *Environmental Science & Technology Letters*. 2015 Aug 11;2(8):215–20.
8. What You Need To Know About Uranium in Private Well Water | Western Upper Peninsula Health Department [Internet]. Available from: <http://www.wupdhhd.org/environmental-health/water-supply-protection-well-program/uranium-and-fluoride-advisory/what-you-need-to-know-about-uranium-in-private-well-water/>
9. Canu IG, Laurent O, Pires N, Laurier D, Dublineau I. Health Effects of Naturally Radioactive Water Ingestion: The Need for Enhanced Studies. *Environmental Health Perspectives*. 2011 Aug 2;119(12):1676–80.

10. Giddings M, Farwell J. Background document for development of WHO Guidelines for Drinking-water Quality. [Internet]. [cited 2018 Mar 20]. Available from: http://www.who.int/water_sanitation_health/publications/2012/background_uranium.pdf
11. Favre-Réguillon A, Lebuzyt G, Murat D, Foos J, Mansour C, Draye M. Selective removal of dissolved uranium in drinking water by nanofiltration. *Water Research*. 2008 Feb;42(4–5):1160–6.
12. Bhangare R, Ajmal P, Tiwari M, Sahu S, Pandit G. Laser fluorimetric analysis of uranium in water from Vishakhapatnam and estimation of health risk. *Radiation Protection and Environment*. 2013;36(3):128.
13. Langmuir D. Uranium solution-mineral equilibria at low temperatures with applications to sedimentary ore deposits. *Geochimica et Cosmochimica Acta*. 1978 Jun 1;42(6, Part A):547–69.
14. Grossmann K, Arnold T, Ikeda-Ohno A, Steudtner R, Geipel G, Bernhard G. Fluorescence properties of a uranyl(V)-carbonate species $[U(V)O_2(CO_3)_3]^{5-}$ at low temperature. *Spectrochimica Acta Part A: Molecular and Biomolecular Spectroscopy*. 2009 Mar 1;72(2):449–53.
15. Zhou P, Gu B. Extraction of Oxidized and Reduced Forms of Uranium from Contaminated Soils: Effects of Carbonate Concentration and pH. *Environmental Science & Technology*. 2005 Jun;39(12):4435–40.
16. Nagy AS, Závodská L, Mátel L, Lesný J. Geochemistry and Determination Possibilities of Uranium in Natural Waters. *Acta Technica Jaurinensis*. 2009;2(1):16.
17. Pereira R, Barbosa S, Carvalho FP. Uranium mining in Portugal: a review of the environmental legacies of the largest mines and environmental and human health impacts. *Environmental Geochemistry and Health*. 2014 Apr;36(2):285–301.
18. Carvalho FP, Madruga MJ, Reis MC, Alves JG, Oliveira JM, Gouveia J, et al. Radioactivity in the environment around past radium and uranium mining sites of Portugal. *Journal of Environmental Radioactivity*. 2007 Jul;96(1–3):39–46.
19. Carvalho FP, Oliveira JM, Malta M. Preliminary assessment of uranium mining legacy and environmental radioactivity levels in Sabugal region, Portugal. *International Journal of Energy and Environmental Engineering*. 2016 Dec;7(4):399–408.
20. Wang Z, Zachara JM, Gassman PL, Liu C, Qafoku O, Yantasee W, et al. Fluorescence spectroscopy of U(VI)-silicates and U(VI)-contaminated Hanford sediment. *Geochimica et Cosmochimica Acta*. 2005 Mar;69(6):1391–403.
21. Gnugnoli G, Laraia M, Stegnar P. Uranium mining & milling: Assessing issues of environmental restoration. *IAEA Bulletin*.

22. Environmental contamination from uranium production facilities and their remediation: proceedings of an International Workshop on Environmental Contamination from Uranium Production Facilities and their Remediation: held in Lisbon, 11-13 February 2004. Vienna: International Atomic Energy Agency; 2005. 262 p. (Proceedings series / International Atomic Energy Agency).
23. Uranium Mining in Virginia: Scientific, Technical, Environmental, Human Health and Safety, and Regulatory Aspects of Uranium Mining and Processing in Virginia [Internet]. The National Academies Press; Available from: <https://www.nap.edu/read/13266/chapter/1>
24. Monitoring and surveillance of residues from the mining and milling of uranium and thorium [Internet]. IAEA; 2002. (Safety Report Series). Available from: https://www-pub.iaea.org/MTCD/Publications/PDF/Pub1146_scr.pdf
25. Dodd B, Tepper G. Uranyl adsorption kinetics within silica gel: dependence on flow velocity and concentration. In: Grim GP, Barber HB, Furenlid LR, editors. SPIE; Available from: <https://www.spiedigitallibrary.org/conference-proceedings-of-spie/10393/2274807/Uranyl-adsorption-kinetics-within-silica-gel--dependence-on-flow/10.1117/12.2274807.full>
26. Planning for environmental restoration of uranium mining and milling sites in central and eastern Europe [Internet]. IAEA; 1996. Report No.: IAEA-TECDOC-982. Available from: https://www-pub.iaea.org/MTCD/Publications/PDF/te_982_prn.pdf
27. Release of sites from regulatory control on termination of practices. Safety Guide. [Internet]. IAEA; 2006. Report No.: No. WS-G-5.1. Available from: https://www-pub.iaea.org/MTCD/Publications/PDF/Pub1244_web.pdf
28. Health and Environmental Impacts of Uranium Contamination in the Navajo Nation Five-Year Plan. House Committee on Oversight and Government Reform. 2008;
29. Method 900.0: Gross Alpha and Gross Beta Radioactivity in Drinking Water. [Internet]. Available from: <https://www.epa.gov/sites/production/files/2015-06/documents/epa-900.0.pdf>
30. Prescribed Procedures for Measurement of Radioactivity in Drinking Water. Research and Development [Internet]. Cincinnati OH 45268: United States Environmental Protection Agency; 1980. Report No.: EPA-600/4-80-032. Available from: <https://nepis.epa.gov/Exe/ZyNET.exe/30000QHM.TXT?ZyActionD=ZyDocument&Client=EPA&Index=1976+Thru+1980&Docs=&Query=&Time=&EndTime=&SearchMethod=1&TocRestrict=n&Toc=&TocEntry=&QField=&QFieldYear=&QFieldMonth=&QFieldDay=&IntQFieldOp=0&ExtQFieldOp=0&XmlQuery=&File=D%3A%5Czyfiles%5CIndex%20Data%5C76thru80%5CTxt%5C00000002%5C30000QHM.txt&User=ANONYMOUS&Password=anonymous&SortMethod=h%7C-&MaximumDocuments=1&FuzzyDegree=0&ImageQuality=r75g8/r75g8/x150y150g16/i425&Display=hpfr&DefSeekPage=x&SearchBack=ZyActionL&Back=ZyActionS&BackDesc=Results%20page&MaximumPages=1&ZyEntry=1&SeekPage=x&ZyPURL>

31. WHAT YOU NEED THE KNOW ABOUT Uranium in Drinking Water. Public Service Announcement. Connecticut Department of Public Health Environmental & Occupational Health Assessment Program; 2006.
32. Edwards K. Isotopic Analysis of Uranium in Natural Waters by Alpha Spectrometry. :33.
33. Singh NP, Wrenn ME. Determinations of actinides in biological and environmental samples. *Science of The Total Environment*. 1988 Mar;70:187–203.
34. Boomer DW, Powell MJ. Determination of uranium in environmental samples using inductively coupled plasma mass spectrometry. *Analytical Chemistry*. 1987 Dec;59(23):2810–3.
35. Hobart D. Periodic Table of Elements: Los Alamos National Laboratory [Internet]. [cited 2018 Mar 20]. Available from: <http://periodic.lanl.gov/92.shtml>
36. Azenha MEDG, Burrows HD, Formosinho SJ, Miguel MGM, Daramanyan AP, Khudyakov IV. On the uranyl ion luminescence in aqueous solutions. *Journal of Luminescence*. 1991 Jan;48–49:522–6.
37. Brewster. *Transactions of the Royal Society of Edinburgh* [Internet]. Edinburgh : Royal Society of Edinburgh; 1788. 596 p. Available from: http://archive.org/details/bub_gb_I_UQAAAAIAAJ
38. DeMent J. *Handbook of Fluorescent Gems and Minerals - An Exposition and Catalog of the Fluorescent and Phosphorescent Gems and Minerals, Including the Use of Ultraviolet Light in the Earth Sciences*. Read Books Ltd; 2013. 114 p.
39. Wang G, Su Y, Monts DL. Parametric Investigation of Laser-Induced Fluorescence of Solid-State Uranyl Compounds. *The Journal of Physical Chemistry A*. 2008 Oct 23;112(42):10502–8.
40. Noda C, Kinnin L. Fluorescence Spectra of Uranyl Ion [Internet]. Available from: <http://webhost.bridgew.edu/cnoda/research/uranyl/index.html>
41. Jones L. Systematics in the vibrational spectra of uranyl complexes. *Spectrochimica Acta*. 1958;9.
42. Kitamura A, Yamamura T, Haseb H, Yamamoto T, Moriyama H. Measurement of Hydrolysis Species of U(VI) by Time-Resolved Laser Induced Fluorescence Spectroscopy. *Radiochimica Acta* [Internet]. 1998 Jan 1 [cited 2018 Mar 27];82(s1). Available from: <http://www.degruyter.com/view/j/ract.1998.82.issue-s1/ract.1998.82.special-issue.147/ract.1998.82.special-issue.147.xml>
43. Chang H-S, Korshin GV, Wang Z, Zachara JM. Adsorption of Uranyl on Gibbsite: A Time-Resolved Laser-Induced Fluorescence Spectroscopy Study. *Environmental Science & Technology*. 2006 Feb;40(4):1244–9.

44. Clark DL, Conradson SD, Donohoe RJ, Keogh DW, Morris DE, Palmer PD, et al. Chemical Speciation of the Uranyl Ion under Highly Alkaline Conditions. Synthesis, Structures, and Oxo Ligand Exchange Dynamics. *Inorganic Chemistry*. 1999 Apr;38(7):1456–66.
45. Bell JT, Biggers RE. Absorption Spectrum of the Uranyl Ion in Perchlorate Media. :18.
46. Michard P, Guibal E, Vincent T, Le Cloirec P. Sorption and desorption of uranyl ions by silica gel: pH, particle size and porosity effects. *Microporous Materials*. 1996 Jan;5(5):309–24.
47. Geipel G. Some aspects of actinide speciation by laser-induced spectroscopy. *Coordination Chemistry Reviews*. 2006 Apr;250(7–8):844–54.
48. Lopez M, Birch DJS. Uranyl photophysics on colloidal silica: an alternative luminescence-enhancing medium for uranyl assay. *The Analyst*. 1996;121(7):905.
49. Ishibashi K, Sakamaki S, Imasaka T, Ishibashi N. Determination of uranium at ultratrace levels by time-resolved laser fluorimetry. *Analytica Chimica Acta*. 1989;219:181–90.
50. Kenney-Wallace GA, Wilson JP, Farrell JF, Gupta BK. Direct determination of uranyl ion by nanosecond dye-laser spectroscopy. *Talanta*. 1981 Feb;28(2):107–13.
51. Sill CW, Peterson HE. Fluorescence Test for Uranium in Aqueous Solution. *Analytical Chemistry*. 1947 Sep;19(9):646–51.
52. Ellerby LM, Nishida CR, Nishida F, Yamanaka SA, Dunn B, Valentine JS, et al. Encapsulation of Proteins in Transparent Porous Silicate Glasses Prepared by the Sol-Gel Method. *Science*. 1992;255(5048):1113–5.
53. Schraml-Marth M, Walther KL, Wokaun A, Handy BE, Baiker A. Porous silica gels and TiO₂/SiO₂ mixed oxides prepared via the sol-gel process: characterization by spectroscopic techniques. *Journal of Non-Crystalline Solids*. 1992 Jan;143:93–111.
54. Siouffi A-M. Silica gel-based monoliths prepared by the sol-gel method: facts and figures. *Journal of Chromatography A*. 2003 Jun;1000(1–2):801–18.
55. Trewyn BG, Slowing II, Giri S, Chen H-T, Lin VS-Y. Synthesis and Functionalization of a Mesoporous Silica Nanoparticle Based on the Sol-Gel Process and Applications in Controlled Release. *Accounts of Chemical Research*. 2007 Sep;40(9):846–53.
56. Hench LL, West JK. The sol-gel process. *Chemical Reviews*. 1990 Jan;90(1):33–72.
57. Zhou Y, Schattka JH, Antonietti M. Room-Temperature Ionic Liquids as Template to Monolithic Mesoporous Silica with Wormlike Pores via a Sol-Gel Nanocasting Technique. *Nano Letters*. 2004 Mar;4(3):477–81.

58. Kruk M, Jaroniec M, Sayari A. Application of Large Pore MCM-41 Molecular Sieves To Improve Pore Size Analysis Using Nitrogen Adsorption Measurements. *Langmuir*. 1997 Nov;13(23):6267–73.
59. Sing KSW, Pierotti RA, Rouquerol J, Siemieniowska T. Reporting Physisorption Data for Gas/Solid Systems. In: Ertl, editor. *Handbook of Heterogeneous Catalysis* [Internet]. Weinheim, Germany; 2008. Available from: <http://doi.wiley.com/10.1002/9783527610044.hetcat0065>
60. Brunauer S, Emmett PH, Teller E. Adsorption of Gases in Multimolecular Layers. *Journal of the American Chemical Society*. 1938 Feb;60(2):309–19.
61. Barrett EP, Joyner LG, Halenda PP. The Determination of Pore Volume and Area Distributions in Porous Substances. I. Computations from Nitrogen Isotherms. *Journal of the American Chemical Society*. 1951 Jan;73(1):373–80.
62. Tran HH, Roddick FA, O'Donnell JA. Comparison of chromatography and desiccant silica gels for the adsorption of metal ion I. adsorption and kinetics. :9.
63. Gurgel JM, Filho LS, Grenier P, Meunier F. Thermal Diffusivity and Adsorption Kinetics of Silica-Gel/Water. :9.
64. Bayramoglu G, Arica MY. MCM-41 silica particles grafted with polyacrylonitrile: Modification in to amidoxime and carboxyl groups for enhanced uranium removal from aqueous medium. *Microporous and Mesoporous Materials*. 2016 May;226:117–24.
65. Dolatyari L, Yaftian MR, Rostamnia S. Removal of uranium(VI) ions from aqueous solutions using Schiff base functionalized SBA-15 mesoporous silica materials. *Journal of Environmental Management*. 2016 Mar;169:8–17.
66. Zhu L, Shi X, Song L, Sun Y, Chen S, Wu W. Mesoporous silica (KIT-6) derivatized with hydroxyquinoline functionalities as a selective adsorbent of uranium(VI). *Journal of Radioanalytical and Nuclear Chemistry*. 2016 May;308(2):381–92.
67. Budnyak TM, Strizhak AV, Gładysz-Płaska A, Sternik D, Komarov IV, Kołodyńska D, et al. Silica with immobilized phosphinic acid-derivative for uranium extraction. *Journal of Hazardous Materials*. 2016 Aug;314:326–40.
68. Zhu L, Yuan L-Y, Xia L-S, Wang L. Incorporation of magnetism into the dihydroimidazole functionalized mesoporous silica for convenient U(VI) capture. *Journal of Radioanalytical and Nuclear Chemistry*. 2016 May;308(2):447–58.
69. Gao B, Yin J, Mao Z-Y, Wang D-J, Zhang L-X, Bie L-J. Synthesis and photoluminescence of blue LED excitable La₄Ti₉O₂₄:Eu³⁺ phosphor for red-light emission. *Materials Research Bulletin*. 2014 Mar;51:185–8.
70. Dodd BM, Tafreshi HV, Tepper GC. Flow-enhanced kinetics of uranyl (UO₂) transport into nano-porous silica gel. *Materials & Design*. 2016 Sep;106:330–5.

71. Zhao M, Li H, Liu W, Chu W, Chen Y. Paper-based laser induced fluorescence immunodevice combining with CdTe embedded silica nanoparticles signal enhancement strategy. *Sensors and Actuators B: Chemical*. 2017 Apr;242:87–94.
72. Rao H-H, Xue Z-H, Zhao G-H, Li S-Y, Du X. Fluorescence emission properties of rhodamine B encapsulated organic-inorganic hybrid mesoporous silica host. *Journal of Non-Crystalline Solids*. 2016 Oct;450:32–7.
73. Li J, Fan N, Wang X, He Z. Cellular level evaluation and lysozyme adsorption regulation of bimodal nanoporous silica. *Materials Science and Engineering: C*. 2017 Jul;76:509–17.
74. Nabavi Zadeh PS, Mallak KA, Carlsson N, Åkerman B. A fluorescence spectroscopy assay for real-time monitoring of enzyme immobilization into mesoporous silica particles. *Analytical Biochemistry*. 2015 May;476:51–8.
75. Dutta RK, Kumar A. Highly Sensitive and Selective Method for Detecting Ultratrace Levels of Aqueous Uranyl Ions by Strongly Photoluminescent-Responsive Amine-Modified Cadmium Sulfide Quantum Dots. *Analytical Chemistry*. 2016 Sep 20;88(18):9071–8.
76. Burns P. The crystal chemistry of hexavalent uranium: polyhedron geometries, bond-valence parameters, and polymerization of polyhedra. :21.
77. Pyykko P, Zhao Y. The large range of uranyl bond lengths: ab initio calculations on simple uranium-oxygen clusters. *Inorganic Chemistry*. 1991 Sep;30(19):3787–8.
78. Hoekstra HR. Uranium-Oxygen Bond Lengths in Uranyl Salts: Uranyl Fluoride and Uranyl Carbonate. *Inorganic Chemistry*. 1963 Jun;2(3):492–5.
79. Gabriel U, Charlet L, Schläpfer CW, Vial JC, Brachmann A, Geipel G. Uranyl Surface Speciation on Silica Particles Studied by Time-Resolved Laser-Induced Fluorescence Spectroscopy. *Journal of Colloid and Interface Science*. 2001 Jul;239(2):358–68.
80. Leung AF, Tsang KK. Temperature dependence of fluorescence decay rates of monovalent-uranyl nitrates. *Solid State Communications*. 1979 Jul;31(4):v.
81. Matsushima R, Sakuraba S. Quenching of the uranyl fluorescence by aromatic molecules. *Journal of the American Chemical Society*. 1971 Dec;93(26):7143–5.
82. Keizer J. Nonlinear fluorescence quenching and the origin of positive curvature in Stern-Volmer plots. *Journal of the American Chemical Society*. 1983 Mar;105(6):1494–8.
83. Mueller J. Fluorescence Workshop UMN Physics: Quenching and FRET [Internet]. 2006 Jun 8. Available from: <http://fitzkee.chemistry.msstate.edu/sites/default/files/ch8990/Fluoro6.pdf>
84. Vaughns C. Stern-Volmer Quenching of Conjugated Polymers: A Study of Fluorophore Concentration. :22.

85. Nelson D. Fresh Water, Natural Composition of - seawater, river, sea, freshwater, temperature, salt, types, source [Internet]. Available from: <http://www.waterencyclopedia.com/En-Ge/Fresh-Water-Natural-Composition-of.html>
86. Scott M. Ocean Chemical Processes - river, sea, oceans, important, salt, types, system, source, effect [Internet]. [cited 2018 Mar 26]. Available from: <http://www.waterencyclopedia.com/Mi-Oc/Ocean-Chemical-Processes.html>
87. Stegen S, Queirolo F, Cortés S, Pastenes J, Ostapczuk P, Backhaus F, et al. Use of the Fresh Water Plants *Zannichellia Palustris* and *Myriophyllum Acuatium* for Biomonitoring of Cd, Pb, and Cu in Anden Rivers of Chile. *Boletín de la Sociedad Chilena de Química*. 2000;45:449–59.
88. Guseva N. The Origin of the Natural Water Chemical Composition in the Permafrost Region of the Eastern Slope of the Polar Urals. *Water*. 2016 Dec 14;8(12):594.
89. Kalf J. Limnology: Major Ions, Carbonate System, Alkalinity, pH [Internet]. Prentice Hall; Available from: <http://web.pdx.edu/~sytsmam/limno/Limno09.6.IonsandANC.pdf>
90. Livingstone D. Chapter G. Chemical Composition of Rivers and Lakes. :75.
91. Shvartsev SL. Geochemistry of fresh groundwater in the main landscape zones of the Earth. *Geochemistry International*. 2008 Dec;46(13):1285–398.
92. JONES L. Determination of force constants. :9.
93. Table of Nuclides [Internet]. [cited 2018 Mar 19]. Available from: <http://atom.kaeri.re.kr:8080/>
94. Knoll GF. Radiation Detection and Measurement. John Wiley & Sons; 2010. 857 p.
95. Reilly D, Ensslin N, Smith H, Kreiner S, Los Alamos National Laboratory (U.S.), Etats-Unis, et al. Passive nondestructive assay of nuclear materials. Springfield, VA: US Department of Commerce, National Technical Information Service; 1991.
96. Model 747 and 747E: Lead Shield [Internet]. [cited 2018 Mar 19]. Available from: <http://www.canberra.com/products/detectors/pdf/747-SS-C40114.pdf>
97. Standard Electrode Coaxial Ge Detectors [Internet]. [cited 2018 Mar 19]. Available from: <http://www.canberra.com/products/detectors/pdf/SEGe-detectors-C49317.pdf>
98. Cryo-Cycle II: Hybrid Cryostat [Internet]. [cited 2018 Mar 19]. Available from: http://www.canberra.com/products/detectors/pdf/Cryo-Cycle_II_C40847.pdf
99. Genie 2000: Basic Spectroscopy Software [Internet]. [cited 2018 Mar 19]. Available from: http://www.canberra.com/products/radiochemistry_lab/pdf/G2K-BasicSpect-SS-C40220.pdf

100. Genie 2000: Gamma Analysis Software [Internet]. [cited 2018 Mar 19]. Available from: http://www.canberra.com/products/radiochemistry_lab/pdf/Genie-2000_Gamma_Analysis_Software_SS-C47691.pdf
101. Model S574 LabSOCS: Calibration Software [Internet]. [cited 2018 Mar 19]. Available from: http://canberra.com/products/radiochemistry_lab/pdf/LabSOCS-SS-C40167.pdf
102. Lux P. Secular and Transient Equilibrium Formula [Internet]. Available from: <http://www.plux.co.uk/secular-and-transient-equilibrium-formula/>

VITA

BRANDON MICHAEL DODD

1900 Fairoaks Road, Powhatan, VA, 23139

(804) 658-7401, doddbm@vcu.edu

Education

- **Ph.D. Candidate in Mechanical and Nuclear Engineering (May, 2018)**
Virginia Commonwealth University (VCU), Richmond, VA, USA
- **Master of Science in Mechanical and Nuclear Engineering (December, 2015)**
Virginia Commonwealth University (VCU), Richmond, VA, USA
- **Bachelor of Science in Mechanical Engineering (May, 2014)**
Virginia Military Institute (VMI), Lexington, VA, USA

Publications

- **Brandon Dodd**, Gary Tepper, Uranyl adsorption kinetics within silica gel: dependence on flow velocity and concentration, SPIE Conference Paper
- **Brandon M. Dodd**, Hooman V. Tafreshi, Gary C. Tepper, Flow-enhanced kinetics of uranyl (UO₂) transport into nano-porous silica gel, *Materials & Design*, Volume 106, 15 September 2016, Pages 330-335, ISSN 0264-1275
- **Brandon M. Dodd**, Gary C. Tepper, Uranyl fluorescence lifetime in nanoporous silica gel: The influence of pore size, pH and water, *Materials & Design*, Volume 151, 5 August 2018, Pages 48-52, ISSN 0264-1275
- Ghochaghi, N. Taiwo, A. Winkel, M. **Dodd**, B. Mossi, K. Tepper, G., 2014, "Electrospun polystyrene coatings with tunable wettability," *Journal of Applied Polymer Science*, 132. (10.)

Conference Proceedings

- American Nuclear Society, Student Conference 2018. “Environmental Contamination from Uranium Processing and Its Impact” **Brandon Dodd***, Braden Goddard and Gary Tepper.
- American Nuclear Society, Student Conference 2018. “Nuclear Engineering at VCU: Nonexistent to Nationally Recognized in 10 Years” **Brandon Dodd**, Daniell Tincher*, Braden Goddard, Sama Bilbao y León and Gary Tepper.
- Energy Materials Nanotechnology, Nanopores. December 2017 “An optical study of molecular transport and accumulation in nanoporous silica gel.” Gary Tepper* and **Brandon Dodd**
- SPIE Photonics and Optics: Radiation Detectors in Medicine, Industry, and National Security XVIII, Summer 2017. “Rapid and accurate detection of uranium in aqueous solutions.” Gary Tepper and **Brandon Dodd***
- American Society of Mechanical Engineers, Student Professional Development Conference, Spring 2014. “The Effect of Deposition Time on Roughness of Superhydrophobic Coating.” **Brandon Dodd**

Provisional Patent

- (62/325,699) Novel Hand-Held, Portable Device to Measure Trace Levels of Uranium in Water Inventors: Gary C. Tepper and **Brandon M. Dodd** (International patent has been filed)